NASA TECHNICAL TRANSLATION NASA TT F-13,605

PREVAPORIZATION OF LIQUID FUEL IN A SMALL RAMJET ENGINE

F. Gehring

Translation of "Die Vorverdampfung von Flossigkraftstoff in einem Kleinen Staustrahltriebwerk". Deutsche Luft- und Raumfahrt, Report DLR-FB-69-67, September 1969, 131 pages.

NATIONAL AERONAUTICS AND SPACE ADMINISTRATION
WASHINGTON, D. C. 20546 APRIL 1971

This is the complete text of the authors dissertation, which was accepted by the University of Stuttgart toward the degree of Doctor of Engineering (Dr.-Ing.).

TABLE OF CONTENTS

TABLE OF ABBREVIATIONS

Notations relating to hydrocarbon fuels

$D_{15.6}^{15.6}$	relative density, referred to water at 15.6°C
i	enthalpy, kcal/kp
K_W	Watson characteristic factor
M	molecular weight
P_{kr}	critical pressure
R	gas constant
s	entropy, kcal/kp degree
s_E	slope of the boiling curve, °C/Vol. %
$\bar{s}_E$	mean slope of the boiling curve, °C/Vol. %
t_{E50}	50% boiling temperature from Engler analysis
$\bar{t}_{E50}$	mean boiling temperature
t_{kr}	critical temperature
$\bar{t}_M$	mean molar boiling point
Δt	correction

The index G instead of E applies for the equilibrium vaporization curve; likewise, other percentages can replace the 50%.

Notations for heat exchange calculation

C_s	black body radiation coefficient, 4.96 kcal/m^2 hr
c_p	specific heat at constant pressure, kcal/kp degree
d_a	outside diameter
d_{gl}	equivalent ("hydraulic") diameter
d_i	inside diameter
F	cowling surface or pipe surface
F'	surface between the fins
F_k	surface wetted by fuel
F_m	average surface (logarithmic mean value)
F_{st}	crosspiece area

f_{av}	configuration factor for offset grouped tube bundles
G	mass flow of fuel, kp/hr
h	half crosspiece height
k	heat transfer coefficient referred to F_k or F_{22} kcal/m^2 hr degree
L	length of the exchange surfaces in the direction of flow
Nu	Nusselt number
Pr	Prandtl number
P	Pressure (partial pressure) of the radiating gases
Q_{11}, Q_{22}	hourly heat transfer to fuel, kcal/hr
Q_{12}	heat flux from combustion gases to fuel
Q_{13}	heat flux from fuel to cooling air
q_{str}	hourly heat transfer by radiation, kcal/m^2 hr
Re	Reynolds number
s	clear offset distance of crosspiece; layer thickness of the radiating body of gas
s_{gl}	"equivalent radius" of the radiating gas body
s_l	distance from the pipe axis along the gas flow
s_q	distance from the pipe axis across the gas flow
T	temperature in ^oK
t	temperature in ^oC
U	wetted circumference of the flow cross section
W	water value, kcal/hr degree
w	flow velocity
α	heat transfer coefficient of surface F, kcal/m^2 hr degree
α'	heat transfer coefficient of surface F'
α_m	mean heat transfer coefficient of surface F_k
α_{sch}	"apparent" heat transfer coefficient of surface F_k
γ	specific gravity, kp/dm^3
δ_w	wall thickness
ε_g	gas body emission ratio
$\varepsilon_{g\infty}$	emission ratio for an infinitely thick gas body
ε_{gw}	proportion of radiative exchange between wall and gas
ε_w	emission ratio of the wall
ϑ	"fin efficiency"

λ	heat conductivity, kcal/m hr degree
ν	kinematic viscosity, m^2/s

Indices for heat exchange calculations

1	heat exchange in engine cowling
2	heat exchange in secondary flameholder
11	referred to fuel duct
12	heated side of the duct, i. e., from the symmetry line in
13	cooled side of the duct, i. e., from the symmetry line out
21	referred to inside of the secondary flameholder tube
22	referred to the surface of the secondary flameholder tube
g	combustion gases
k	fuel
ko	convection
krü	curved fuel line
l	air
m	logarithmic or arithmetic mean
st	crosspiece
str	radiation
v	offset tube bundle
w	wall
t'	initial temperature
t''	final temperature

Notations for the ramjet engine and test

B	fuel consumption kp/hr	
B_r	reduced fuel consumption	$B \frac{p_o}{p} \sqrt{\frac{T_o}{T}}$
b	specific fuel consumption, kp/hr kp	
b_r	reduced specific fuel consumption	$\frac{B}{S} \sqrt{\frac{T_o}{T}}$
c_s	thrust coefficient	$\frac{S \frac{p_o}{p}}{\frac{S_o}{\alpha} w_p F}$
c_{s_r}	reduced thrust coefficient	

F	internal cross section area
g	acceleration of gravity
H	flight altitude
Ma	Mach number
M_d	turning moment
m	richness of mixture (ratio of the actual to the stoichiometric fuel/air ratio)
n	revolutions per minute (or second)
p	pressure
S	engine thrust
S_r	reduced engine thrust $S\frac{p_o}{p}$
w_r	reduced speed $w\sqrt{\frac{T_o}{T}}$
α	stoichiometric fuel/air ratio
ε	angular delay
ϑ	moment of inertia, cm kp sec
ς	density, kp sec^2/m^4
ω	angular velocity

Indices related to the ramjet engine and test

0	referred to the standard atmosphere at sea level
1	in the intake diffusor - intake cross section
1'	in the collecting diffusor - intake cross section
2	in the combustion space - intake cross section
3	in the combustion space - final cross section
4	in the final nozzle cross section
th	theoretical

PREVAPORIZATION OF LIQUID FUEL IN A SMALL RAMJET ENGINE

F. Gehring

ABSTRACT. The combustion chambers of small subsonic ramjet engines for rotor tip drive are relatively short. Complete combustion of the air-fuel mixture within the engine cannot be achieved by the injection of liquid fuel. The combustion efficiency, however, can be improved by eliminating the time interval from liquid fuel injection to fuel droplet evaporation, which is relatively long in comparison to the time the fuel is present in the combustion chamber. In order to improve the combustion efficiency the liquid fuel is heated up by the dissipated heat of the ramjet engine to such an extent that it evaporates immediately during expansion in the injection system. The application and functional reliability of this fuel pre-evaporation system is small tip drive ramjet engines is demonstrated and proved by means of tests. The influence of the operational parameters, such as velocity of air flow, altitude, air-fuel ratio, fuel flow rate and pressure on the caloric state of the fuel before injection and after expansion is the subject of a theoretical investigation. N70-23774

1. INTRODUCTION AND STATEMENT OF THE PROBLEM

For the dissipative continuous process in the subsonic region, the /13* thermodynamic efficiency of ramjets is less than ten percent. In order that the losses remain as low as possible, one can among other things attempt to utilize the fuel optimally in the engine; that is, one tries for complete

---

*Numbers in the margin indicate pagination in the original foreign text.

combustion of the air-fuel mixture. This requirement can no longer be met in conventional short ramjets with direct injection of liquid fuel, because the preparation of the fuel, up to the point of vaporization and final mixing with the combustion air takes too long (required residence times longer than about 2/100 second).

In the engine, the liquid fuel must go through the following phases which are long in relation to the residence time:

injection
jet breakup
droplet formation
droplet vaporization

These phases are then of somewhat shorter duration:

macromixing
micromixing
ignition
combustion

If acceptable operation is to be attained for ramjet engines with combustion chambers lengths below about 600 mm, it is necessary, among other things, to reduce the pretreatment time of the fuel.

This can happen in two ways:

First: Use of initially gaseous fuel (e. g., propane). But this solution is not very advantageous because of the bulk of gaseous fuel under pressure.

Second: The liquid fuel is preheated under pressure to the extent that during the pressure release in and behind the injector nozzle, it fully or partially vaporizes spontaneously, depending on the operating conditions. /14

The ramjet engine, first suggested by Lorin in his publications during the years 1907-1913 /24, 25/ and thus also known as the "Lorin engine" is temptingly simple in design. Because of that advantage, it is of interest for air travel.

The ramjet engine reaches its best efficiency in the supersonic region at Mach numbers of 3 to 4. In this range it is superior to all other air-breathing engines. But with decreasing Mach number, its efficiency drops so strongly that in the subsonic region it is no longer useful for direct propulsion of aircraft.

In spite of the headstrong development of air travel in the last two decades, Lorin's idea has until this day been realized only in a few test airplanes and missiles, because aircraft development is still groping its way into the region of Mach numbers productive for ramjet engines.

The welcome possibility of circumventing the disadvantages of shaft drive in helicopter design spurred development of the jet-driven rotor at the beginning of the 1940's. The Focke-Wulf firm was the first to plan use of ramjet engines for rotor drive in their "driving wing" (Triebflügel) of Tank in 1944, /26/, only two years after the first flight test was performed with an engine developed by E. Sänger /27, 28/.

After 1945 the use of ramjet engines to drive helicopter rotors was of interest in the USA, and the development was pressed with great expense. Thus the McDonnell company, in cooperation with NACA /11, 12/ developed engines of round and oval cross section, which were tested on their helicopter "Little Henry" /29,30/. The Hiller company invested more than two million dollars in ramjet development for their helicopter "Hornet" /31, 32/ and may have collected the greatest experience in this field. /15

They made about 25 ramjet helicopters in various versions for quite varied applications. In the Netherlands, the Nederlandse Helicopter Industrie built the ramjet helicopter "Kolibrie", powered by TJ-5 engines. It received a civil airworthiness certificate (CAR) after two and one-half years of testing /33/. In Germany, the firm of Daimler Benz was interested in the development of small ramjet engines /34/.

With the engine lengths in these developments (500 to 700 mm) it must have been necessary to accept very considerable combustion losses. The reasons for the limits on length are:

a) Ramjet engines placed at the ends of the rotor blades are subjected to high centrifugal forces. These result in corresponding bending moments at the ramjets, so that the design of longer engines is made difficult.

b) In the ideal case, these engines would have to be made curved (radius of engine curvature = rotor radius), so that the engine input and exhaust planes would be perpendicular to the corresponding tangents to the rotor blade path. Such curved engines are very difficult to make; thus the straight engine is preferred. Because of the diffusor aerodynamics the intake cross section should be as nearly perpendicular to the incident air flow as possible. The effect of this is that the longer the straight engine becomes, the greater is the angle between the long axis of the engine and the rotor blade axis. Simultaneously, the angle between the thrust vector and the tangent to the blade path increases, and with it, the radial component of thrust, which is lost to effective thrust. The obliqueness of the incidence of air flow on the engine, and the resulting outside air resistance, also increase to the same extent. This resistance is particularly noticeable in forward flight of the helicopter, in which the obliquity of the incidence of the air flow changes cyclically.

c) The aerodynamic center of such an engine body lies ahead of its center of gravity and the elastic axis of the rotor blade; the engine is aerodynamically unstable. Thus an additional torsional moment acts on the rotor blade. This is greater, the longer the engine is. Some help can be provided by a stabilizing fin; but the fin produces additional

/16

drag and it is difficult to design its attachment to the engine.

d) Moments from second-order centrifugal forces which act on the engine work against rotor blade angular control and cause additional blade stress in torsion. The equation for the sum of these moments is

$$M = \omega^2 \sin\varphi \int x^2 dm$$

in which: dm = mass element of the engine

φ = angle between the longitudinal axis of the engine and the plane of the rotor disk

x = distance of the mass element from the elastic axis of the rotor blade

As the engine becomes longer, the distance x increases, and thus moment M also increases.

Therefore, for relatively small ramjet rotors, one is forced to such short engines that injection of liquid fuel can hardly still be defended.

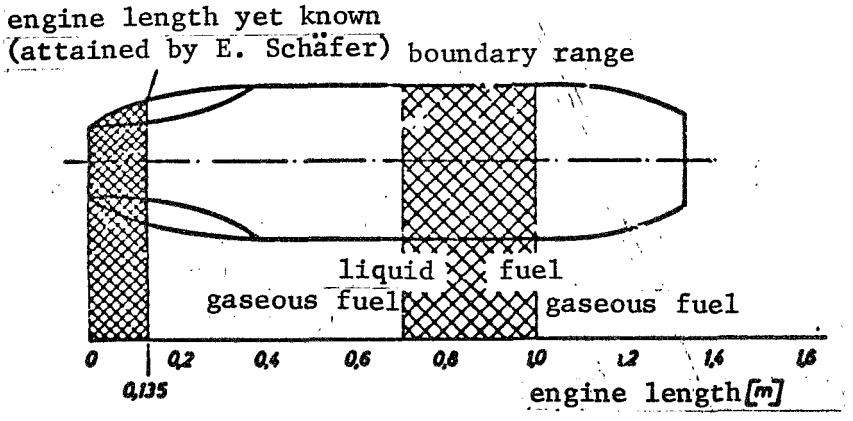

Limits for liquid injection of fuel

It was soon well established that the ramjet rotor is not useful /17
for commercial helicopter construction because it is uneconomical, primarily due to the poor efficiency of the ramjet engine in the subsonic region.

But for other applications — short-range helicopters and expendable equipment — the advantages of these rotors also appear to be clear: cheap manufacture of the device, due to the extraordinarily low weight per unit power and the simplicity of the ramjet engine and the entire engine system. It could hardly be made more simple. These engines are also no less interesting for driving propellors and heater fans employed for special purposes.

E. Schäfer carried out experiments with extremely small ramjet engines on a miniature rotating arm at the Research Institute for Physics of Jet Propulsion in 1955, toward the realization of ramjet propellors /34/. The rotating arm of 500 mm diameter was driven by two ramjets of only 30 mm diameter and 135 mm length. Acetylene and propane gas served as fuel.

The bulk of the pressurized gaseous fuels was not favorable for the practical application of this engine; and as Schäfer wrote in his report: "It must be the goal of future work to attack the problem of mixture preparation and combustion of liquid fuels in the small ramjet engines considered here. The results of this work would be of great interest not only for the ramjet propellor, but also for many other problems of combustion technology".

The German Helicopter Study Society in 1959 obtained a research contract on a small helicopter with ramjet engines /35/. Propane gas was still planned for operation of the small blade-tip ramjet engines. But this project gave rise to investigation of the idea expressed by Schäfer in a talk: "To vaporize liquid fuel before it is mixed with the combustion air". /18

The result of these investigations is reported in this work. Its goal is: to show the potential of fuel prevaporization and its application in small blade-tip ramjet engines; and to investigate the effects of the working parameters, such as incident flow velocity, flight altitude,

mixture richness, fuel throughput and pressure, at different ratios of jet output cross section to combustion chamber cross section, on the enthalpy/entropy state of the fuel before the injection nozzle and after its discharge. And, what is especially important, it will be demonstrated experimentally that such fuel prevaporization is functionally sound in a ramjet engine.

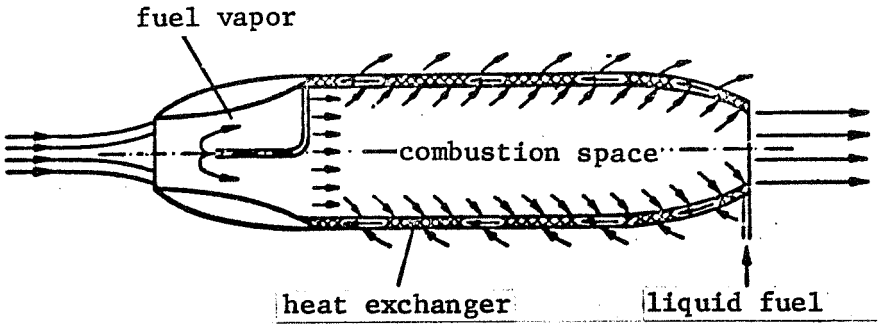

Schematic diagram of a ramjet engine with liquid fuel prevaporization by utilization of lost heat.

2. TECHNOLOGY OF HYDROCARBON FUELS AND THEIR VAPORIZATION /19

2.1. Liquid Fuels

The liquid fuels which come into consideration today for operation of a blade-tip ramjet engine are primarily automobile and aviation gasoline, Diesel oils, and the Diesel-type jet fuels classified by the designations JP-1, JP-4, and JP-5. For military purposes, special fuels such as alcohol are of limited interest because of their almost invisible jet of flame gases.

The present investigation will be primarily concerned with the "standard" fuels, such as are used commercially in large amounts. Still, the results obtained in this work could also be applied to special fuels under appropriate circumstances.

All these fuels used for the operation of jet engines, whether liquids or gases at atmospheric pressure, belong to the great family of hydrocarbons. In general, however, the fuels are not pure materials, but a mixture of a large number (several hundred) hydrocarbon homologs. Considered roughly, the paraffinic-naphthenic compounds make up the major portion; then there follow the aromatic components, with the olefins in the last place. Sulfur and lead tetraethyl occur in fractional percentages by weight or volume, depending on the type of fuel.

Characterization of these individual types of fuels by fixed chemical and physical characteristics is quite difficult, however, and even impossible, because commercial fuels are mixtures of individual components, which are produced in various plants. These mixtures must meet a specification /20 which allows considerable tolerance. This is not least conditioned by the large number of crude oil fields (or by production from various coals) and the resulting necessary variety of crude oil compositions.

For example, if one had the analysis of a standard automobile gasoline that was used in the tests, it would be possible to make phase diagrams for that gasoline, at significant expense and up to a certain degree of accuracy. These would not, however, include the individual hydrocarbon homologs, but would apply only for a selected mean characteristic of this gasoline. Thus one works as if he were dealing with a pure hydrocarbon. If one relates the "same" standard automobile gasoline to a later time or especially to another company, one can safely say that these phase diagrams no longer apply. One must make considerable compromises with their accuracy.

2.2 Physical Properties

A group of properties is used to characterize the type of hydrocarbon oil. Their relation to the chemical structure of the oils has been determined through experiments. The following properties are particularly important for fuel vaporization:

2.2.1. Distillation Characteristics

Being mixtures, the mineral oils have no boiling point, but a more or less broad boiling range. In petroleum technology, this is determined by distillation analysis in the laboratory [1,2]. One of the most common distillation procedures is that of Engler or A. S. T. M. (American Society for Testing Materials). The result is shown in tables, or in the form of a "boiling curve". The boiling analysis of the standard automobile gasoline used for the tests is given at the end of this chapter. The related curve is presented in Figures 1 and 2. /21

In these diagrams the temperature is plotted against the volume percent of the fuel which has distilled. The lower part of Figure 2 shows the curve mentioned along with the boiling range curves for the most commonly used airplane fuels. It is apparent that the various fuels can differ considerably in the slope and temperature level of their boiling range curves. The ranges themselves have different widths at constant

volume percent of distillate, and these ranges increase for all the fuels shown with increasing yield of distillate. The boiling point spread within a given type of fuel is therefore less for the more volatile components than for the higher-boiling ones, which expand this range greatly at the end of the distillation.

The following characteristics are derived from distillation analysis:

2.2.2 50% Boiling Temperature $t_{E\ 50}$

The 50% boiling temperature is defined as that temperature at which 50% by volume of the starting material has distilled over in Engler distillation analysis. But this value is characteristic only for narrow-boiling fractions. The same definition also applies to the 10% boiling temperature $t_{E\ 10}$ and the 90% boiling temperature $t_{E\ 90}$.

2.2.3 Slope of the Distillation Curve s_E or $\bar{s}_E$

This is understood to mean the slope of the distillation curve in degrees Celsius per volume percent. The mean slope $\bar{s}_E$ is defined either as /22

$$\bar{s}_E = \frac{t_{E\ 70} - t_{E\ 10}}{60}$$

or

$$\bar{s}_E = \frac{t_{E\ 90} - t_{E\ 10}}{80}$$

2.2.4 Mean Boiling Temperature $\bar{t}_E$ (Boiling Index)

The mean boiling temperature is obtained by taking the arithmetic mean of $t_{E\ 10}$, $t_{E\ 30}$, $t_{E\ 50}$, $t_{E\ 70}$, and $t_{E\ 90}$:

$$\bar{t}_E = \frac{t_{E\ 10} + t_{E\ 30} + t_{E\ 50} + t_{E\ 70} + t_{E\ 90}}{5}$$

It is also often calculated by adding the temperatures at 5, 15, 25 . . . . 85, 95 percent distillate by volume, and dividing the sum by ten.

2.2.5 Mean Molar Boiling Temperature $\bar{t}_M$

For the mean boiling temperature $\bar{t}_E$ the amount of distillate is measured in percent by volume. This temperature represents a volume-mean boiling temperature. But in the physical view this relation is not quite satisfactory as a characteristic value for a mineral oil, because the ratio of density to molecular weight decreases with increasing boiling point. From this it can be seen that mineral oils with the same mean boiling temperature, but with different slopes for the Engler curve, can show significant differences in mean molecular weight and thus also in vapor density.

In order to remedy this condition, the concept of the "mean molar boiling temperature" $\bar{t}_M$ has been introduced. In this case the mean value is referred to the equimolar amount of distillate. The value of $\bar{t}_M$ is obtained by decreasing the mean boiling temperature $\bar{t}_E$ by a correction, Δt: /23

$$\bar{t}_M = \bar{t}_E - \Delta t$$

The value of the correction depends on the slope of the Engler distillation curve, $\bar{s}_E$, defined in 2.2.3, between the 90% and 10% points. Figure 3 shows Δt as a function of $\bar{s}_E$ according to /1, 2/.

2.2.6 Watson Characteristic Factor K_W

Out of several proposed characteristic values intended to give a relation between the chemical structure of a type of oil and its physical properties, the Watson characteristic factor still proves best. The purely empirical relation on which it is based allows no exactness in the results. Nevertheless, the characterization of an oil which it gives is quite useful.

The Watson characteristic factor is defined as follows:

$$K_W = 1{,}22 \frac{\sqrt[3]{T_s}}{D^{15{,}6}_{15{,}6}}$$

Here T_s is the boiling temperature in $^{\circ}K$ and $D^{15.6}_{15.6}$ is the relative density at $15.6^{\circ}C$, referred to water at $15.6^{\circ}C$.

For mixtures of oils, the boiling temperature T_s is replaced by the 50% boiling temperature defined in 2.2.2 or by the mean molar boiling temperature defined in 2.2.5, depending on whether we are dealing with a fraction having narrow boiling limits, or with one having widely spaced boiling limits. /24

From the quality of the oil, the boiling temperature, and the density, which are contained in K_W, other properties can be determined. These include the viscosity, the specific heat, the heat of vaporization, and the heat content. The corresponding tabulations are in /1, 2/.

2.2.7 Physical Properties of the Standard Automobile Gasoline used for the Tests

These characteristics were determined or calculated according to the definitions above, as follow:

50% boiling temperature	$t_{E\ 50}$	$= 87^{\circ}C$
mean boiling temperature	$\bar{t}_E$	$= 94.1^{\circ}C$
mean slope of the boiling curve	$\bar{s}_E$	$= 1.21\ ^{\circ}C/Vol\ \%$
correction from Figure 3	Δt	$= 7^{\circ}C$
mean molar boiling temperature	$\bar{t}_M$	$= 87.1^{\circ}C$
Watson characteristic factor	K_W	$= 11.8$

and also

density	$D^{15.6}_{15.6}$	$= 0.73$
molecular weight	M	$= 94$
gas constant (848/M)	R	$= 9.02$
critical temperature	t_{cr}	$= 274^{\circ}C$

critical pressure P_{cr} = 38 kp/cm^2 abs

2.3 Critical State

The critical state of a material is characterized by the absence of wet vapor in the transition from vapor to liquid; i. e., the transition is direct. The related state variables are the critical temperature t_{cr}, /25
the critical pressure p_{cr} and the critical volume v_{cr}. At the critical point, which is established by these parameters, therefore, the liquid is no longer separated from the vapor, and both states have the same density.

If the critical temperature is exceeded, a boundary between gas and liquid can no longer be detected. Even if the pressure is set very high, no phase separation can be obtained. If the temperature drops below the critical value at constant pressure, only the liquid form of the material can be obtained, and vaporization is prevented by the critical pressure.

The critical state variables t_{cr} and p_{cr} of hydrocarbon mixtures are higher than those of the homologs they contain. The separation of the critical points of the homologs is the greater, the further apart their boiling points are. The values of t_{cr} and p_{cr} can be determined from the already-defined concepts $\bar{t}_E$, $\bar{s}_E$, K_W, $\bar{t}_M$, and the molecular weight, according to /1, 2/. These are shown graphically or numerically in the upper part of Figure 2 for the fuels mentioned.

For hydrocarbon homologs the liquid and gaseous states are separated by the vapor pressure curve (vapor tension curve), which ends at the critical point. Mixtures, which include all the fuel types considered here, and which have a boiling range at constant pressure, have a two-phase region between liquid and vapor. In this region the liquid and the vapor are of different composition. The limiting lines of these regions are designated as the vaporization line along the liquid, and the dew line along the vapor.

Both lines join at the critical point, in analogy with the vapor pressure curve of a single material. Its exact course near the critical point cannot be determined by calculation, however, and can only be found by experiment. This is caused by abnormal vaporization and condensation phenomena near the critical point and potential phase separation even above the critical point. The parameters t_{cr} and p_{cr} must not be the maximal values on the limiting curve, as still higher temperatures and pressures can appear. Above these maximum values, phase and composition differences are no longer possible, even for mixtures. /26

2.4 Equilibrium Vaporization Curves and Vapor Pressure Diagrams

In order to study and evaluate the problem of fuel vaporization it is necessary to follow the course of the state of liquid fuel used during the vaporization process by means of a state diagram for this fuel. As is shown later, the vapor pressure diagram with vaporization and dew lines for the fuel concerned has proved very good for this purpose. But even with the Engler distillation analysis described in 2.2.1 and the boiling curve obtained from it, it is still not possible to draw such a pressure-dependent vapor and dew point diagram for the hydrocarbon mixture concerned, because the Engler analysis is not carried out at constant pressure. Thus no vaporization equilibrium can appear, as is the case, for instance, in the pressure drop at and following the fuel injection jet of a ramjet engine.

For mineral oils in a closed system, that is, when all the phases present remain in contact with each other, and newly-formed phases are not removed, the vaporization equilibrium is represented by the so-called equilibrium vaporization curve [1]. This is plotted like the Engler curve, but at constant pressure, as a function of volume percent and temperature. It can be determined from the distillation properties of the mixture concerned by the methods given in [1]. /27

Figure 1 shows this equilibrium vaporization curve for the standard automobile gasoline used in the tests. The similarity to the Engler curve, which is also shown, is apparent. The part of the curve between 10 and 90 volume percent distillate can be replaced by a straight line, to a good approximation, while the analysis shows the ends of the line to be more or less strongly curved.

The concepts defined in 2.2.2 and 2.2.3 naturally apply also for the equilibrium vaporization curve, except that the index E is replaced by the index G.

The equilibrium vaporization curve for higher pressure appears if one plots the temperature of the initial point $t_{G\ 0}$ (vaporization point) of the curve, and the endpoint $t_{G\ 100}$ (dew point) as log p vs. 1/t. The critical point for the type of fuel being considered is also plotted, and connected with straight lines to the points $t_{G\ 0}$ and $t_{G\ 100}$. These two lines are the vapor pressure curve (vaporization line) and the dew pressure curve (dew line) of the fuel considered, because in a pT diagram plotted according to this scale (abscissa 1/T, ordinate log p) the vapor pressure curves of single materials are nearly linear [1, 2, 9]. Thus one has obtained the vapor pressure diagram, such as is shown in Figure 19.

Now the vaporization and dew points can be read from the equilibrium vaporization curve, in this diagram, for any chosen pressure below the critical point. One can see that with increasing pressure the temperature difference between the vaporization line and the dew line becomes steadily smaller, reaching zero at the critical point (see also Figure 1).

We have already referred in 2.3 to the inaccuracy of the course of /28
the vaporization and dew lines near the critical point. Just as for the temperatures $t_{G\ 0}$ and $t_{G\ 100}$, one can now draw straight lines to the critical point from the temperatures at other volume percentages of distillate, such as $t_{G\ 25}$, $t_{G\ 50}$, and $t_{G\ 75}$. Then these lines subdivide the equilibrium vaporization curve to be read at any pressure in the same proportion of volume percent distillate as that of the initial curve at

1 atmosphere absolute pressure. Therefore, if one knows the pressure-temperature curve of the expansion process in the fuel injection jet for a fuel vaporization process, and if this curve falls in the region between the vaporization and dew lines, then by means of this vapor pressure diagram one can for any expansion phase determine the vapor and liquid proportions in volume percent. Thus one can determine at any time the extent to which the vaporization, or in some circumstances, the condensation, has proceeded.

2.5 Expansion in the Fuel Injection Jet

The total heat - entropy diagram has proved best for thermodynamic study of the expansion process in a jet, since the amounts of work and heat can be read off as line segments. But because of the varied nature of the forms of the passages in injection jets, it is impossible to determine generally valid expansion curves. Thus one must follow the expansion process in the heat-entropy diagram for each jet form at a known "chamber condition".

In order to make a generally valid statement in spite of that, it is expedient to include the range of all possible conditions in place of an individual expansion. For the present expansion process this range is limited by the lines of two theoretical state curves. One of these is that of adiabatic expansion, i. e., the state curve for constant entropy. The other is the pure throttle expansion at constant enthalpy. /29
The curve of constant entropy is the more important for this investigation, because it is more or less the criterion for the possible vapor state of the fuel, while the isentropic curve marks off only the higher superheated vapor states. From these two curves, it is also possible to draw conclusions on the approximate course of the actual expansion curve.

As has already been discussed in 2.1, the fuels under consideration are made up of many hundreds of hydrocarbon homologs. It is impossible to make up vapor tables or diagrams which take into account the caloric

behavior of the individual hydrocarbons in such a mixture. This mixture can be replaced, however, by an assumed single material of the same density, which remains liquid up to the mean molar boiling temperature, completely vaporizes at this temperature, and above it is in the superheated vapor region. Thus one takes the characteristic data explained in 2.2 as representative of the actual fuel, and for these data, which represent the mean values, draws the necessary diagrams. This method is sufficiently accurate for the current investigation, and with it one can make definitive statements on the possibility of fuel vaporizaton.

To determine the course of the isentropic and isenthalpic curves mentioned, it is necessary to have temperature-entropy and enthalpy-temperature curves, in which these state curves appear as straight lines. The enthalpy-entropy curve mentioned initially can be neglected, because only the limiting curves for the process are to be determined.

Drawing of the temperature-entropy and enthalpy-temperature diagrams is quite time-consuming and encumbered with approximations; but the accuracy is adequate for the thermodynamic considerations undertaken. Figures 4 and 5 show these diagrams for the standard automobile gasoline used in the tests. The diagrams were developed by the methods given in [1]. /30

Thus to obtain the limiting curve for all expansion processes from one initial condition, one need only enter the diagram at the appropriate "chamber condition", and from this point trace out the thermal behavior of the fuel on the line entropy = constant or enthalpy = constant.

2.6 Heating up and Vaporization

Vaporization of a liquid fuel in a ramjet engine can follow thermodynamically different paths.

Let us consider these possibilities in a temperature-entropy or enthalpy-entropy diagram, such as are given in Figures 4 and 6 for standard automobile gasoline.

If liquid fuel is heated, it is converted into the state of saturated vapor as soon as the temperature reaches the saturated vapor temperature at the prevailing pressure. The expansion process can then be started near the upper limiting curve (saturated vapor limit). Thus one certainly obtains superheated vapor with the usual hydrocarbon mixtures used as fuels, if the level of the counter-pressure is reached.

In several technological devices, such as blowtorches and gasoline stoves, as well as in the combustion chambers of some turbojets, the vaporization process works in the way just described. In order to avoid cracking of the fuel in turbojets, air is mixed with the fuel and this mixture then heated /36-42/.

If one wishes to avoid during the heating phase of the fuel the saturated vapor region and its related bubble boiling, then one must work with with higher pressures, near or above the critical pressure. In this case the heating up to the "chamber condition" proceeds exclusively in the liquid phase along the lower limiting curve. The starting point for expansion can be below the critical point, but the lower it is, the more the curve approaches that for pure throttle expansion. In contrast to the previous case, here the saturated vapor region is not crossed until the expansion phase, or not at all. The final state is again in the superheated vapor region. To be sure, there are also "chamber conditions" in the supercritical region from which the course of expansion leads relatively slowly through the saturated vapor region, or it can even end there. This occurs if the temperature of the fuel is only a little above the critical value, and the pressure very much above. Then because of the high pressure the enthalpy and entropy may have become so low that the expansion curve can no longer get over the apex of the upper limiting curve, and thus leads into the saturated vapor region.

/31

The possibilities which have been described for fuel vaporization are due to the particular caloric behavior as characterized by the course of the saturated vapor boundaries for this material in the temperature-entropy or enthalpy-entropy curves, in which the entropy increases with increasing values of t and i (see Figures 4 and 6).

These possibilities for fuel vaporization can be more or less well realized in a ramjet engine. The problems which appear are treated in Chapter 4 by means of the computer and test results, in combination with the vapor pressure diagram described in 2.4.

INSTITUTE FOR APPLIED CHEMISTRY
Hans Gockel, Chemical Engineer
Public commissioned expert in commercial chemistry, under oath
Stuttgart-Feuerbach • Wienerstrasse 13
Bank: Feuerbach Peoples Bank, Girokonto No. 86 • Postal Checking account No. 321 35 Post Office Box 172 Telephone 8 35 59

German Research Institute for
Air and Space Travel, Design Division
7023 Stuttgart Airport

Your designation: Order No. 85
Your communication of: No. 8900, 7/11/66

Our designation: Go/Kl-3
7 Stuttgart-Feuerbach, 23 November 1966

VK Investigation Number 443

Sample material: Standard automobile gasoline Received: 8/11/66
Submitted by: German Research Institute for air and Space Travel
Taken from

Color and outward appearance:	clear, reddish liquid	
Density at 15°C:	0.731	
Acid value:	0.21	mg/100 cm^3
Sulfur (total):	0.03	% by weight
Corrosion (Cu):	negative	
Solid residue from evaporation at 160°C	2.2	mg/100 cm^3
Type	-	
Density Number	32	
Sulfonation number	-	
Iodine number	-	
Anti-knock agent (TEL)	0.004	Volume %

Boiling behavior according to ASTM/Standard Engl. Convention

Begin	36	°C	5%	48	°C
10%	52	"	15%	56	"
20%	59	"	25%	63	"
30%	66	"	35%	71	"
40%	76	"	45%	81	"
50%	87	"	55%	93	"
60%	101	"	65%	109	"
70%	117	"	75%	125	"
80%	132	"	85%	140	"
90%	149	"	95%	163	"

KZ. = 94.9

up to 50°	7.5%		
" " 70°	34 %	Yield	98%
" " 100°	59.5%	Residue	1%
" " 150°	90 %	Loss	1%
" " 200°	-	Final	184°C
" "	-		

up to 75° (including distillation loss) 39%

Evaluation

This sample of standard gasoline is of acceptable standard commercial quality. The specific gravity, together with the Di. number, shows that the aromatic portion is unusually low.

3. EFFECT OF THE RAMJET OPERATING PARAMETERS ON THE STATE OF THE FUEL VAPOR

/33

3.1 Heat Exchange in the Engine Cowling. Fuel Heating

In the ramjet engines described here, the liquid fuel is heated with waste heat. Since part of the heat loss is taken off through the engine cowling, the fuel must be introduced in the proper way for this heat exchange process. The introduction of fuel onto or into the engine covering is determined by theoretical considerations of heat exchange, and to a large degree also by design and technological requirements.

Because of the weight, it is not desirable to run a separate fuel line in some manner along the engine cowling with engines for blade tip drive, although it could be done simply and economically with tubes. It is more appropriate to use the engine cowling for fuel transport. Simultaneously, the cowling material is cooled.

This solution leads to a double cowling. The annular clearance is supported by crosspieces and subdivided so as to provide favorable fuel supply, and also to stand the fuel pressure, which in some circumstances is very high.

Different paths can be used for design, either through welding together specially produced tubes, or by milling channels out of the solid material. The manufacturing possibilities were decisive for the selection of the solution actually realized.

In the ramjet engines used in the tests, as shown in Figures 32 to 35, the fuel is lead through a channel with square cross section, which is coiled helically through the annular space of the engine double mantle. The heat exchange for this solution will be calculated below. The calculation procedure used is based on the methods used in references [3] through [6] for computation of heat exchange in finned tubes and finned surfaces.

/34

To do this, the cross section of a finned surface is reflected in a line of symmetry which runs across the fins. Thus one obtains adjacent channels of rectangular cross section, which are heated on one side and cooled on the other side. The heat conductivity problems in the channel wall are thus the same on both sides of the symmetry line, but with the signs reversed.

The following figure shows the cross section of a channel element and the designations which apply to it.

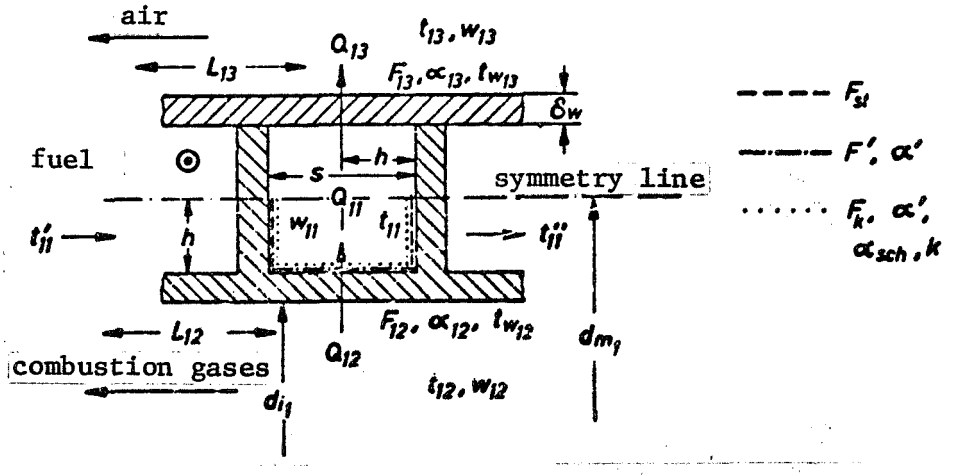

Without introducing serious errors, the calculations can be simplified as follows:

1. The channel walls are thin in comparison to the engine cowling diameter. Thus the curvature of the outer and inner cowlings can be neglected for calculation of heat conduction in the walls. /35
2. It is assumed that there is no heat flow perpendicular to the cross-pieces; this flow is only radial.
3. The brazed joint between the outer cowling and the cross-pieces is neglected; i. e., it is assumed that the material runs

solidly through, instead of there being a brazed joint.

In order to comprehend to some extent the multiple temperature and velocity conditions in the combustion chamber, the following additional simplifying assumption is introduced:

4. The wall and gas temperature, as well as the gas velocity, are assumed to be constant through the length of the combustion chamber.

The square cross section of the channel, the uniform wall thicknesses, and the homogeneous construction material allow the following equalities in this case:

$$\delta_{w_{12}} = \delta_{w_{13}} = \delta_{w_{St}} = \delta_{w_4}$$
$$h_1 = h_2 = h$$
$$s_1 = s_2 = s = 2h$$
$$\lambda_{w_{12}} = \lambda_{St_{12}}; \quad \lambda_{w_{13}} = \lambda_{St_{13}}$$

a) Coefficient of thermal conductivity, k

For the heated (index 12) and cooled (index 13) sides of the channel, the thermal conductivity coefficient is:

$$\frac{1}{k_{12/13}} = \frac{1}{\alpha_{sch_{12/13}}} + \frac{F_{K_{12/13}}}{F_{12/13}} \cdot \left(\frac{1}{\alpha_{12/13}} + \frac{\delta_{w_4}}{\lambda_{w_{12/13}}} \right)$$

α_{sch} is designated as the so-called apparent heat transfer coefficient. The following equation applies for it:

$$\alpha_{sch_{12/13}} = \alpha_{rm_{12/13}} \left[1 - (1 - \vartheta_{12/13}) \frac{F_{St_{12/13}}}{F_{K_{12/13}}} \right] \qquad (1)$$

Here ϑ is the "fin efficiency": /36

$$\vartheta_{12/13} = \frac{\tanh h \sqrt{\frac{\alpha_{m_{12/13}} \cdot 2}{\lambda_{w_{12/13}} \cdot \delta_{w_1}}}}{h \sqrt{\frac{\alpha_{m_{12/13}} \cdot 2}{\lambda_{w_{12/13}} \cdot \delta_{w_1}}}} \qquad (2)$$

b) Heat transfer from the combustion gases to the inner cowling. According to Hausen, the Nusselt number for heat transfer from the combustion gases to the inner cowling (forced convection) is

$$Nu_{12} = 0.024 \left[1 + \left(\frac{d_{i2}}{L_{12}}\right)^{2/3}\right] Re_{12}^{0.786} \cdot Pr_{12}^{0.45}$$

and the heat transfer coefficient is

$$\alpha_{12_{Ko}} = \frac{Nu_{12} \cdot \lambda_g}{d_{i_1}}$$

The heat transfer is increased by radiation from the combustion gases. The heat transfer coefficient for this is:

$$\alpha_{12_{Str}} = \frac{q_{Str}}{(t_g - t_{w_{12}})}$$

Since the radiating gas contains CO_2 and H_2O, the individual radiations are determined separately and added to give the total radiation:

$$q_{Str} = q_{CO_2} + q_{H_2O}$$

The total radiation is decreased, however, by about 2 - 7% due to opposing effects of the individual radiations. Assuming this factor to be 4%, we have

$$q_{Str} = 0.96 (q_{CO_2} + q_{H_2O})$$

The amount of heat transferred per hour per square meter of wall surface by gas radiation is, for CO_2 or H_2O radiation /37

$$q_{str\ CO_2/H_2O} = C_s\left[\varepsilon_{gw_g}\left(\frac{T_g}{100\,°K}\right)^4 - \varepsilon_{gw_w}\left(\frac{T_g}{100\,°K}\right)^4\right]$$

Within the brackets, the term ε_{gw} is to be determined for the gas temperature in the first expression and for the wall temperature in the second expression. According to E. Eckert /7/ the radiative exchange ratio ε_{gw} is given by the equation:

$$\varepsilon_{gw\ CO_2/H_2O} = \frac{1}{\frac{1}{\varepsilon_g} + \frac{1}{\varepsilon_{g\infty}}\left(\frac{1}{\varepsilon_w} - 1\right)}$$

ε_g and $\varepsilon_{g\infty}$ for CO_2 and H_2O can be taken from diagrams /6, 8/ as functions of the product of s and p. In this case s is replaced by the "equivalent radius" s_{gl}. Here it is equal to 0.95 d_{i1}. The necessary partial pressures of CO_2 and H_2O are dependent on the richness of the mixture, m. They can be determined from the partial composition of the flame gases in volume proportions (mole fractions). The emission ratio of the wall ε_w is set equal to 0.65.

Now one obtains the following expression for the heat transfer coefficient α_{12} :

$$\alpha_{12} = \alpha_{12\,H_2O} + \alpha_{12\,str}$$

The increase in heat transfer due to dissociation of the flame gases (CO_2, H_2O) is still so slight at the prevailing combustion temperatures that this effect can be neglected.

c) Heat transfer from the outer cowling to the air.
According to Jürges-Merkel, the heat transfer in turbulent flow along a plane wall (cowling curvature neglected) is given by

$$Nu_{12} = 0.057\,Re_{12}^{0.76}\,Pr_{12}^{0.76}$$

Then the heat transfer coefficient α_{13} for transfer from the outer cowling to the air becomes /38

$$\alpha_{13} = \frac{Nu_{13} \cdot \lambda_L}{L_{13}}$$

d) Heat transfer from the surface F'_{12} to the fuel or from the fuel to the surface F'_{13}

According to Hausen-Kraussold the expression for liquids is

$$Nu'_{12} = Nu'_{13} = 0{,}024\left[1+\left(\frac{d_{gl}}{L_H}\right)^{2/3}\right] Re^{0{,}8} Pr^{0{,}33} \underbrace{\left(\frac{\eta_{H\ddot{u}}}{\eta_{Wu}}\right)^{0{,}14}}_{=1}$$

The last term in this equation can be set equal to one here, because there is provision for continuous intimate mixing of the fuel stream, which is especially stratified due to centrifugal force. Because we are dealing with tube flow in rectangular cross section, the equivalent hydraulic diameter must be inserted. Then the heat transfer coefficient becomes

$$\alpha'_{12} = \alpha'_{13} = \frac{Nu'_{12/13} \cdot \lambda_K}{d_{gl}}$$

With consideration of the curvature of the flow channel, α'_{12} or α'_{13} become

$$\alpha'_{13\,Krü} = \alpha'_{13,Krü} = \alpha'_{12/13}\left(1+3{,}54\,\frac{d_{gl}}{d_{mg}}\right)$$

e) Mean heat transfer coefficients m_{12} and m_{13} for the surfaces F_{k12} and F_{k13}

This heat transfer coefficient depends on the cross-piece height h to the distance between cross-pieces, s. For h/s = 1/2, one obtains

from the corresponding diagram in [6]:

$$\alpha_{m_{12}} = \alpha_{m_{13}} = 0{,}93\,\alpha'_{12/13\ \text{korr}}$$

This mean heat transfer coefficient can now be inserted into Equations (1) and (2). /39

f) Fuel temperature increase

The amount of heat transferred to the fuel per hour is

$$Q_{11} = Q_{12} - Q_{13} \tag{3}$$

or with the water value, $\dot{W}_{11} = G_{11}\, c_{p_{11}}$

$$Q_{11} = W_{11}\,(t''_{11} - t'_{11}) \tag{4}$$

The quantity of heat added or removed per hour is

$$Q_{12/13} = k_{12/13}\, F_{K\,12/13}\, \Delta t_{m_{12/13}} \tag{5}$$

Δt_m is the mean temperature difference. It is assumed that $t'_{12} \approx t''_{12}$ and $t'_{13} \approx t''_{13}$. Then, because there is countercurrent flow and the difference in the temperature differences is very small, one gets, instead of the mean logarithmic temperature difference, Δt_m as the difference of the arithmetic mean temperatures of the two materials.

$$\Delta t_{m_{12}} = t_{12} - \frac{t'_{11} + t''_{11}}{2}$$

$$\Delta t_{m_{13}} = \frac{t'_{11} + t''_{11}}{2} - t_{13}$$

If these two equations are substituted into Equation (5), and then Equations (4) and (5) into Equation (3), one can solve Equation (3) for the fuel temperature t''_{11} at the conclusion of the heating process, obtaining

$$t''_{11} = \frac{k_{12} F_{K\,12}\,(2t_{12} - t'_{11}) + k_{13} F_{K\,13}\,(2t_{13} - t'_{11}) + 2\dot{W}_{11}\, t'_{11}}{2W_{11} + k_{12} F_{K\,12} + k_{13} F_{K\,13}}$$

The course of the calculations shown, with the formulas used, was confirmed by the test results; they agreed well (see Figure 15). The calculation applies, however, only for the last two possibilities for heating described in 2.6; that is, as long as no bubble boiling occurs. But bubble boiling is, as is shown later, not desirable for operation of the ramjet engine; it would complicate the calculations and make their result uncertain. /40

This heat exchange process was programmed for the investigation in 3.2 and 3.3.

The corresponding flow diagram is shown in Figure 7. In order to obtain the necessary increase in fuel temperature ahead of the injection jet in the test runs, it was necessary to follow the first heat exchange with a second one. For this purpose, the secondary flameholder in the test ramjet engine was designed as a heat exchanger, as shown in Figure 33. The calculations set up for this were based on the well-known formulas and relations which agree best with experiments. The calculations are shown in the flow diagram of Figure 8.

3.2 Operating Parameters, State and Efficiency Characteristics of the Ramjet Engine

Prevaporization of fuel for blade-tip ramjet engines on an aircraft is reasonable only if the safe operation of the engine is guaranteed for all flight and operating conditions occurring. In order to investigate the effect of potential operating parameters on the state of the fuel before the injection jet, the heating process of 3.1 was carried out for a wide variety of these parameters. The necessary starting data, such as state and efficiency characteristics for the ramjet engine as functions of important design and operating parameters were taken from the theoretically derived design tables of Sänger-Bredt /13/. Calculation of these tables is based on n-octane (C_8H_{18}) as fuel. The controlling reason for this choice was the fact that, with reference to its chemical /41

and thermodynamic properties, n-octane has an intermediate position among the fuel mixtures considered.

This condition agrees with the present investigation, as n-octane is a characteristic member of the liquid paraffins, which scarcely differ with respect to their heating powers in mixtures. As already mentioned in 2.1, these paraffins appear predominantly in the usual fuel mixtures. For comparison with gasolines it is helpful that the critical values of these mixtures are of the same order of magnitude as those of the hydrocarbon homologs of n-octane (p_{cr} = 25 atm abs; t_{cr} = 296°C).

In order to limit still more the number of free parameters, the tables were based on a standard atmosphere.

The program for the heating process was provided with the following variables

Flight Mach number ..... Ma
Flight altitude..... H
Jet orifice ratio..... F_4/F_2
Mixture richness..... m

and with the state and efficiency characteristics resulting from them. The values are summarized in the following table: /42

	flight altitude H = 0 and 4 km											
Ma	0,3				0,5				0,7			
m	0,4	0,6	0,8	1,0	0,4	0,6	0,8	1,0	0,4	0,6	0,8	1,0
F_4/F_2	0,3	0,3	0,3	0,3	0,3	0,3	0,3	0,3	0,3	0,3	0,3	0,3
	0,4	0,4	0,4	0,4	0,4	0,4	0,4	0,4	0,4	0,4	0,4	0,4
	0,5	0,5	0,5	0,5	0,5	0,5	0,5	0,5	0,5	0,5	0,5	0,5
	0,6	0,6	0,6	0,6	0,6	0,6	0,6	0,6	0,6	0,6	0,6	0,6
	0,7	0,7	0,7	0,7	0,7	0,7	0,7	0,7	0,7	0,7	0,7	0,7

Such a computer program, with only 4 parameters and 120 combinations, appears very simple on quick consideration. But since the material values for the fuel, the combustion gases, the cooling air, and the wall material which enter into the calculation depend on the temperature, and in large part also on the pressure, the four parameters raise up a great number of possible material variables. Thus such a heat exchange computation can be solved only by iteration.

In spite of some problems it was possible to establish temperature- and pressure-dependent state curves for materials up to the most extreme values, and to enter these as polynomials into the computer. This was able, at each iteration step, to read out the newly appearing material value by interpolation from the "curves". Only with this supplementary program could the computation time be held within acceptable limits.

3.3 "Chamber Conditions" of the Fuel

The computer program described in 3.1 and 3.2 led, in a Mach number, mixture richness, fuel temperature ratio space, for H = constant, to equipotential surfaces which describe possible "chamber conditions" (Figure 9). The dimensionless fuel temperature ratios, t''_{11}/t_{cr}, are shown for the flight altitudes of 0 km and 4 km. In this set of altitudes, these surfaces are staggered from below upward.

This was not foreseen originally. It was expected, rather, that the fuel would be heated less at 4 km altitude because of its lower initial temperature and the more intense cooling of the outer cowling. But because the fuel flow is less at higher altitude, due to the better efficiency of the engine, so that the specific heat input becomes greater, the staggering mentioned above takes place; the fuel temperatures are greater at higher altitude. /43

Within the altitude surfaces, an increase in the mixture richness also causes higher fuel temperatures, because of the resulting higher combustion chamber temperatures. The rise in the incident flow velocity for the engine (Mach number) counteracts this tendency, however, primarily because of the greater fuel flow.

The diagram shown is for the jet orifice ratio $F_4/F_2 = 0.5$. As can be seen from Figure 10, variation of this design parameter does not significantly change the fuel temperature ratio t''_{11}/t_{kr}.

Figure 11 gives information on the amounts of heat exchanged and the fuel flow; Figure 12 on the parameters w_2, w_3, t_3, ϑ_3 and p_3; and Figure 13 on the thrust coefficient c_{sth} and the thrust S_{th}. In all cases these values are shown over the the mixture richness and peripheral velocity for the two altitudes 0 and 4 km. The percentage distribution of the amount of heat removed from the combustion chamber via the engine cowling is shown in Figure 14. More than 50% of this heat will be returned to the engine through the fuel, while the remainder is lost to the outside air. From this diagram it is also apparent that by insulation of the engine outer cowling still more heat could be added to the fuel with the same exchange surfaces.

4. EXPERIMENTAL RESULTS AND CONCLUSIONS FROM COMPUTER RESULTS

Experiments with the ramjet engine, as in Figure 33, on the system described in Chapter 5, have confirmed the usefulness of the theoretical assumptions and predeterminations of Chapters 2 and 3.

With the fuel temperatures attained at the end of heating, it is demonstrated that: liquid fuel can be heated sufficiently with the heat loss from a ramjet engine for blade-tip drive that after expansion in the injection jet it appears entirely in the vapor phase. The functional efficiency of such fuel prevaporization was demonstrated with these experiments.

4.1 Fuel Temperature and Pressure Along the Heating Section

Figures 15 and 16 (17 and 18) show the experimental measurements of temperature and pressure as a function of fuel consumption at measuring points I - V along the heating section. The peripheral air flow around the engine during measurement was nearly constant at 0.37 Ma. An acceleration of 540 g occurred. Three different jet orifice ratios, F_4/F_2, are shown as parameters in the diagrams.

At the actual fuel consumption, which was considerably above the theoretical, about 50% of the required final fuel temperature could be attained. The remaining 50% had to be provided from the secondary flameholder designed as a heat exchanger. On the average, the final temperatures at maximum fuel flow of about 90 kp/hr were about 320°C. The effect of the jet orifice ratio on the fuel temperature is not very great, as the calculation in 3.3 has also shown. On the other hand, small temperature differences at constant fuel flow also affect the related fuel pressure. Because the higher the temperature and thus the specific volume, the higher must be /45
the corresponding pressure in order to obtain the same flow at constant fuel

jet openings. This temperature-pressure dependence was determined from the fuel flow control used. Because the fuel valve is ahead of the rotor, the pressure is a function of the rate of rotation and the fuel column in the rotor.

It can also be seen from the diagrams that the pressure drop in the heat exchanger system is slight. On the average, it was only about twelve percent, in spite of effective throttling points caused by flow reversal. This absolute loss is without great importance, however, with the pressure levels which are available, and is not dependent on the pressure level. The pressure drop calculation, detemined by consideration of the effects of tube flow, heat addition, centrifugal force, and throttling points was confirmed very well by the pressure measurements. These measurements were made under extreme conditions. It was also confirmed that there is no need at all to fear limitation of heat uptake ability in the heat exchange tube due to attainment of the local sonic velocity in the flowing fuel /9, 10/. Under the most extreme conditions, maximum fuel flow and maximal heat addition, with an input velocity of 3 m/s the velocity ahead of the injection jet was still not as high as 8 m/s. Only in the jet orifices did the local sonic velocity of 165 m/s appear, limiting the capacity of the orifices; that is, the maximal flow was reached.

4.2 Evaluation of Fuel Prevaporization in the Vapor Pressure Diagram

In the vapor pressure diagram explained in 2.4 the conditions in fuel prevaporization can be studied intensively, and their development can be followed clearly. Such a diagram for the standard automobile gasoline used in the tests is shown in Figure 19. The course of heating /46
is shown for the measuring points I - V for the three fuel flows, corresponding to the experimental results. At measuring point I ahead of the injection jet the final temperature has been reached, from which the discharge leads to a counterpressure. Depending on the operating conditions, this is between 0.5 and 1.5 atm. abs. Let us consider first the case of maximum fuel flow of 90 kp/hr (line a) with a final temperature of 315°C and a pressure of 57 kp/cm^2.

As already mentioned in 2.5, it is not practical for this investigation to determine the actual expansion course. It is better, as done here, to establish the possible range of expansion conditions through the isentropy and if necessary, also by the isenthalpy. The course of these limiting curves was determined from the corresponding state diagrams in Figures 4 and 5. These curves, which diverge at right angles in the enthalpy-entropy diagram, are here first close together, and then diverge, enclosing a wedge. Now the actual expansion curve lies within this wedge, depending on the shape of the injection jet. The plotted isentropy, which in this pT diagram on a distorted scale (abscissa 1/T, ordinate log p) similarly follows nearly a straight line, crosses only the hot vapor region while coming out from the supercritical region. Thus the hot vapor phase is ensured for the expanding fuel, because the actual expansion curve must in every case fall to the right of this adiabatic curve. The isentropy can thus be considered as if it were a "criterion with certainty" for the vaporization process. In the second case also (line b), with a flow of 75 kp/hr and the final state $t = 290^{\circ}C$, $p = 44$ kp/cm^2, the behavior is much the same.

In the last case (line c) the heating is at subcritical pressure, and the fuel state passes through the two-phase region below the critical point. There the liquid and gaseous aggregate condition appears simultaneously, with differing chemical compositions. The saturated vapor states of individual hydrocarbon homologs are also present. /47

Because we made for this study the simplifying assumption that we would treat this gasoline as if it were a single material, with its phase diagram based on the mean molar boiling temperature, these saturated vapor states in the present diagram lie on the line of the mean molar boiling temperature.

The final state of this heating process is no longer in the supercritical, but still in the superheated vapor region, which the expansion curve of ordinary hydrocarbon fuels cannot leave.

If the heating process passes entirely through the two-phase region, so that only hot vapor is present ahead of the injection jet, no significant problems are to be expected in the operation of the ramjet engine. If, on the other hand, this process ends in the two-phase region, then a flame-out cannot be prevented. If bubble boiling occurs, the individual vapor bubbles are pushed together by the centrifugal force into larger vapor bubbles filling the entire cross section of the channel. These grow still more at the end of the heating. Now if the injection jet is "loaded" alternately by liquid and gaseous aggregates, the irregular fuel supply immediately extinguishes the engine. This condition has made the use of the engine in these tests considerably more difficult. More about this appears in 4.5.

At higher Mach numbers, the fuel pressure increases automatically in rotor operation. In our example, that means a new position of the initial point for expansion, and thus for the other expansion conditions. Also, the chances for complete vaporization become poorer with increasing pressure (see also 2.6). It might therefore be appropriate to reduce /48 excessively high pressures by a built-in throttle.

With the present circulation conditions, increase of the peripheral velocity to Ma = 0.65 brings with it a pressure of 180 kp/cm^2. Now if one follows the isentropic expansion curve from this new pressure, with the temperature assumed to be the same, then for the first case, which previously ran without any problem into the hot vapor region and which is now designated as a', we have a completely new situation.

The isentropy curve enters the two-phase region quite near the critical point, running down the line of the mean molar boiling temperature until it reaches the lower limiting curve of the saturated vapor region (see also Figure 4). From there on it would, with the supposed single material, again appear in the hot vapor region. Actually, however, it reaches that area only after first passing over the dew line.

In the next case (b') the conditions become still worse. The isentropic expansion ends in the two-phase region. But since the actual expansion runs to the right of that line, the hot vapor condition could still be attained. At the least, the expansion curve arrives at that part of the two-phase region in which only a slight portion of the extremely high boiling components are still not vaporized. The third case (c') no longer escapes from the central part of the two-phase region.

To study fuel vaporization under flight conditions, the computer results of 3.3 were likewise converted into a vapor pressure diagram (Figure 20). The fuel n-octane, on which the calculation is based, is thus exchanged for the test gasoline. This mental manipulation can be made readily, because the two fuels have similar physical behavior and the investigation is primarily directed toward qualitative results. In this diagram, the significant scattering of the "chamber conditions" of the fuel, due to the operating parameters, is clearly expressed.

Contrary to the temporary assumption in Figure 19, the computer result here shows that with increase of the peripherical velocity there is not only a pressure increase, but a simultaneous decrease in the fuel temperature ahead of the injection nozzle. That is, the starting point for expansion in the prevaporization process becomes less favorable with increasing Mach number, not only through the increase in fuel pressure, but also through less heating of the fuel.

The temperatures reached in the current example are entirely enough to provide one hundred percent fuel vaporization at the mixture richnesses of $m = 0.7$ to 1.0 which primarily occur in "cruising operation", at any flight altitude and at any Mach number. With lower richnesses of the mixture and higher peripheral velocities, one arrives at the two-phase region after expansion. Because this is a case of partial load, of of relatively short duration, such as starting, idling, etc., vaporization which is only partial can be accepted, especially as there is a chance

that the residue will be decreased on the way to and in the combustion chamber.

On the other hand, it is more important that under partial load conditions the "chamber condition" does not end in the two-phase region. As discussed above, this would lead to significant perturbations in operation. This "free side product" of rotor operation, the fuel pressure, is favorable in this case. For very large rotors, which run with correspondingly low rates of rotation, this could be inadequate.

4.3 Engine Size and Fuel Heating

If we vary the size of a ramjet engine while maintaining the geometric proportions, the thrust changes in the same degree, as does the fuel consumption. Thus we may accept the simplifying, theoretically correct assumption of constant thrust coefficient. But for this consideration it can also be said, with sufficient accuracy, that the amounts of heat transferred change in the same degree. For the heating process, this means that the fuel temperature will remain the same, within certain limits, independent of the engine size. If one wishes to increase the fuel temperature, he must increase the heat exchange surface, and must therefore increase the specific length. /50

4.4 Liquid Fuels and Their Suitability for Prevaporization in the Ramjet Engine

The maximum fuel temperatures attained with the test engine are about 350°C. With some improvements these could be raised to 380 - 400°C. Lengthening the engine would provide a further temperature increase; but since it would make the engine more slender, it is not acceptable for a blade tip engine on grounds of strength and aerodynamic stability. Therefore a maximum fuel temperature of only about 400°C can be attained in rotor operation.

Considering the fuel temperature range determined in 3.3 and required for flight, and the discussions in 4.2, it becomes clear that the critical temperature of the fuel to be used must not be much below 300°C. Thus the liquid fuels which can be considered for a blade-tip ramjet engine with fuel prevaporization are, as can be seen from Figure 2, primarily automobile and aviation gasoline and perhaps also the turbine fuel JP 4. Fuels of more diesel-like character such as JP 1 and JP 5 are not usable, except perhaps for stationary rotors.

Along with the thermodynamic bahavior, the chemical behavior of the fuels in prevaporization must also be considered. It had been feared that cracking might produce low-volatility components and solid carbon particles in the heat exchange channels. Actually, even after long test /51
operation, extremely thin, anthracite-black deposits of solid carbon particles and lead could be detected in the heat exchange tube of the secondary flameholder, which was heavily loaded thermally. No viscous liquid deposits formed. To the contrary, the surfaces of the channels in the engine cowling, which had been copper-plated for manufacturing reasons, remained completely clean up to the connection of the succeeding exchange spiral. The deposits appeared only from that point onward. Before and in the injection nozzle they took on a whitish grey color. In 4.6 there is a report on their effect on operation of the engine.

Presumably the less volatile fuels (JP 1, JP 4, and JP 5) form more deposits. This is one more reason why they are not particularly well suited for prevaporization in a ramjet engine.

4.5 Effect of the Fuel Prevaporization on Combustion Chamber Temperature, Fuel Combustion and Engine Thrust

The combustion chamber temperature at cross section 3 of the ramjet engine is shown in Figure 21 as a function of the fuel flow. The measurements were carried out for two versions of the engine: first for the engine with fuel prevaporization as in Figure 33 and second for the engine of Figure 32, in which the fuel had to be used for cover cooling

(cooling of the brazing) and was thus prewarmed (see also Figures 17 and 18).

Comparison of the combustion chamber temperatures at the various jet orifice ratios shows that the temperatures are significantly higher (11.5 - 13.5%) with prevaporization than without. They also climb steadily with increasing fuel consumption, while they remain nearly constant with the other engine.

Result: With prevaporization, as with gaseous fuels, the preparation time can be shortened, and better and more timely combustion attained. In the engine without prevaporization (only prewarming) a considerable portion of the fuel burned only after leaving the engine. This is also the cause of the constant temperature of the combustion chamber in this case. /52

These observations are reflected in the exhaust jet of the two engine versions. This is shown in the pictures made during night tests, presented in Figure 25. The flame pictures without prevaporization are in the left column, and those with prevaporization in the right column. The exposure time was the same for all photographs, 15 seconds at aperture 8. In one case, the background is shown, because the two nights were of different brightness. The fuel flow increases from top to bottom.

The exhaust jet may be described as follows:

a) Flame picture without fuel prevaporization

Iris-blue flame with a core about 2 - 3 cm thick glowing yellow. Flame edges very frayed with hooks bent forward and bright yellow glowing flecks, the size and frequency of which increases with the fuel flow.

b) Flame picture with fuel prevaporization

Iris-blue flame with dark blue, weakly glowing core the size of the nozzle exit. Edges also strongly frayed with cumulus-like edges and individual eruptions glowing bright yellow. The intensity of the flame is less.

The flame pictures should be amplified by the following comments: Blue flames are designated as not glowing. As a rule, they indicate good combustion, having no significant incandescent radiation, but only gas radiation. This is infrared radiation from carbon dioxide and water vapor. /53

Generally, a yellow glow in a hydrocarbon flame occurs only if there is insufficient oxygen directly available and the gas exceeds the decomposition temperature of its hydrocarbon components without burning taking place. Therefore the combustion is generally more protracted in a glowing flame than in a non-luminous one. Its radiation, however, can be a multiple of the pure gas radiation.

With these facts in mind, therefore, the flame pictures also indicate more favorable combustion with fuel prevaporization.

Considering the thrust measurements in Figures 26 and 27, one might conclude from the result that the fuel prevaporization diminishes the thrust yield. The cause for this result, unexpected in view of the previous considerations, is to be sought not in the different fuel supply but in the different shapes of the secondary flameholders in the two versions of the engine.

The secondary flameholder used for fuel heating in the engine of Figure 33, with its tubing coil and the additional supports against centrifugal force, obstructs the engine considerably more than the small conical flame holder of the other version (Figure 32). This

greater obstruction means greater internal resistance, which affects the thrust to an increased degree in such a small engine. The larger flameholder, and the lower velocity in the combustion chamber because of it naturally result in better combustion, so that the higher combustion chamber temperature and the more favorable flame picture cannot be ascribed solely to the vaporized fuel.

The less favorable secondary flameholder must not be interpreted as /54
a disadvantage of fuel prevaporization, because it is easily possible to have part of the heat exchange completed therein occur elsewhere. For example, the engine nozzle or the primary flameholder could be used. Insulation of the outside of the cowling would also have a very good effect on heating, as mentioned in 3.3. Also, increased fuel velocity in the exchange channels improves the heat transfer coefficient α via the Reynolds number Re; but changes in that respect could not be performed in the course of this work.

Of the thrust attained, it must be said that it does not represent the absolute optimum, since the engine in its rotation must work in an atmosphere contaminated by its exhaust. Some improvements for the engine are under discussion; they would also have a positive effect on the thrust.

It is interesting to compare the combustion chamber temperature curves with the thrust curves (Figures 21 and 26). The similarity of the curves in both engine versions clearly shows the theoretically based relation between the combustion chamber temperature, the jet velocity, and the thrust.

In Figures 28 and 29 the efficiency curves are recalculated to the CINA (Commission Internationale de Navigation Aérienne) conditions. The formulas used are contained in the table of abbreviations.

The curves presented in Figure 30 serve to determine the optimum jet orifice ratio. The experimental curves contradict the theory, which

predicts greater air flow and thus greater thrust with increasing orifice ratio. Discussion of the many-layered and not entirely comprehensible arguments would be too extensive here. /55

4.6 Control of the Fuel Supply

The fuel supply is regulated by a ball valve mounted on the mast holding the rotating arm. The valve can be remotely controlled from the control desk. Because the valve is upstream from the rotor, the fuel pressure at the engine is dependent on the rate of rotation of the rotor and on the fuel column present in the rotor.

This type of control gave several problems: Because the injection nozzle and its position with respect to the ignition spark were not well suited for starting, propane gas was introduced into the engine at an appropriate point for initial ignition. For the engine to start, the ignition had to occur at 180 RPM (u = 56 m/s) at the latest. If the fuel valve was opened at the beginning of combustion, the fuel flowed into the heat exchanger, which had been preheated by the propane flame. There it immediately began to vaporize, and the resulting vapor pressure forced the gasoline back into the rotor again until equilibrium between vapor pressure and external pressure was reached. Only as much gasoline as could be forced through the fuel jet in the form of vapor could flow. Furthermore, the entire liquid-vapor system began to oscillate, as the flowmeter float showed. Only rarely was the situation improved by an increase in the rate of rotation, because simply not enough gasoline was let into the rotor, and no corresponding outward pressure could be built up. In addition, the engine stopped at higher rotational rates because of insufficient fuel supply.

If gasoline was supplied to the engine even before ignition, it was possible to overcome the vapor pressure building up with combustion and to start the fuel flow. Now, since the outward pressure had not

yet reached the critical pressure, if bubble boiling started and the bubbles were not separated from the fuel injection jet, the engine died immediately, if the propane gas supply was cut off too soon. Cut off too late, the gas blowing in from the side distorted the flame so strongly that the engine again died.

The engine could only be started acceptably with the following procedure: The rotating arm was brought up to the speed at which ignition could occur. Then the fuel valve had to be opened completely, so that the line in the rotor was full of gasoline and the pressure was maximal. Only then was the engine ignited with propane gas. If combustion started, the rotation was quickly accelerated, so that the fuel reached the critical pressure as rapidly as possible. But the fuel supply must also be throttled, because otherwise the fuel supply would have been too high because of the increasing pressure, and the excess fuel would have killed the engine. Also during this time the propane gas had to be turned off again. Afterward, the control could be regulated up and down within certain limits, because the bubbles coming from the control valve condensed again with increasing pressure.

All these problems can be avoided if the fuel flow control is moved to the injection nozzle. Then at any control position the line in the rotor is full of fuel, and the pressure is only a function of the rotational rate (see Figure 23). With certain rotors, of course, the control can be omitted entirely and the size of the injection jet can be designed for a definite, constant operation.

As already discussed in 4.4, carbon and lead deposits appear as a whitish grey layer in the injection nozzle and of course in the line ahead of it, after long operation. These deposits can be removed easily by mechanical means. They cause a gradual "growth" of the fine orifices in the injection jet. In order to achieve the same fuel flow in spite of this, the valve must be opened further. But the maximum fuel flow becomes steadily smaller, because the local sonic velocity sets in earlier

due to the orifices becoming smaller.

This problem can also be counteracted with an appropriately designed regulatable injection jet. This could also take on the function of a starter jet, because propane can not be considered for practical use of such engines.

4.7 Effect of the Injection Jet on the Fuel Temperature

The effect of the injection jet on combustion and thus also on the fuel temperature can be seen from Figure 24. The measurements for this simple variation clearly show how important the design and arrangement of the jet are for combustion. A fine distribution over the entire fresh air stream is especially necessary for gaseous or prevaporized fuels. In this respect, liquid fuel in combination with turbulence nozzles are more advantageous. The individual fuel droplets, because of their greater mass and because of the centrifugal force, are much more exposed, which leads to far greater mixing than with gaseous fuels.

The form and position of the injection jets make up one of the most difficult problems for ramjet engines working under centrifugal force. Long development with many tests is necessary here in order to arrive at an optimum.

4.8 Distribution of the Combustion Gas Temperature Across the Combustion Chamber Cross Section

Calculation of the heat exchange presupposes knowledge of the wall temperatures in the combustion chamber.

Although the effect of centrifugal force on the thrust of ramjet engines has been investigated extensively elsewhere, primarily in America /11, 12/, no experience could be found on the distribution of the combustion gas temperatures across the combustion chamber cross section under centrifugal force. /58

Figure 22 shows the experimental values determined at section 3 of the ramjet engine, in the plane of the rotor. As expected, the maximum temperatures are displaced toward the outside wall in the direction of the centrifugal force. Even so, the strong temperature drop at the inside wall was surprising.

It is interesting to note how the temperature curve is reflected in the flame tracing on the inner wall of the engine nozzle. Deposition of combustion gas residues made this photograph possible.

5. EXPERIMENTAL EQUIPMENT /59

5.1 Ramjet Engine

5.1.1 General

When the engines needed for the tests were designed and built, only theoretical tables on supersonic ramjet engines were available /13/. Broader foundations could not be obtained either in or out of the country. The results which had been obtained up to this time were still subject to military secrecy. Thus the engine itself had to be developed, at some cost in time.

Aside from the central problem of fuel prevaporization, there were many far more difficult problems, the solutions of which were of decisive importance for the functioning of the engine; for example: design of the collecting diffusor, flameholding, ignition of the air-fuel mixture, development of the fuel injection jets, strength problems (due to the enormously high centrifugal forces), material problems, cross-sectional ratios for the intake, combustion chamber, and nozzle, and deviation of the actual engine parameters and efficiency values from the theoretical statements at hand.

Although the advantages of flat engines (oblong, oval cross section) for blade-tip drive were well known with respect to combustion technology, the development was carried out only for engines of circular cross section. This was because of manufacturing reasons.

The most important development stages are shown in Figure 31.

5.1.2 Engine Design

The engine developed and used for the experiments consisted of three components which joined together: collector diffusor, central section, nozzle (Figures 32, 33, and 35).

The dimensions and characteristic data are: outside diameter 130 mm; maximum length 500 mm; weight, about 4.5 kp. The theoretical gross thrust was 20 kp, and the attainable gross thrust about 15 kp (thrust coefficient $c_s = 0.75\ c_{sth}$). These values are for an incident flow velocity of 230 m/s at 0 km altitude and a mixture richness of $m = 1$. /60

Ramjets for rotor drive require a wide control range. Thus the diffusor used here is designed as a collector diffusor, which automatically adjusts for changed input conditions, so that it controls the proper area ratio F_1/F_2 of the undisturbed flow over a relatively wide range of variation. Considered strictly, it is built as an intermediate form of intake and collector diffusor, so that the dimensions can be kept smaller (see Figure below). The calculation is based on the experience of the NACA reported in reference /19/ (see also /14-18/).

The diffusor portion is composed of two rotational bodies of aluminum, turned from a solid piece.

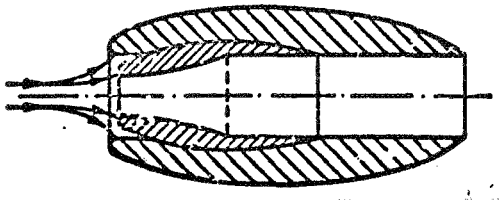

Comparison of a pure collector diffusor with a combined diffusor (intermediate form of intake and collector diffusor) at the same aerodynamic stress on the outer surface.

The cylindrical senter section of the engine consists of an inner and an outer cowling (material CK 35) with a total wall thickness of only 6 mm. In the inner cowling a helical slot has been milled 4 mm wide and 4 mm deep, with a pitch of 5 mm. The outer cowling, previously electroplated with a 20-micrometer layer of copper, was shrunk onto the inner one under a protective gas (Figure 34). After the shrink fitting both parts, likewise under a protective gas, were brazed in a box oven. Only after /61
that could the engine supports of 25CrMo4 be welded to the outer cowling. Several attempts to do this earlier failed. The double mantle did not seal because of the one-sided stress conditions during brazing.

The engine nozzle, with a circular arc contour, was pressed from deep-drawing sheet 1 mm thick.

The flameholders (Figures 36 and 37) required extensive and tedious experiments; they showed that the best results were obtained with two flameholder planes. The test engine has a star flameholder (material Nimonic 75), which is followed by a conical secondary flameholder. In the engine version of Figure 33, the secondary flameholder is designed as a heat exchanger.

5.2 Rotating Arm Test Stand

5.2.1 General

The ramjet engine was to be run under operating conditions. The rotating arm test stand appeared to be the most economical equipment for the purpose. An existing small rotating arm for helicopter model rotors was rebuilt into this configuration. In doing so, it was necessary to make allowances for many approaches which were not entirely satisfactory in view of the design (Figure 38).

5.2.2 Construction

The rotor of the rotating arm is composed of three parts: rotor central section, long rotor arm, and short rotor arm.

The rotor arms are of glass fiber plastic. This construction with glass fiber rovings was immediately obvious for the predominantly uniaxial stress field produced by centrifugal force (/20, 21, 22/). Because of the high strength of glass fiber, with respect to its weight, it was possible to build the rotor arms light and slender. /62

Two half-shells on a supporting Styrofoam core joined to make a rotor arm. The fuel supply at the ends of the arms was through loop gaskets as in the Hütter-Hänle procedure.

In order that the long rotor blade with a NACA 0014 profile could retain aerodynamic stability, it was necessary that the center of gravity, referred to the blade depth, be brought forward at least to the t/4 line. For this purpose a bare copper wire 9 mm thick was embedded in the leading edge of the blade for the full length of the blade. Similarly, both the fuel and measuring lines were moved as far forward in the blade as possible.

A center section of 25CrMo4 (Figure 39) at the outside flange of the long rotor arm is divisible in the horizontal plane. Here the engine is attached by means of a tongue and groove connection and four special shear screws. The balancing weight is screwed on to the short rotor arm. It houses an air brake, which allows loading the engine with known values of resistance (Figures 40 and 41). The center segment of the rotor (a turned and welded part of CK 35) is semi-gimbal mounted (see Figure 40). One degree of freedom, in the vertical direction, allows the rotor to be balanced statically without taking it off the tower. The other degree of freedom, in the horizontal plane, is necessary for the measurement of rotational moments with the pressure gauge mounted on the center section.

The rotor weight and the forces which appear in operation are carried on the tower head. This rests on a neck groove. It gets its power via three V-belts and a Borg-Warner free-wheeling mount from a 3.5 kW electric motor.

5.2.3 Technical Data /63

1. Dimensions
   Circular path of the engine R = 3 m
   Circular path of the balancing weight R = 1 m
   Rotor plane above ground 2.0 m

2. Rotor designed for u = 0.9 Ma $\hat{=}$ 300 m/second, with n = 955 RPM, ω = 100 1/s at a maximum engine weight of 5 kp.

3. Braking power of the air brake on the balancing weight, 30 mkp at n = 955 RPM; u_{brake} = 100 m/second. Actuation of the air brake by Rotax linear actuator A 0901/L. Normal actuation load 114 kp; maximum actuation load 180 kp; static load 450 kp.
   28 volt, 3.5 amp.; positioning speed 5.0 cm/7 seconds.

4. Electric drive motor N = 3.5 kW
   Power for running at n = 318 RPM, N = 3.36 kW. Peripheral velocity at the engine then u = 100 m/second.

5.3 Fuel System

The fuel system for the rotating arm test stand is designed for various test possibilities. Two types of fuel are introduced into the engine separately and simultaneously. This was intended for the use of liquid fuel (e. g., gasoline) and propane gas, a precaution which later proved extremely useful; only in this way could the problems of initial ignition by introduction of propane gas be eliminated.

The liquid fuel was forced from a standard commercial drum to the level of the rotor by excess pressure (produced with a hand pump). It passed through a cutoff valve, the fuel flow meter, and, on the tubular pole, a fine filter (Figure 42). Figure 44 shows the transition from the fixed /64
to the rotating part of the tower head, sealed with retaining rings.

The desired fuel flow was adjusted with a ball cock, which was fastened to the tower pole and remotely controlled from the control desk with a flexible cable.

The propane gas line ran parallel to the gasoline line. The gas, under a pressure of about 6 atm. (gauge), was taken from a bottle in the liquid phase. So that the large amounts needed would always be available without icing up the lines and fittings, the gas bottle was followed by an electrically heated vaporizer with with an output per liter of 24 kp/hr. The flow or pressure could be regulated as needed with two pressure reducing valves (Figure 43).

5.4 Ignition System

The quite difficult problem of starting the engine was solved with a high voltage spark system.

From a DC source, a low voltage line led through the ignition push-button to a Bosch vibrator ZS/VA 24/1 mounted on the tower head. It is supplied with 24 volts and provides a high voltage ignition current at about 15,000 volts. Transmission of the direct current to the rotating part of the tower head can be seen in Figure 44. The copper cable mentioned in 5.2.2, in the rotor leading edge, also serves to conduct the high voltage ignition current to the spark plug.

The special requirements of the ramjet engine slowed the development of a special spark plug (Figure 35). The Beru company took on this problem. The insulator required special attention, because there was no

experience indicating whether such an indicator would be strong enough under high acceleration. /65

The plug weighs only 7 grams. The unusual length of its center electrode is striking. It allows the experimental placement of the spark at different positions of the engine cross section, within a certain range.

As already mentioned in 5.1.2, the entire center part of the engine makes up a heat exchanger, so that the spark plug could be inserted only ahead of or behind the central section. The first possibility was chosen. It allowed placing the ignition spark in the stationary turbulence zone behind the flameholder, where the flow velocity of the air-fuel mixture is small or even zero /23/. Because the chemical reaction for production of a flame requires a certain residence time for the air-fuel mixture, such zones form the best provision for ignition. They are also the reason that the flameholder is able to maintain the flame in the combustion space.

If the cold engine is started, the fuel leaves the injection jet, which is designed for vaporizing operation, in the liquid form, because heat exchange has not yet taken place. The expanding fuel jet is at first in large drops. It mixes very poorly with the fresh air, and makes the initial ignition considerably more difficult. In order to avoid this problem without extensive starting jet development, propane gas was used for the initial ignition. Once the air-fuel mixture is ignited, it continues to burn spontaneously. The spark need not be maintained for the entire burning time.

5.5 Control and Monitoring System

A multilayer protective shield separates the control desk from the rotating arm test stand.

The electrical monitoring and control equipment is collected at the left side of the control desk. The fuel control system is to the right, on and beside the desk (Figure 42).

A linear potentiometer, driven by the air brake positioning motor, provides voltage division dependent on the position. This is read out by a voltmeter having an indicator which passes through an angle of 90°, according to the leaves of the air brake. The potentiometer is supplied through the measuring slip ring (Figure 46) from a 12 volt DC source. /66

The positioning motor is controlled with two push-buttons, one each for "open" and "close". The necessary sliprings are in the tower head (Figure 44). The positioning speed, or the time for full extension, is 7 seconds at 28 volts supply.

The time can be increased, slowing the positioning, by lowering the voltage (at most 13 volts).

5.6 Centrifugal Test Stand for Miniature Pressure Gauges

The extreme conditions under which the fuel pressure measurement at the engine must be made required the development of miniature pressure gauges, as explained in 6.5.1. They are designated briefly as MD gauges.

The effect of centrifugal force on these transducers and on their reading could be studied by means of a 6kW test stand built for the purpose. It allowed exposure of the MD gauges to a maximum acceleration of 5,000 g. Figures 61 and 62 show the construction of the test stand and the positioning of the "samples".

A steel tube, connected to the MD gauge, is inset into the front of the long rotor portion. This tube can be filled with liquids of different specific gravity. At the MD gauge, these produce a pressure which depends on the centrifugal force and which can be calculated

exactly. The effect of a definite acceleration on the statically calibrated MD gauge can be determined from the difference between the calculated and indicated values. Alcohol (γ = 0.7894 kp/dm^3) and manometer sealing liquids (bromides) (γ = 1.0; 1.5; 2.0; 2.5; and 3.0 kp/dm^3). It is possible to obtain different pressures at the same rotational rate for the rotor. /67

A magnetic inductive pickup reads the rate of rotation from a disc fitted with six permanent magnets, and indicates it on an electronic frequency counter. A carrier-frequency measuring bridge indicates the strain in the two MD gauge membranes. Unbalance of a Wheatstone bridge is also used. Rate of rotation and strain are then printed simultaneously by a printer (Figure 61).

6. MEASURING TECHNIQUE

/68

6.1 Fuel Flow Measurement

The fuel flow is indicated by a flowmeter working on the floating element principle (Figure 43). A scale of percentage of the maximum fuel flow is engraved on the replacable measuring tube. The true flow can be read from a calibration curve which depends on the material characteristics.

6.2 Rotational Rate Measurement

The rate of rotation for the spinning-arm rotor was determined in two ways: with a photoelectric tachometer for running surveillance at the control desk, and with a magnetic-inductively controlled frequency counter for the measuring and recording system.

The impulses required for both measurements of rotational rate come from an aluminum ring screwed to the turntable at the tower head. This ring is divided by black segments into 100 light-dark fields, and is provided with 60 permanent magnets (Figure 45).

The magnetic inductive pickup, a coil with a soft iron core, feeds the impulses produced by the magnets into an electronic frequency counter. A Schmitt trigger connected between the two forms the sharp and not entirely well defined pulses from the pickup into square pulses which are then reliably read by the counter. A printer connected to the counter allows the rate of rotation to be printed out along with other experimental values of interest. (Figures 48, 49, and 50).

6.3 Thrust Measurement

The engine thrust was measured with deceleration tests. The moment for the entire rotor arm, which was needed for this measurement,

was determined experimentally (Figure 51). /69

Another measuring system provided a considerably more convenient determination of the rotational moment up to the maximum rate of rotation for the engine. An ordinary torsiometer could not be built in because of the shaft-less construction of the tower head. The path which was followed for the solution is shown in Figure 47. An inductive force gauge (measuring range 50 kp or 500 kp) is supported on the rotor center section, 100 mm from the center of rotation, in tension, to be sure, but replaceable. The rotor, which is movable about the vertical axis, can be adjusted over the force gauge with two adjusting screws on the rotatable tower head. Because the force gauge can be mounted in reverse, it is possible with this arrangement to transmit the reaction forces in both directions between the rotor arm and the working elements running with it through the gauge, and to measure them.

It is also possible to measure, up to the maximum drove speed, the turning moment of the rotor at any time. Thus its air resistance, as well as the braking force of the drive elements, can be determined. For determination of the effect of centrifugal force on the indication of the force gauge, it was mounted so that during acceleration of the arm it is free of transmission forces, and is subject only to centrifugal force. Together with the static calibration, performed on the arm with a rotary force meter, a corresponding calibration protocol for the rotational moment measuring system could be set up.

The signals from these pickups are recorded by a carrier-frequency measuring bridge, converted by an analog-digital converter, and printed out together with the related rotational rates. (Figures 48, 49, and 50).

A power meter was used for repeated checks of the thrust measurements. With it, the electrical power used by the drive motor could be determined exactly (Figure 54). From the power diagram of the motor, measured on a water-turbulence brake test stand, the power produced could be determined.

The values determined in this way confirmed the accuracy of the preceding measurements (Figure 52). /70

6.4 Temperature Measurement

Miniature sheathed thermocouples measure the temperatures at the ramjet engine (Figure 39). These elements, because of their good mechanical strength and the small dimensions of the temperature sensors, prove particularly useful at the prevailing high acceleration forces. Furthermore, their heat resistance and their complete insensitivity toward external influences such as pressure, humidity, and chemical corrosion satisfy the requirements.

Sheathed Chromel/Alumel thermocouples measure the fuel temperatures at the ramjet engine. The temperature response range of these elements extends from -200°C to +900°C (depending on the sheath material and diameter). In order to meet the requirements for measuring points, which were often changes at short notice, the mhermowire (1 mm thick) was obtained in lengths, and the individual leads welded together and sealed pressure-tight as needed. Figure 53 shows the measuring heads, designed as screw caps, with which the hard-brazed thermoelements can be introduced pressure-tight into the measuring points. The fuel temperature directly before its emergence from the injection jet was likewise measured with the temperature-measuring orifices illustrated in Figure 53.

At the end of the central part of the engine, a movable sheathed platinum-rhodium/platinum thermocouple can be introduced through a special screw fitting (Figures 39 and 53). It allows measurement of the combustion gas temperature and of the temperature profile across the inside diameter of the engine. The temperature response range of the thermocouple, sheathed with the material platinum + 10% rhodium, goes up to 1,400°C and for a short time to 1,600°C.

The thermal potentials are conducted through compensating lines and the measuring slip ring to the analog-digital converter. An electronic amplifier increases the potentials of the Chromel/Alumel thermocouples to the extent that the temperatures of the measuring points can be read on the visual indicator of the analog-digital converter, or printed out by the printer, directly in ^{o}C. However, the temperatures of the points with the platinum-rhodium/platinum thermocouple must be determined from the amplified and recorded potentials by means of the thermocouple calibration line. /71

For both elements, the temperature of the cold junction was also considered.

6.5 Fuel Pressure Measurement

6.5.1 General

Because of the position of the fuel pressure measuring points on the ramjet engine in a rotating system, only transducers, out of all the possibilities for pressure measurement, can be considered. They measure the fuel pressure (mechanical quantity) and produce electrical analog values. It is then relatively simple to transmit the electrical signal from the rotating system to the recording equipment.

The extreme conditions to which pressure measurements are subjected at the engine place unusual demands on the transducer:

a) Because of the limited possibilities for positioning within the engine connecting section, the maximum allowable dimensions are preset. The transducer must not be higher than 12 mm, and must not exceed 25 mm in diameter.

b) At a tip acceleration of up to 2000 g, the error indication should not be more than 2% of the measuring range. That is, per g it must not be

more than 0.001%. But these high accelerations are not shock impulses of a few milliseconds duration; rather, they act during the entire test run, and affect the transducer through the complete measurement. /72

c) Temperature changes such as occur during operation on the rotating arm must not affect the measurements.

d) The transducer must be compact, rigid, and light, so that its mechanical stress and deformation will remain within limits.

e) The pickup should be simple, reliable, and universally attachable.

These requirements made up the criterion against which the offerings of firms in and out of the country were tested, and the possibility of using their transducers were investigated. But none of the pickups offered satisfied the requirements.(1)

There was neither time nor money to commission a special development. Thus our own transducer was developed within a few weeks. It met the specific requirements completely, without containing measuring electronics which were particularly complex and difficult with respect to material and production. It could be produced with the means at hand.

The result of this development is shown in Figure 55. It is a miniature pressure gauge (MD gauge). The paper clip beside it serves for size comparison. Independent of the pressure range, the outside dimensions are: height, 11 mm; diameter, 24 mm. The weight is only 26 g.

---

(1) Not until a year later did an American company market subminiature gauges with semiconductor strain gauges as the measuring elements, at a price of DM 2,000 - DM 3,000.

6.5.2 Measuring Principle /73

The measuring principle of the MD gauge is based on the elastic deformation of a solidly clamped membrane by the force $K = \Delta p \cdot F$ (Δp = pressure difference at the membrane surface F).

6.5.3 Construction

The transducer is designed as a double membrane, because the slight elastic deformation of a single membrane would have given too small an output and because, as is shown in 6.5.5, a full bridge circuit was necessary. The construction of the MD gauge can be seen from Figure 55. It is made of two parts (material 16MnCr5), into each of which a membrane is screwed. These membrane-carrying rings are brazed together, pressure-tight, under a protective gas. The gauge housing so formed receives considerable rigidity because of the relatively strong wall. The pressure medium is conducted into the interior of the gauge through a section of tubing, which is also brazed in place. Two disks permanently close off the spaces with the measuring elements outside the membranes. In the outer housing of the MD gauge, two slots are provided, each of which accepts a steel wire with which the gauge is fastened at the measuring position.

6.5.4 Measuring Element

A strain gauge is glued to the outer center of each membrane of the MD gauge. It stretches, as soon as mechanical forces (liquid or gas pressure) act on the membrane (active strain gauges). Two more strain gauges are applied to the inside of the two gauge covers (Figure 55). The covers are of the same material as the membranes, so that with the same temperature of cover and membrane, the gauges are exposed to the same temperature as at the measuring position. Because they have the same temperature curve (resistance change of the strain gauge itself as a function of temperature), they are used for compensation (compensation strain gauges or passive strain gauges). /74

The four active and passive strain gauges are connected in a full Wheatstone bridge circuit (Figure 55). In this bridge circuit, the effects of the diagonally opposite resistances add, while the effects of adjacent resistances counteract each other. This is used in the MD gauge to increase the output signal and to compensate for the temperature effect. With the full bridge circuit it is also possible to lead the measuring signal through the slip ring without distortion.

Experiments with other bridge circuits were entirely unsatisfactory.

6.5.5 Static Calibration

Static calibration of the MD gauges was performed by means of the control desk of a strength testing machine and of the pendelum dynamometer built in for force measurement. The pressure was applied in steps to the MD gauge, and the stretch read out with a carrier frequency measuring bridge.

The static calibration curves of the MD gauges are shown in Figures 56 and 57.

6.5.6 Dynamic Calibration

Basically, the MD gauges were tested on the centrifugal test stand described in 5.6, with and without pressure loading. The effect of centrifugal force on the MD gauges was studied first without pressure loading. The test was extended up to 5,000 g. At this extreme peak load no indication of mechanical or electrical limits was detected.

The stretch values recorded up to 2,000 g, shown in Figures 56 and 57 as functions of the acceleration, show strong hysteresis between acceleration /75
and runout, but the greatest stretches indicated are very slight. The maximum error was 1% of full scale, or 0.0005% per g. With pressure loading, the deviations of the stretches from the static calibration were significantly stronger, because the effect of the centrifugal force on the

membrane which is bulged out by the applied pressure, and so also on the deformed strain gauges, is considerably greater than on a plane membrane and a non-deformed strain gauge. This deviation from the static calibration increases linearly with increasing pressure (Figures 56 and 57).

It was surprising to find that with increasing acceleration the difference between the static and dynamic calibrations decreased. This phenomenon can be clarified as follows: with increasing mechanical stress in the plane of the strips, the strain gauges connected in the full bridge "harden" because of the deformation caused by the centrifugal forces. Thus the error of the full bridge becomes smaller with increasing centrifugal force.

In order to obtain information on the effect of the orientation of the grid of the strain gauge with respect to the stress direction in the plane of the strain gauge on the deformation of the gauges by centrifugal force, also in the plane of the gauges, two strain gauges (active gauges) were applied to the top and bottom of a round metal sheet, in the same direction. The two compensation gauges were placed on a separate piece of metal in such a way that the centrifugal force acted perpendicularly to the plane of the gauge and so caused no deformation of the measuring grid. This arrangement allowed investigation of the effect mentioned above on the centrifugal test stand (Figure 62). The disc with the active gauges was rotated between 0° and 90° during the test, while the metal piece with the compensating gauges stayed in the same position. The result of this study is shown in Figures 59 and 60.

The effect of time under stress was also measured with the system described. This study showed that the indicated extension remained constant during the time necessary for the later tests. /76

These MD gauges were developed in a very short time and could still be improved in many details, but they have proved very good at this stage of development.

7. SUMMARY

/77

This work was a theoretical and experimental investigation on the problem of using liquid hydrocarbon fuels for relatively short blade-tip ramjet engines.

By means of fuel phase diagrams it was possible to show various paths for hot vapor production, with their advantages and disadvantages. Heating at supercritical conditions appeared to be the most advantageous type, although in this case the greatest amount of heat must be exchanged. Heating under subcritical conditions can cause considerable difficulty because of vapor bubble formation, especially in starting.

Heat exchange calculations and experiments done under true-to-life conditions have confirmed that, by means of the heat loss of a short ramjet engine for blade tip drive, liquid fuel can be heated to the temperature region necessary for immediate, spontaneous and complete vaporization during the expansion process in the injection jet.

Hydrocarbons for which the entropy increases with increasing values of enthalpy or temperature on enthalpy-entropy or temperature-entropy diagrams are particularly well suited for this purpose.

The functional efficiency of such fuel prevaporization has been shown by experiments with a ramjet engine on a rotating arm test stand.

With the rather simply produced vapor pressure diagrams of liquid fuels, it is simple to judge whether and to what degree they are suitable for prevaporization. It is also possible to follow the heating and expansion curves in this diagram in relation to the aggregate condition, and from this to draw conclusions about the possible operating range.

/78

The automatically self-adjusting supercritical fuel pressure in rotor operation is very welcome for the prevaporization process. But as the

pressure increases further with increasing rate of rotation, the chance for complete vaporization drops to the same degree, because the enthalpy and entropy of the fuel decrease with increasing pressure.

Changed flight operating conditions produce a very significant scattering of the "chamber conditions" of the fuel before expansion in the injection jet. But the fuel temperatures attainable with a blade-tip ramjet engine are sufficient to produce complete fuel prevaporization for the usual long-term operating conditions. For part-load working conditions, which are usually of short duration, it is possible that only part of the fuel is prevaporized.

With increased mixture richness and flight altitude, the fuel temperature increases also. It decreases with increasing peripheral velocity of the engine. The effect of the jet orifice ratio on the fuel temperature is slight.

Only automobile and aviation gasoline can be considered as liquid fuels for this purpose, because the heat exchange capacity of a blade-tip ramjet engine is limited.

There need be no fear of viscous deposits due to cracking processes in the heat exchanger. However, very thin solid carbon and lead deposits can form in the heat exchanger channels and in the injection jets, which are under heavy thermal loading. Problems in the jets must be considered.

Combustion chamber temperature measurements and flame pictures show the favorable effect of prevaporization on combustion in the chamber. Efficiency measurements again brought to light the bad effect of internal obstruction on the thrust of such small engines.

The fuel control system used on the test stand, with the throttle valve upstream of the rotor, did not prove suitable in the experiments. Better results would be produced with a controllable injection jet. /79

Fuel temperature measurements with various injection jets showed that a fine distribution covering the whole fresh air stream is necessary, especially for gaseous fuels.

For the experimental technique, the fuel pressure measurement at the engine is particularly interesting. We developed our own miniature pressure gauges for the extreme conditions under centrifugal force. They were tested in a centrifugal test stand, with loads up to 5,000 g, and were entirely satisfactory with respect to strength and measuring electronics. They proved good in practical measuring operation.

The ramjet engine developed for the tests needs to be put into first class working order. It is the result of a year of work, which should be continued in several directions if the engine is to be perfected.

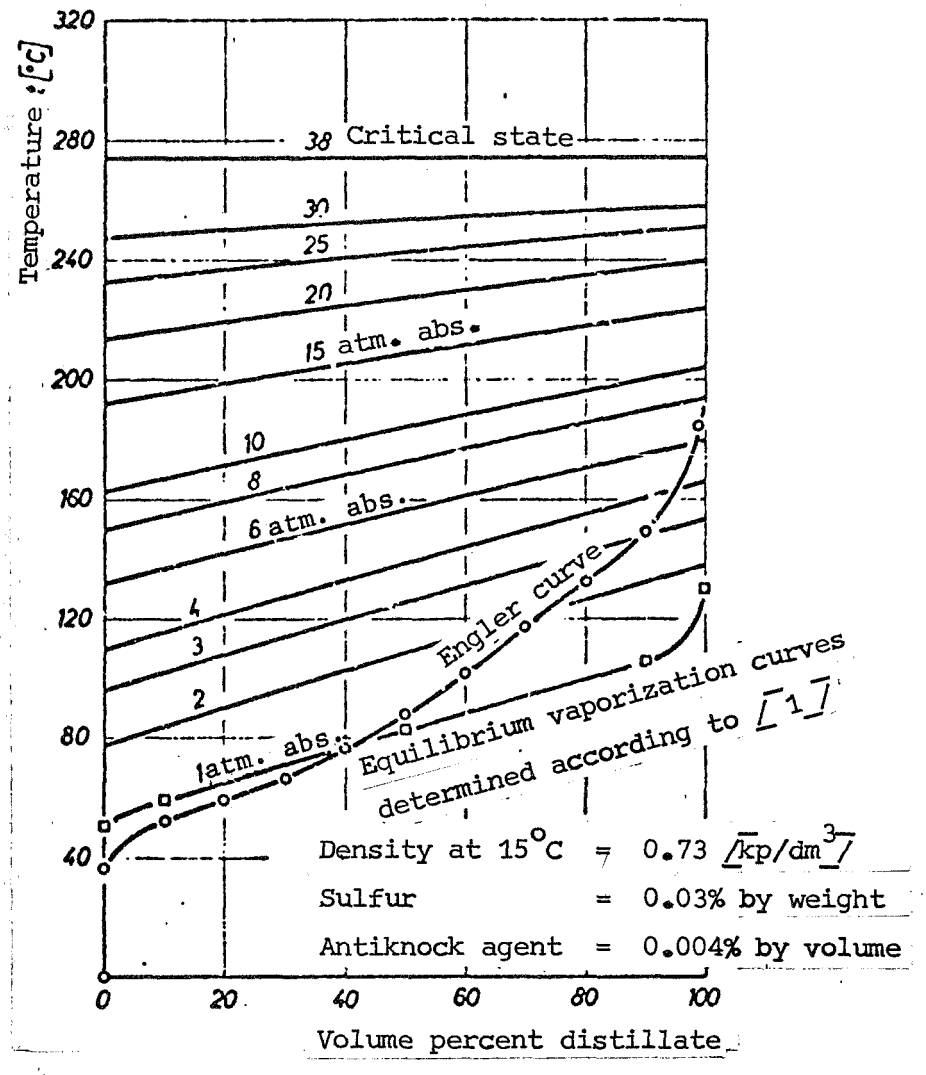

Figure 1. Distillation analysis according to Engler (ASTM) and equilibrium vaporization curves in a closed system at different pressures for the standard automobile gasoline used in the test runs.

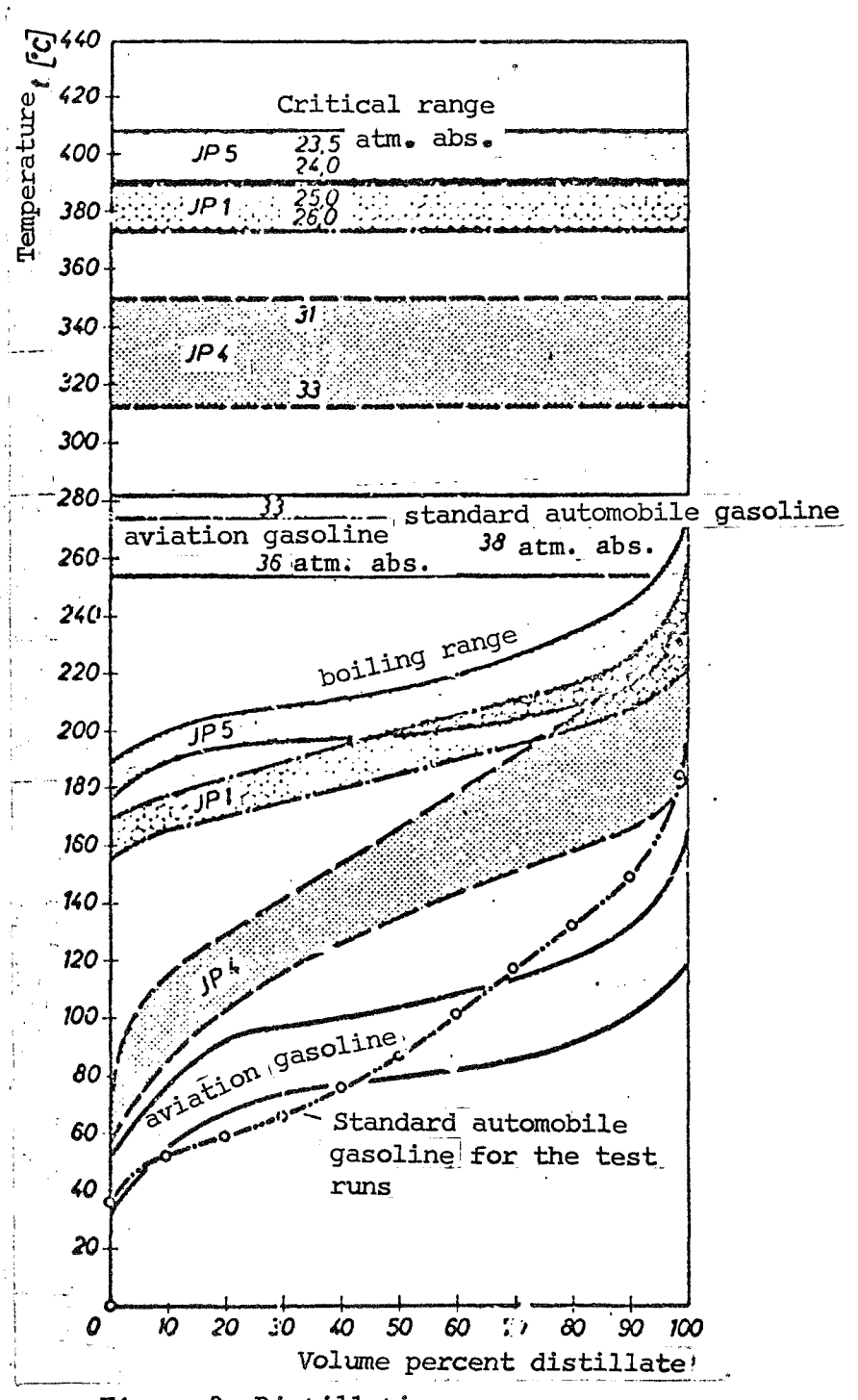

Figure 2. Distillation curve ranges and critical regions for aviation fuels.

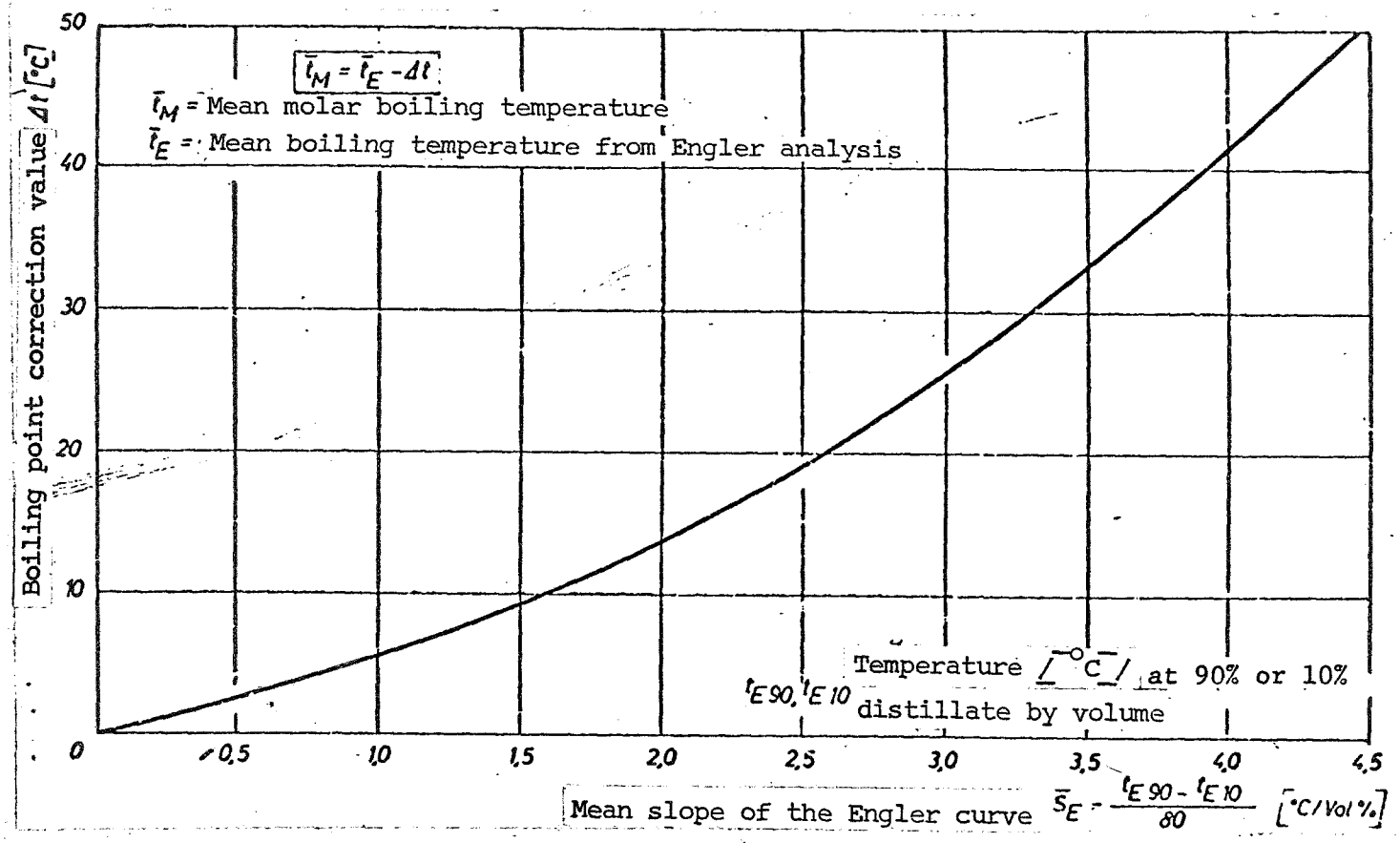

Figure 3. Diagram according to reference [1,2]. Determination of the mean molar boiling temperature $\bar{t}_m$ from the Engler (ASTM) distillation curve.

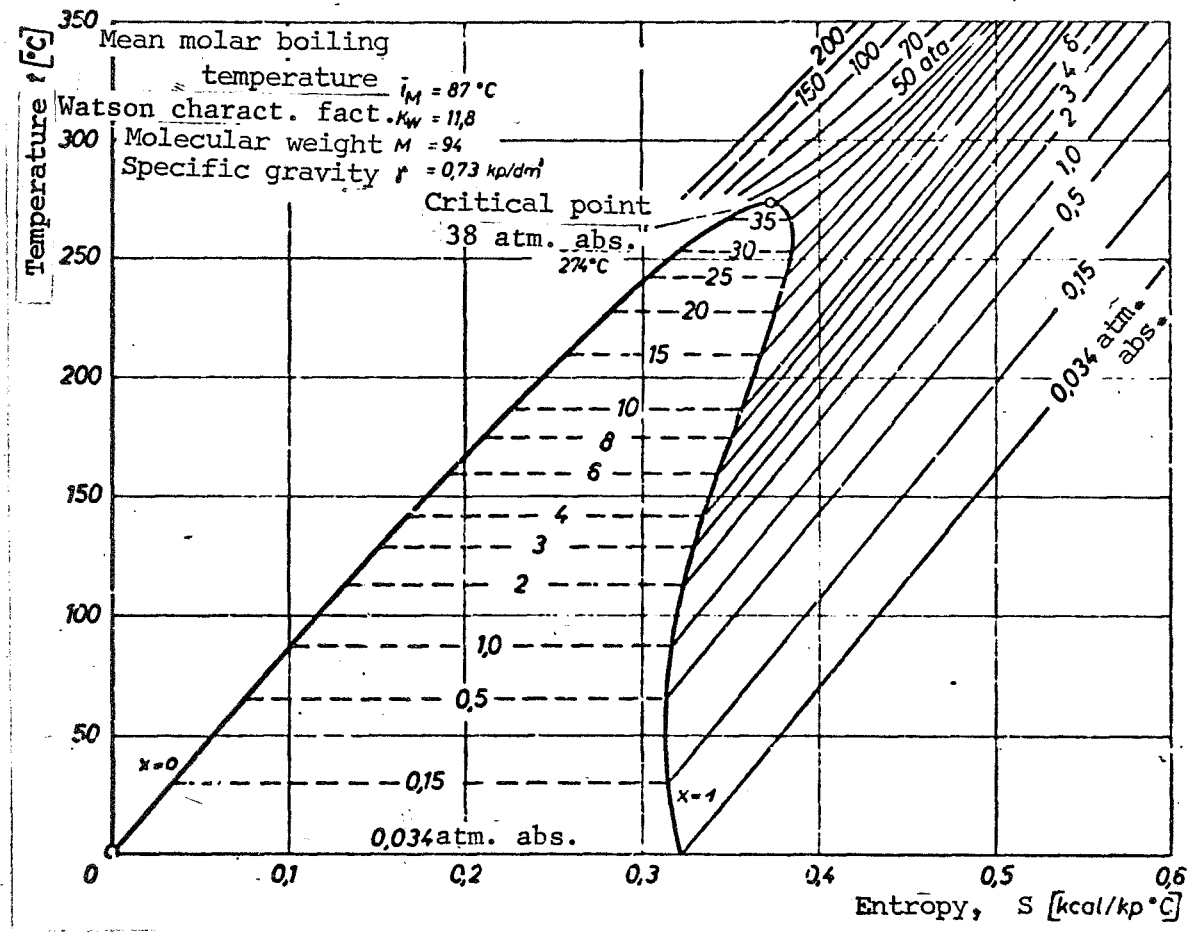

Figure 4. Temperature-entropy diagram for standard automobile gasoline, calculated for the mean molar boiling temperature.

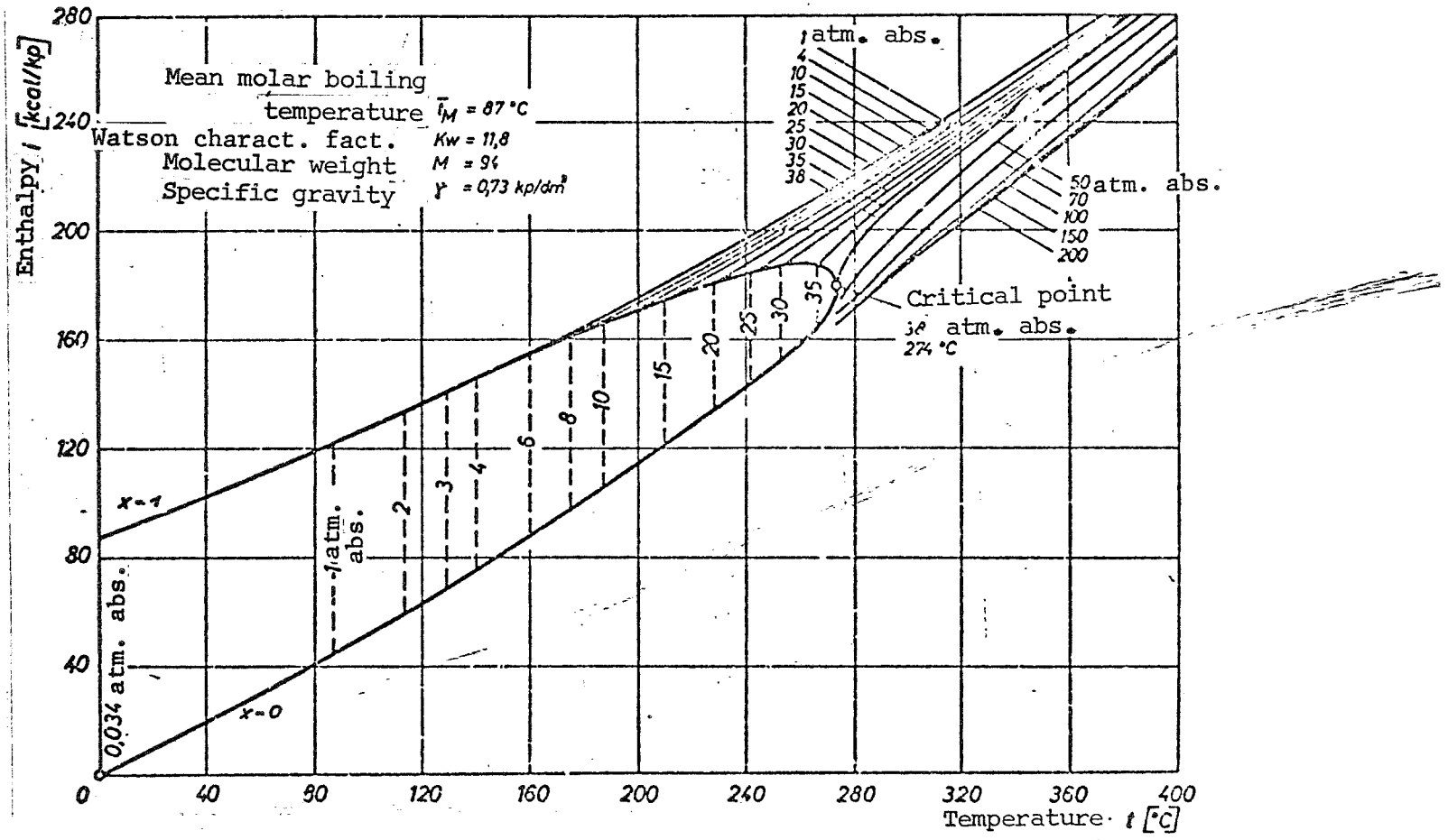

Figure 5. Enthalpy-temperature diagram of standard automobile gasoline, calculated for the mean molar boiling temperature.

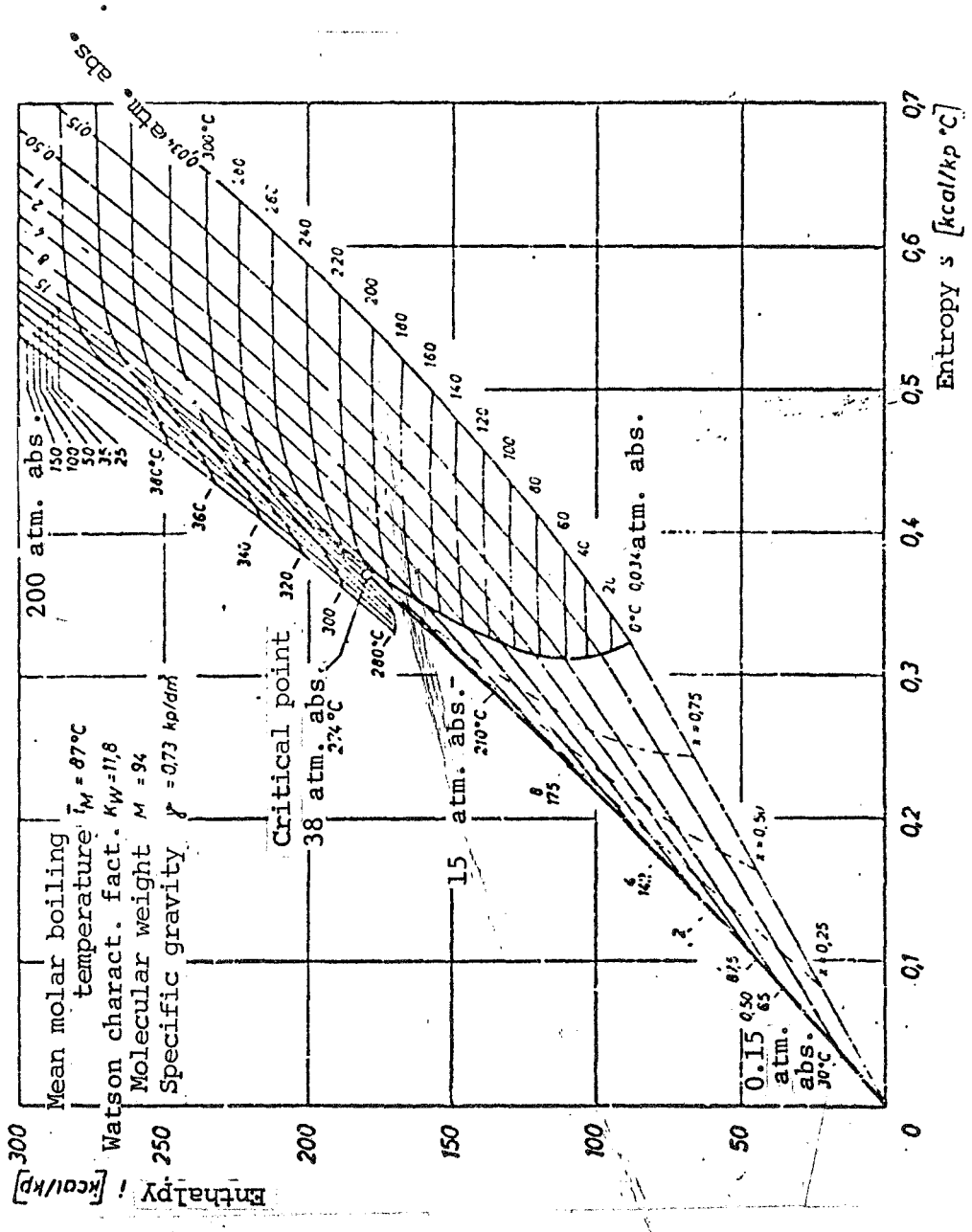

Figure 6. Mollier enthalpy-entropy diagram for standard automobile gasoline. Calculated for the mean molar boiling temperature.

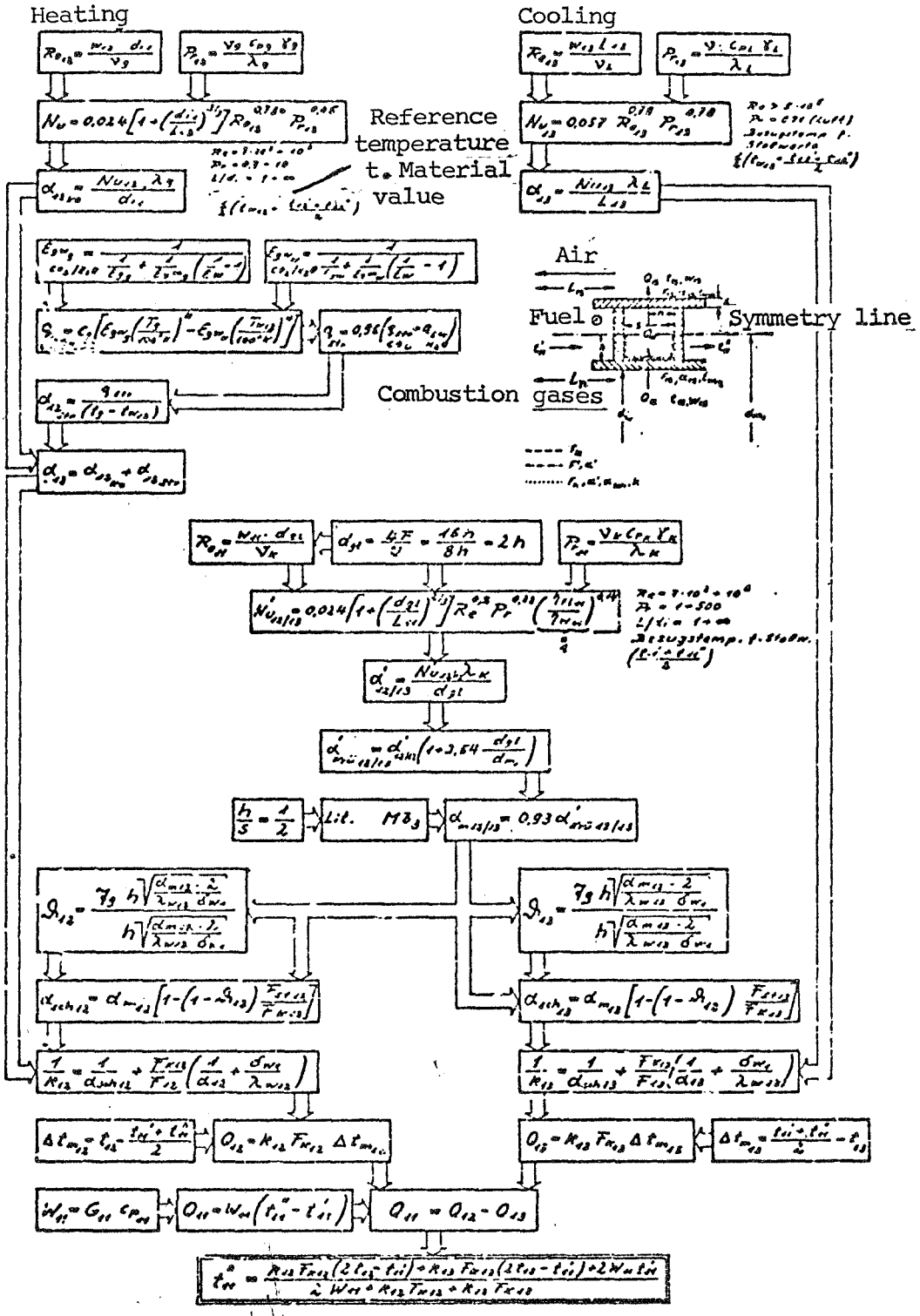

Figure 7. Flow diagram for heat exchange in the engine cowling.

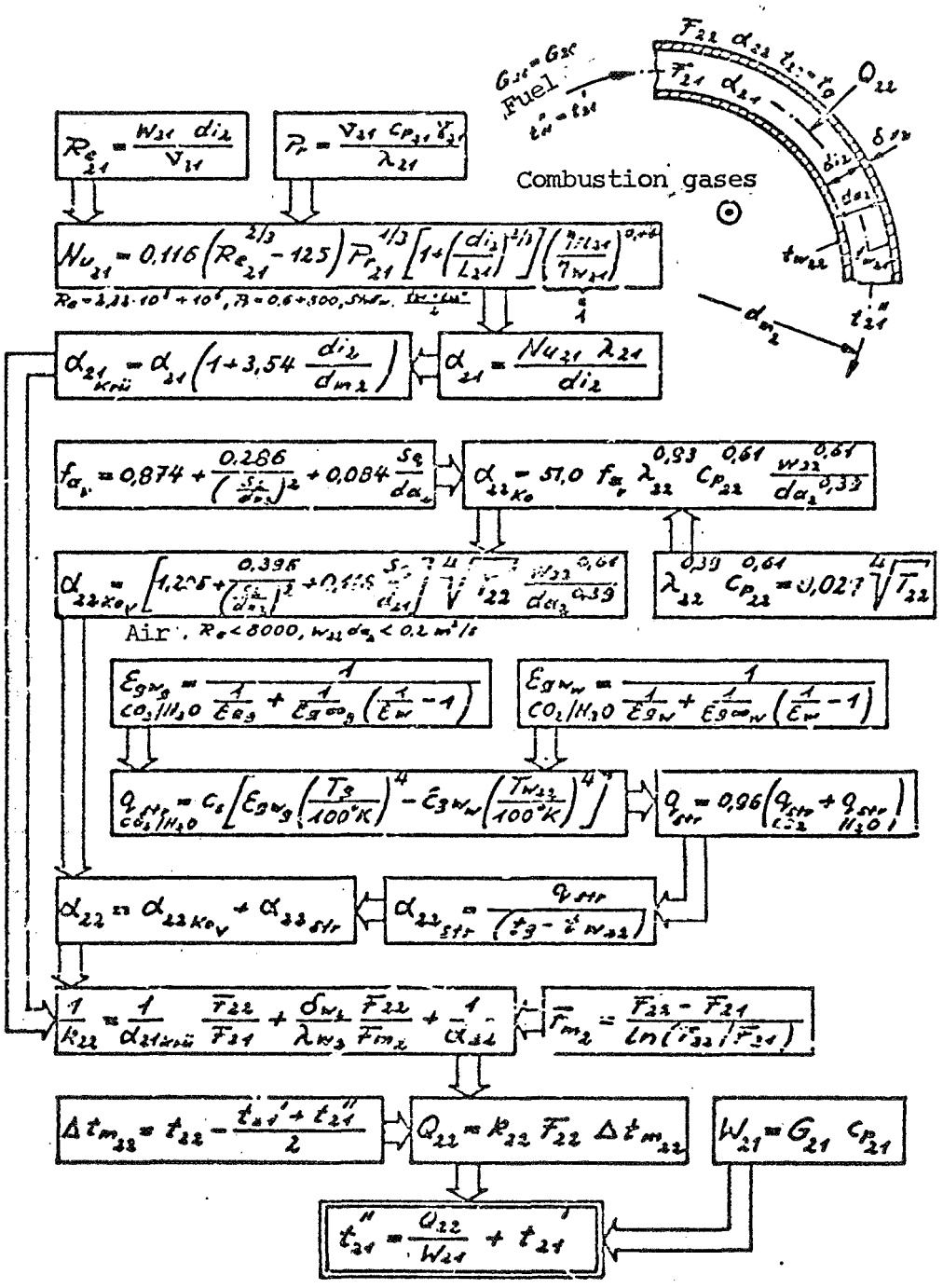

Figure 8. Flow diagram of the heat exchange in the secondary flameholder.

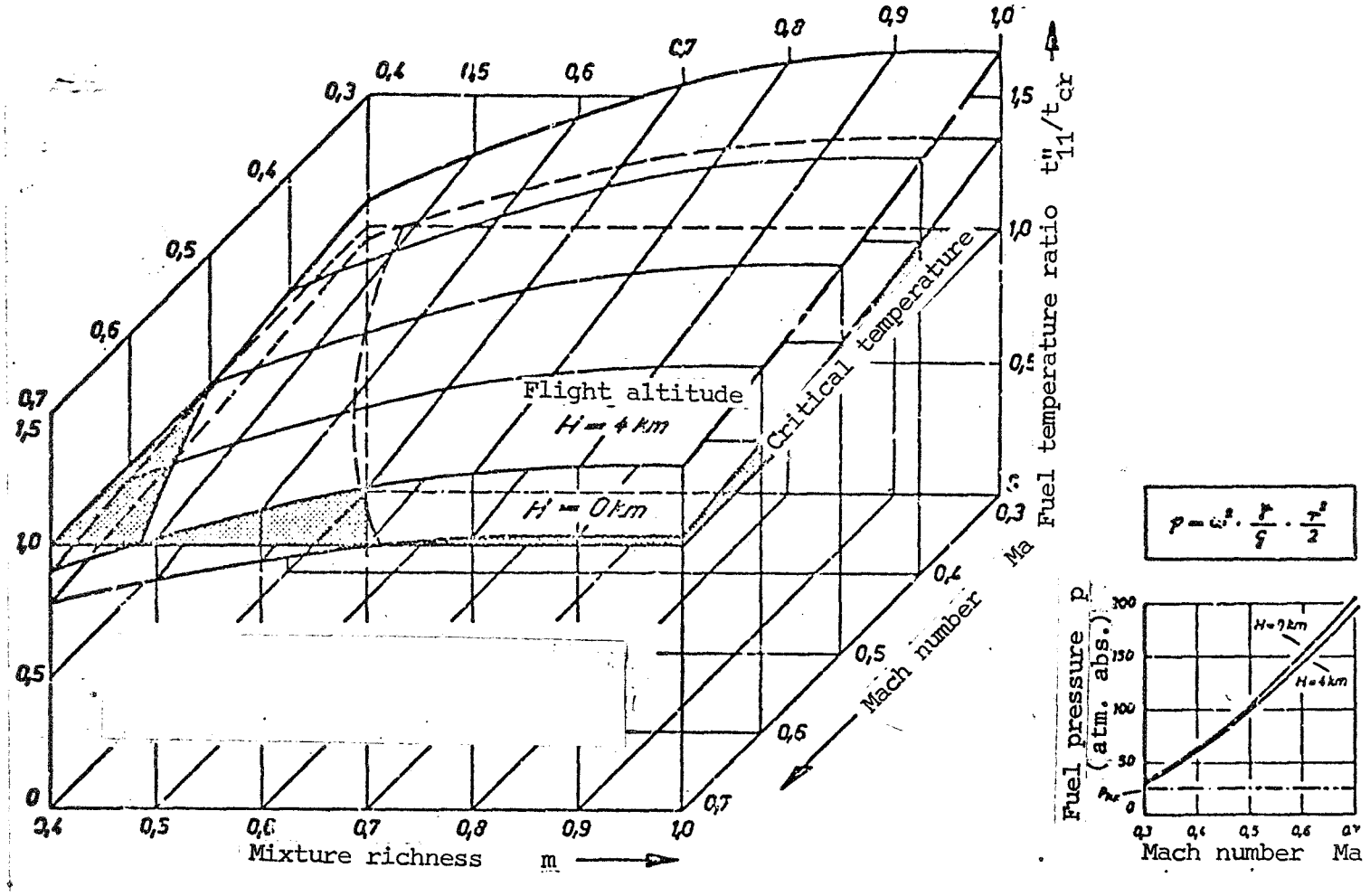

Figure 9. Fuel temperature ahead of the injection jet, t''_{11}, as a function of the mixture richness, incident flow velocity, and flight altitude. Calculated for n-octane (t_{cr} = 296°C). Rotor radius r = 3m, jet orifice ratio F_4/F_2 = 0.5; engine of Figure 32.

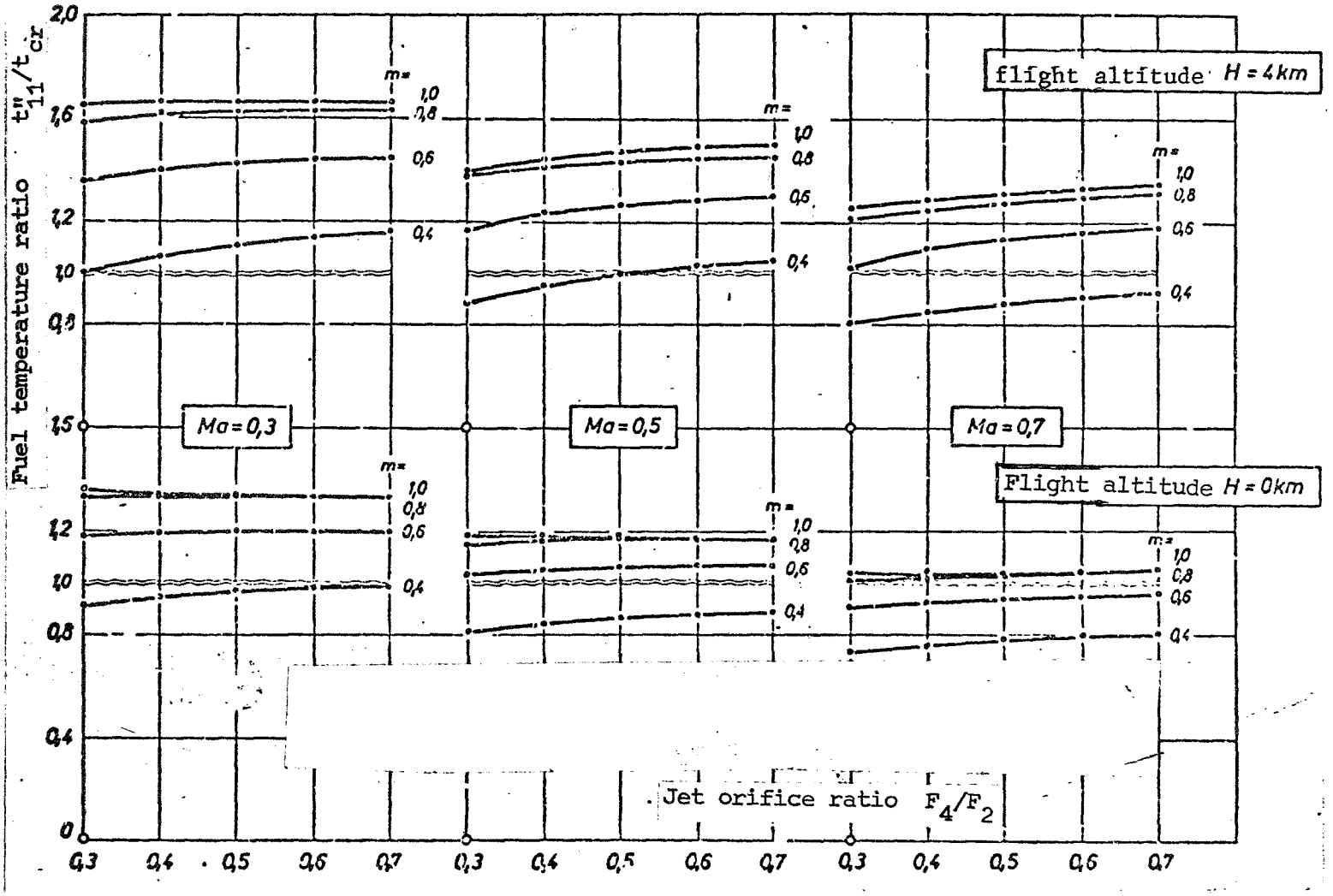

Figure 10. Fuel temperature ahead of the injection jet, t''_{11} as a function of the jet orifice ratio F_4/F_2 at different incident flow velocities and flight altitudes. Calculated for n-octane (t_{cr} = 296°C); engine of Figure 32, rotor radius r = 3m.

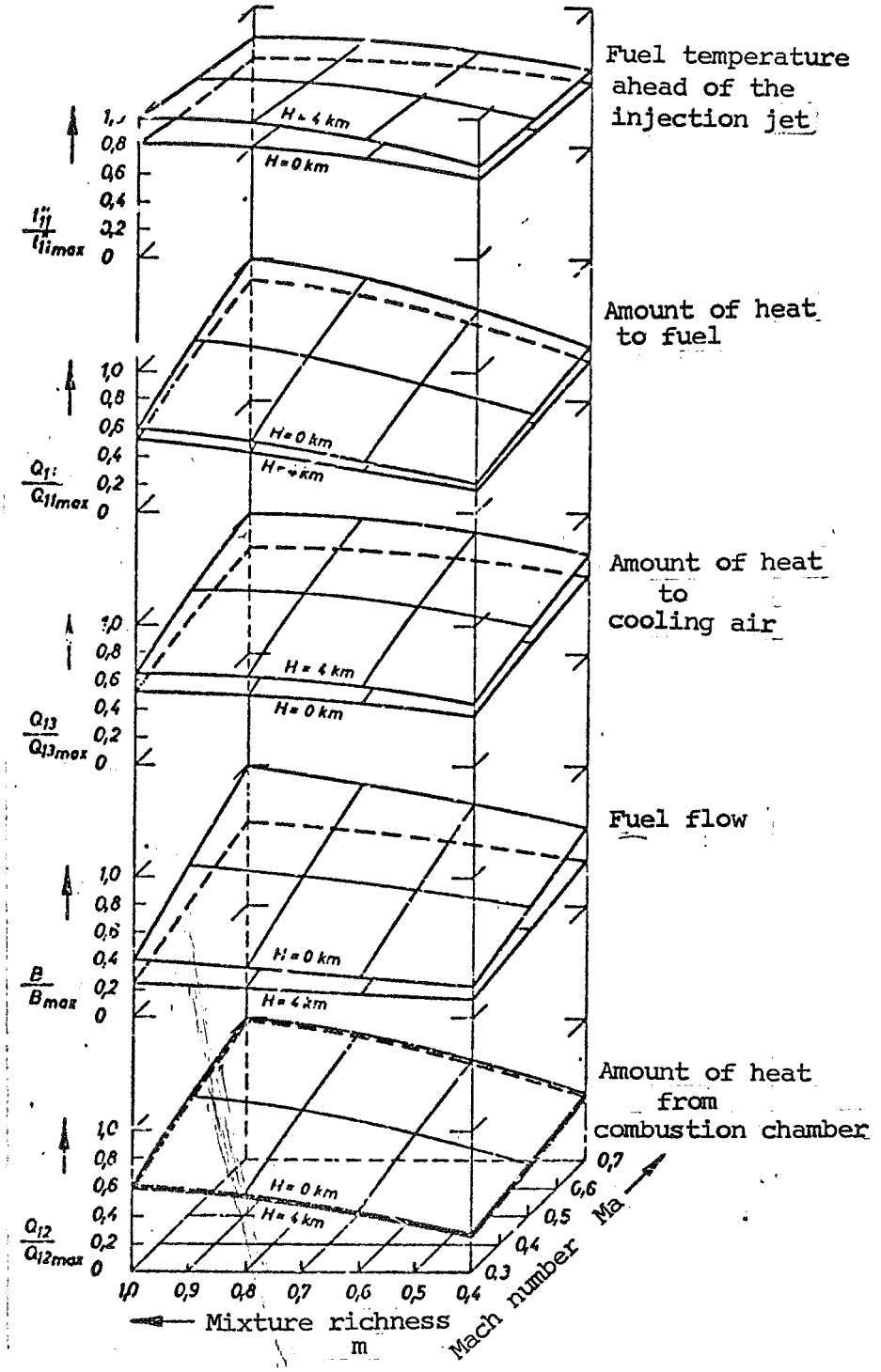

Figure 11. Effect of mixture richness, Mach number, and flight altitude on fuel flow, fuel temperature, and amount of heat transferred.

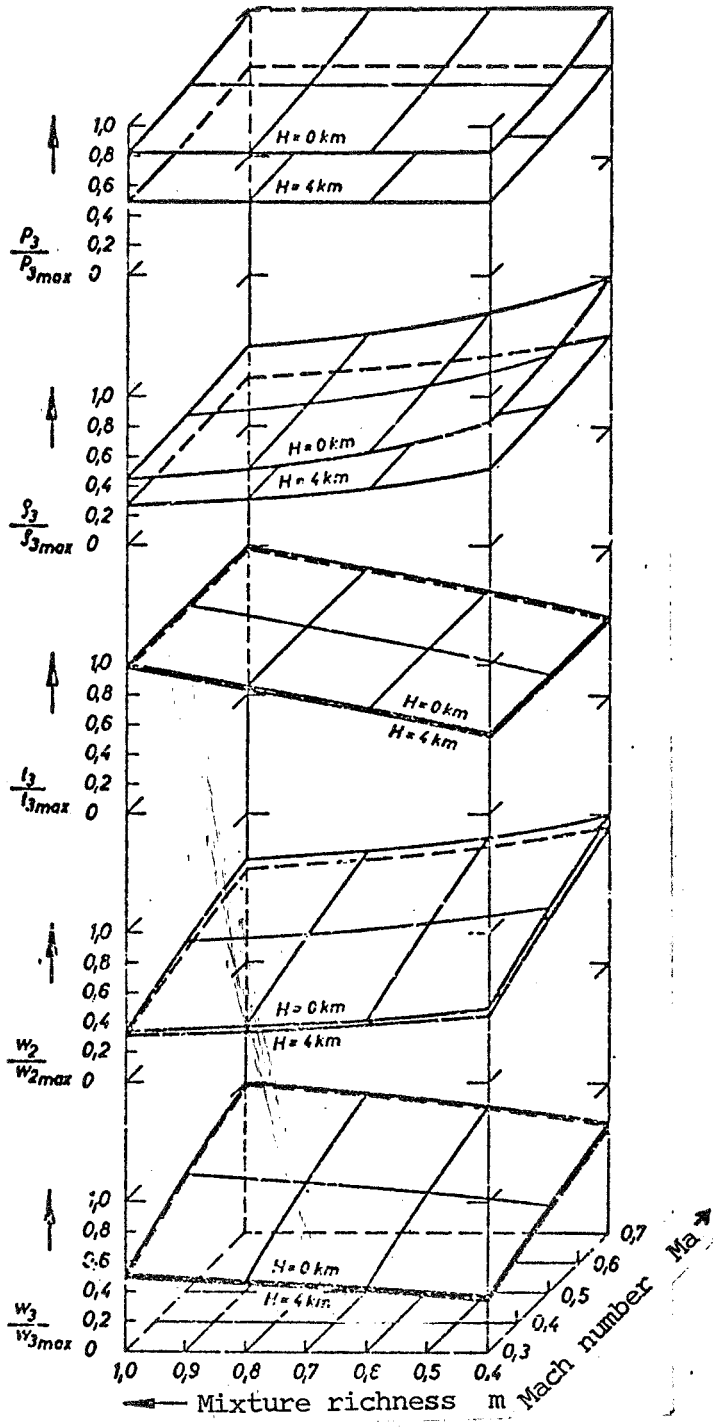

Figure 12. Effect of mixture richness, Mach number, and flight altitude on pressure, density, temperature, and flow velocity in the combustion chamber.

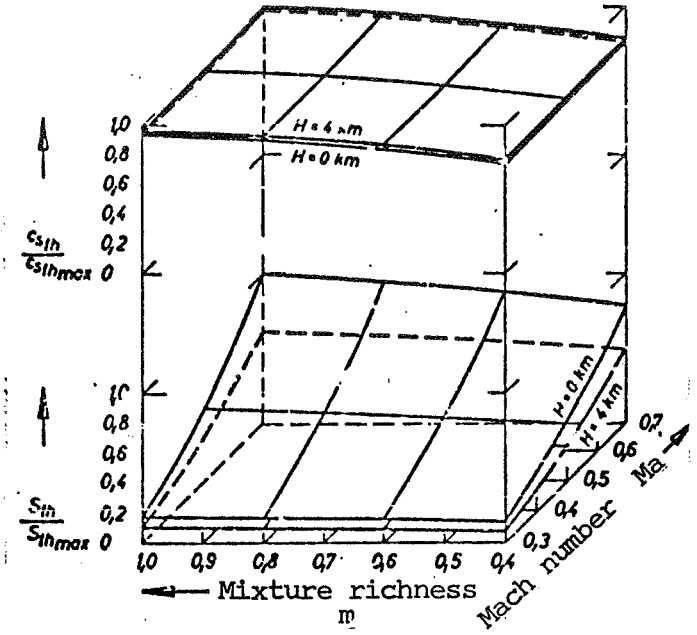

Figure 13. Effect of mixture richness, Mach number and flight altitude on the theoretical thrust and thrust coefficient.

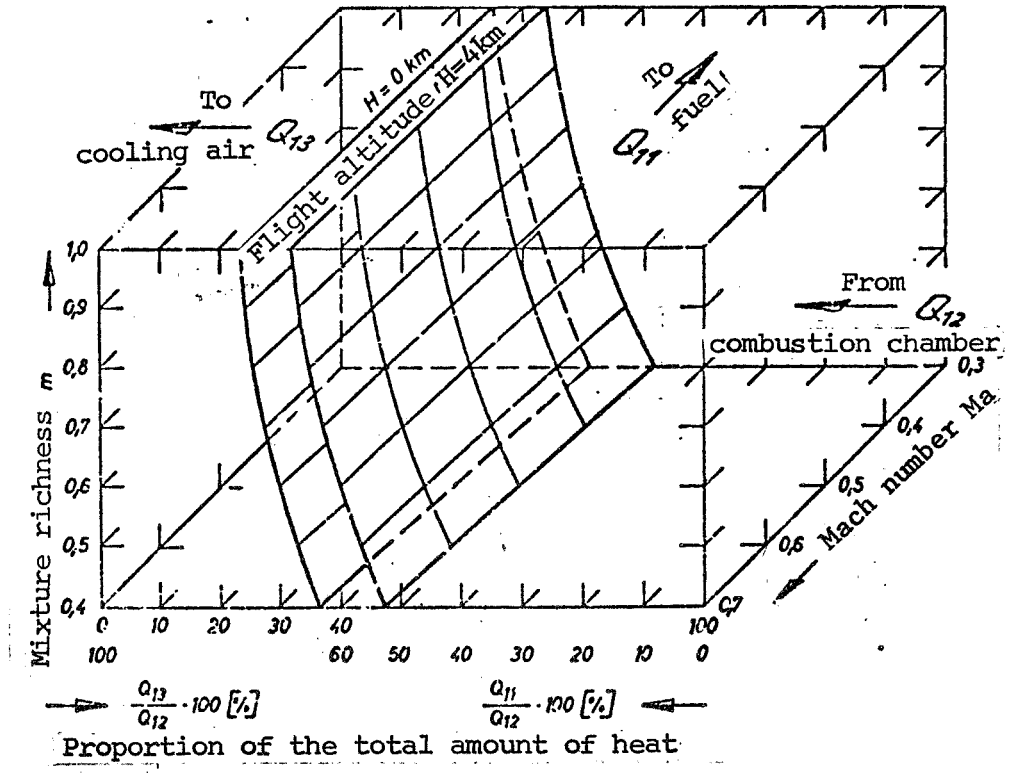

Figure 14. Percentage distribution of the heat given off by the combustion chamber to the heat exchange cowling.

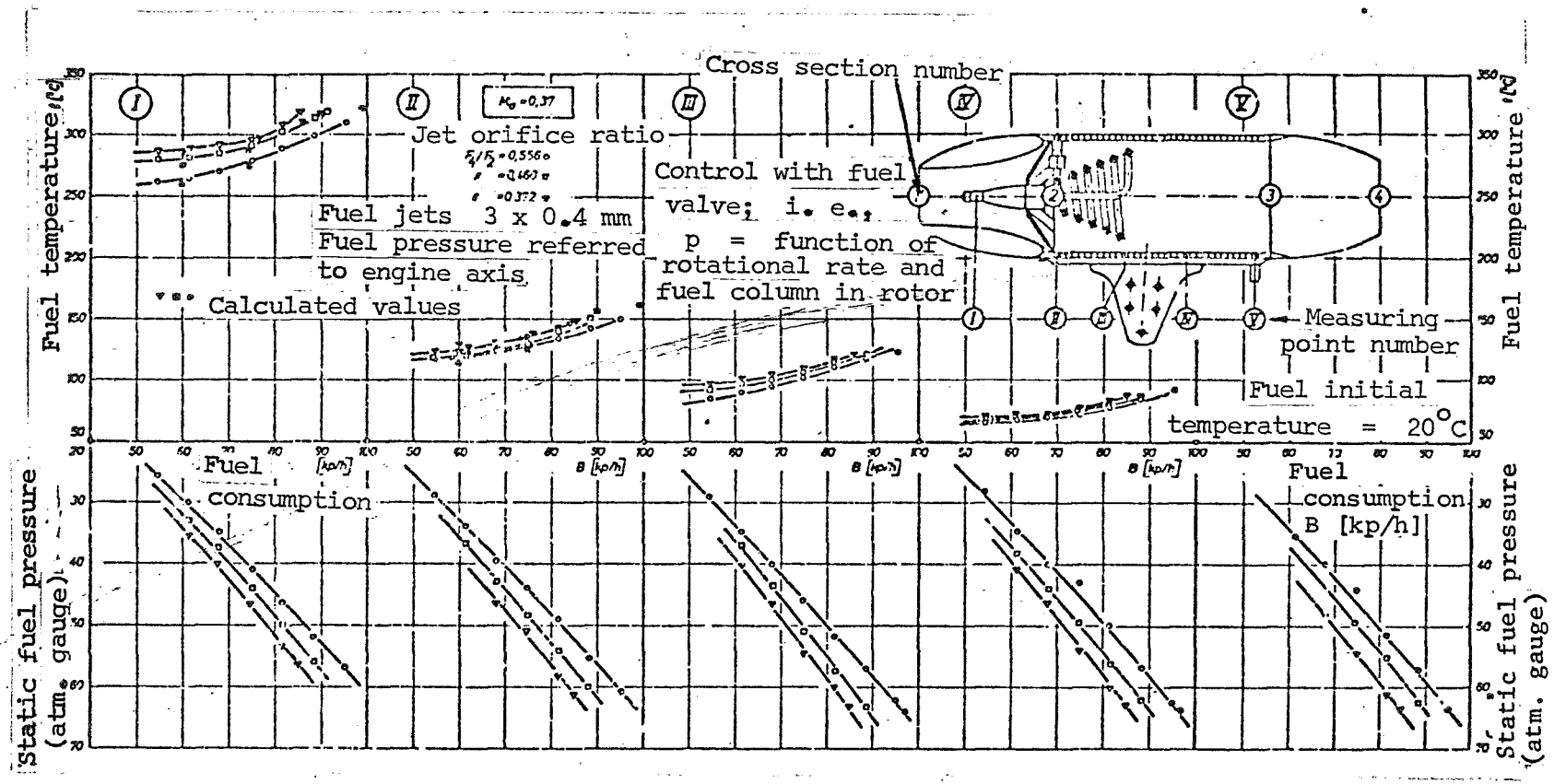

Figure 15. Temperature and pressure measurements in the ramjet engine of Figure 33 with fuel prevaporization.

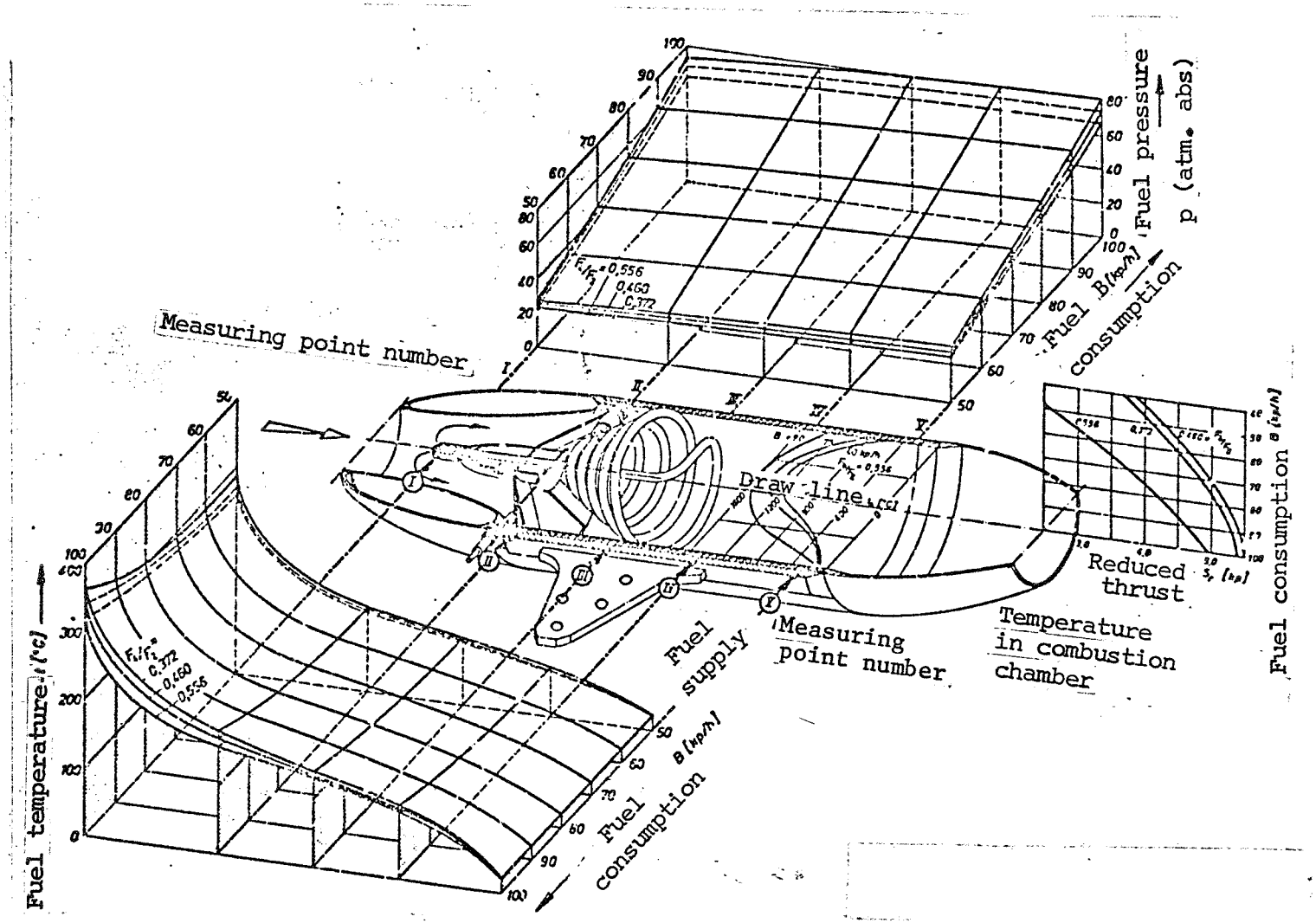

Figure 16. Experimental measurements on ramjet engine with fuel prevaporization.

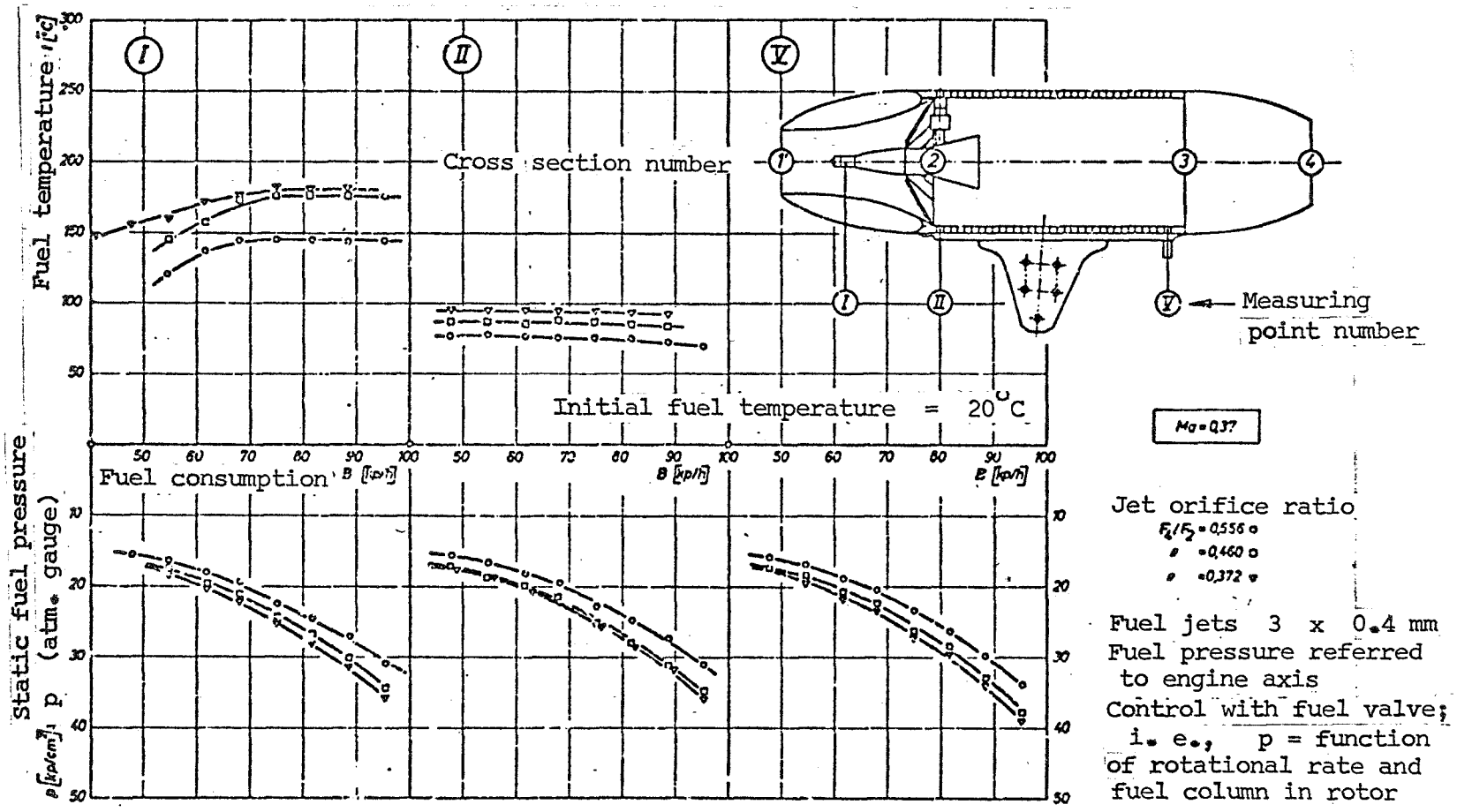

Figure 17. Temperature and pressure measurements on the ramjet engine of Figure 32 with fuel prewarming.

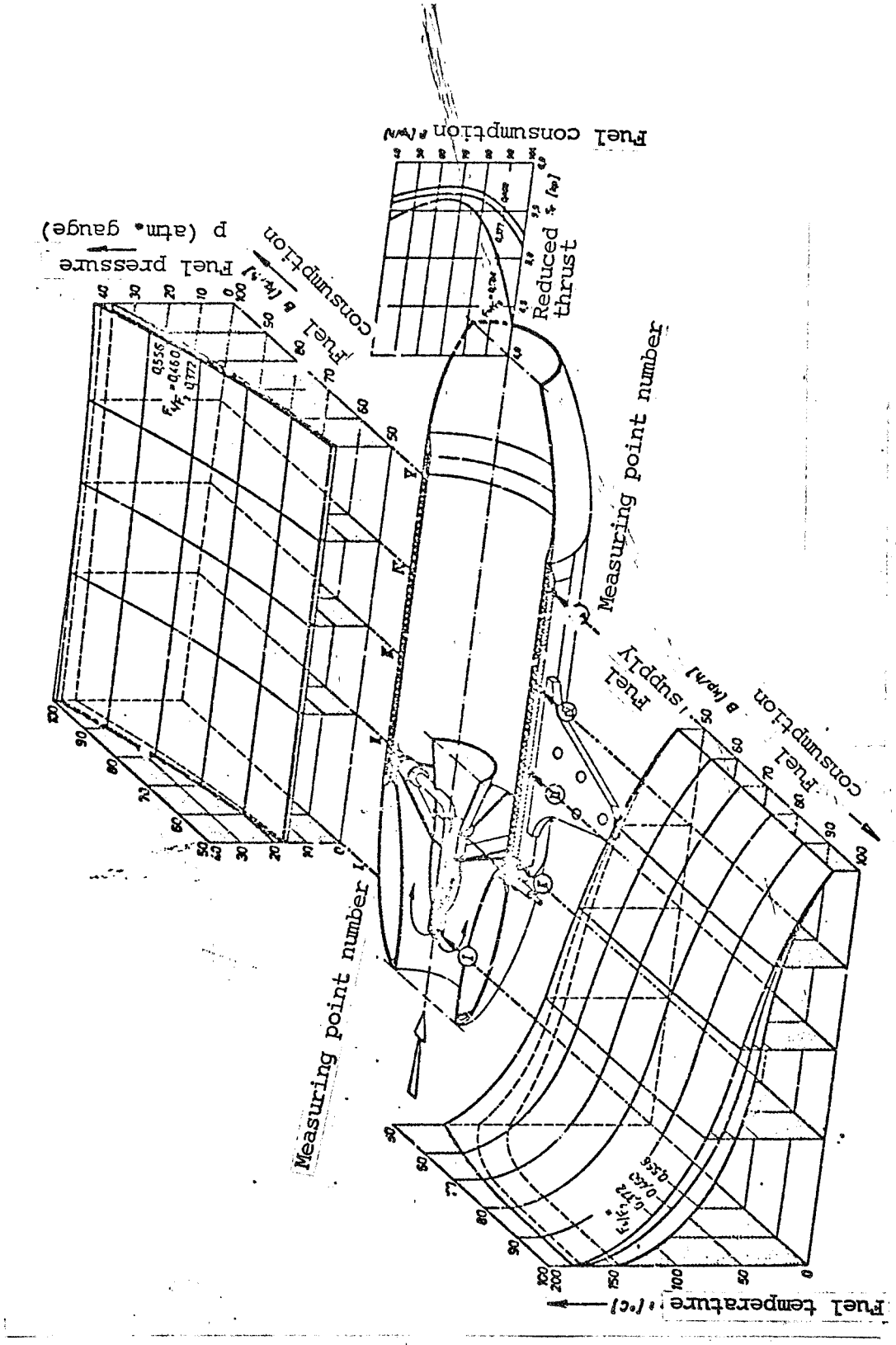

Figure 18. Experimental measurements on the ramjet engine with fuel prewarming.

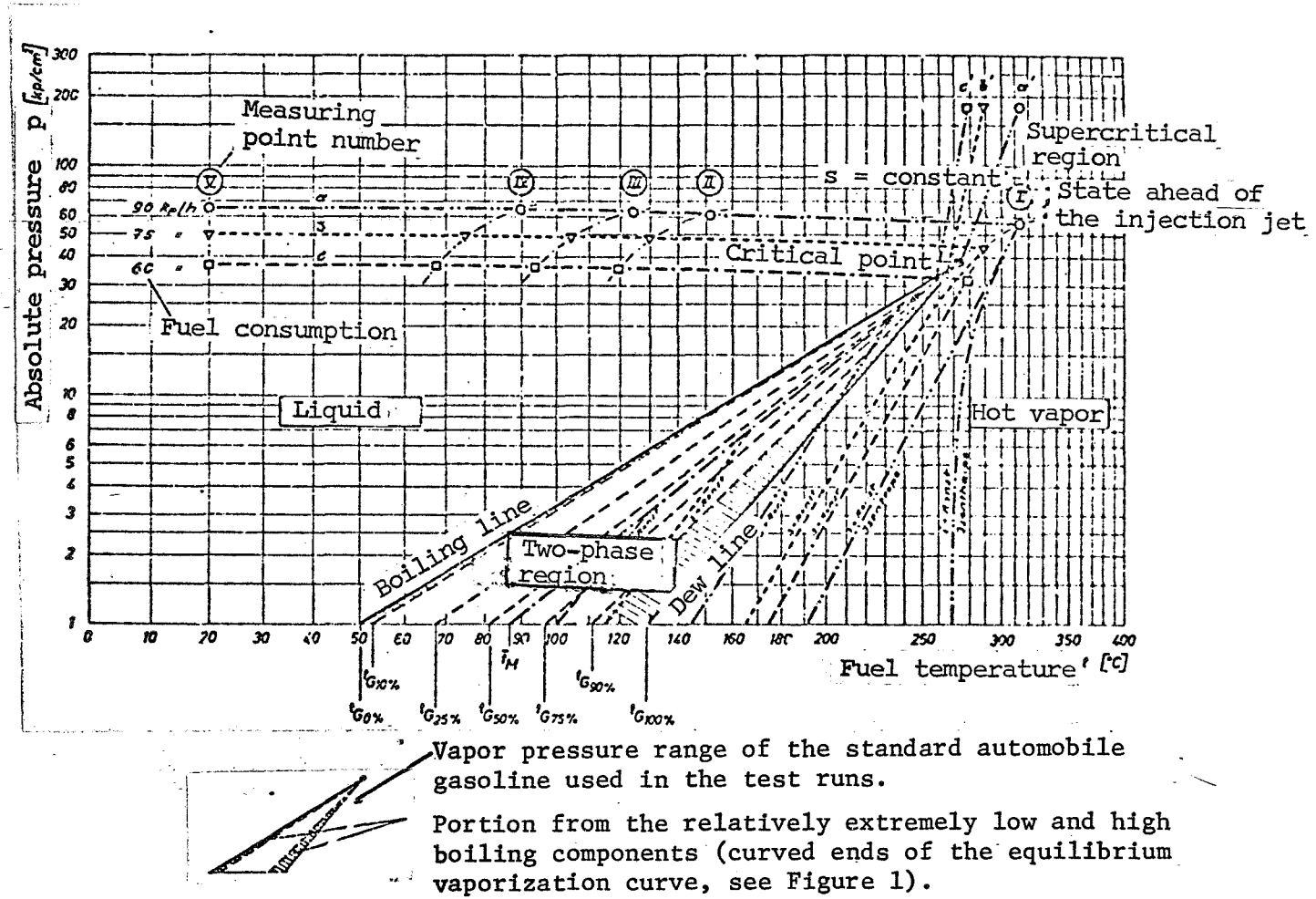

Figure 19. Log p vs. 1/T diagram for the fuel prevaporization of standard automobile gasoline attained in the investigation. The isentropy and isenthalpy were determined from the temperature-entropy or enthalpy-temperature diagrams based on the mean molar boiling temperature (Figures 4 and 5). The actual expansion curves run to the right of the corresponding isentropy.

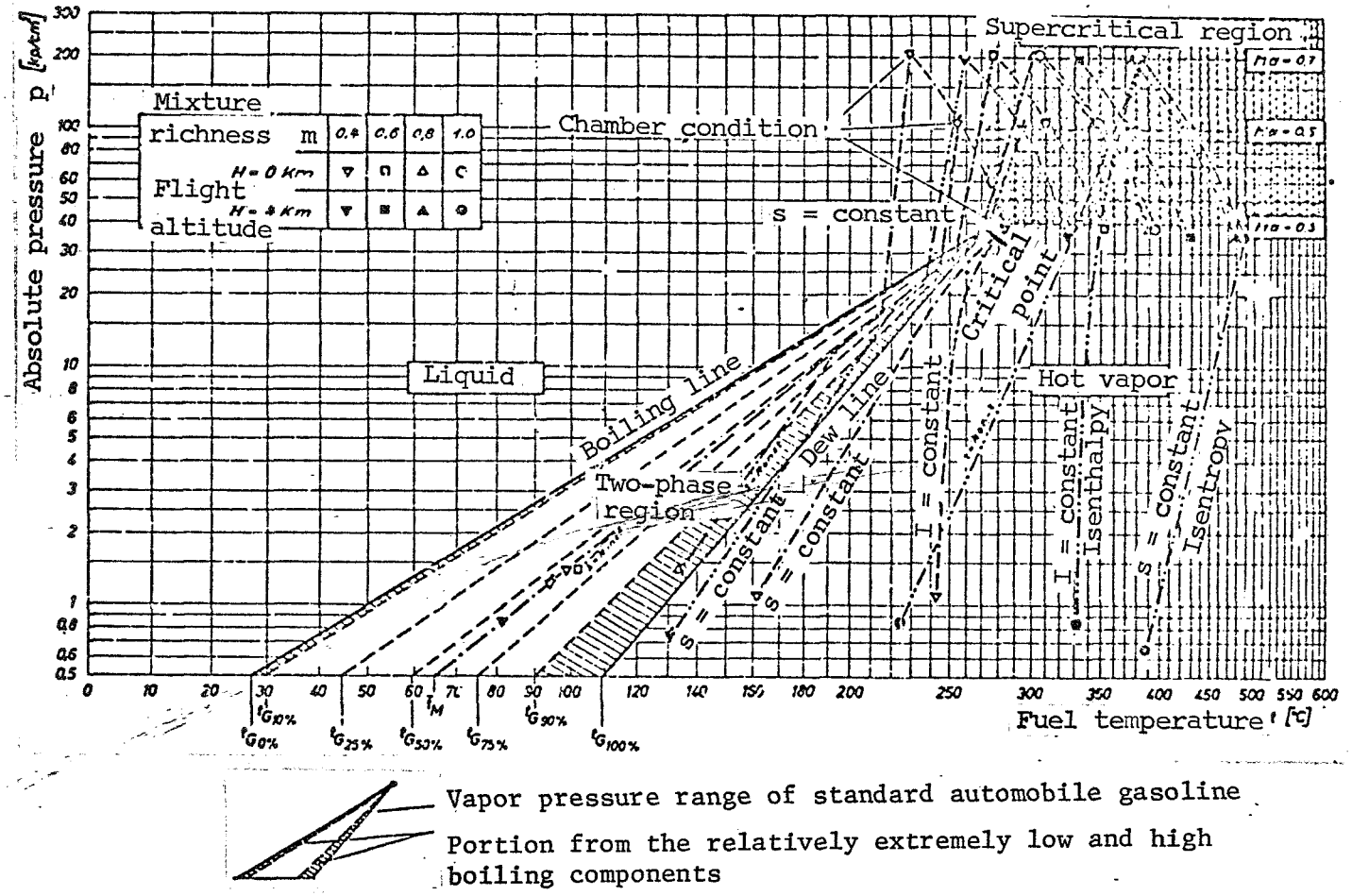

Figure 20. Log p vs. 1/T diagram of fuel vaporization for standard automobile gasoline for the "Chamber condition" determined via calculation (see 3.2 and 3.3). The actual expansion curves run to the right of the corresponding isentropy.

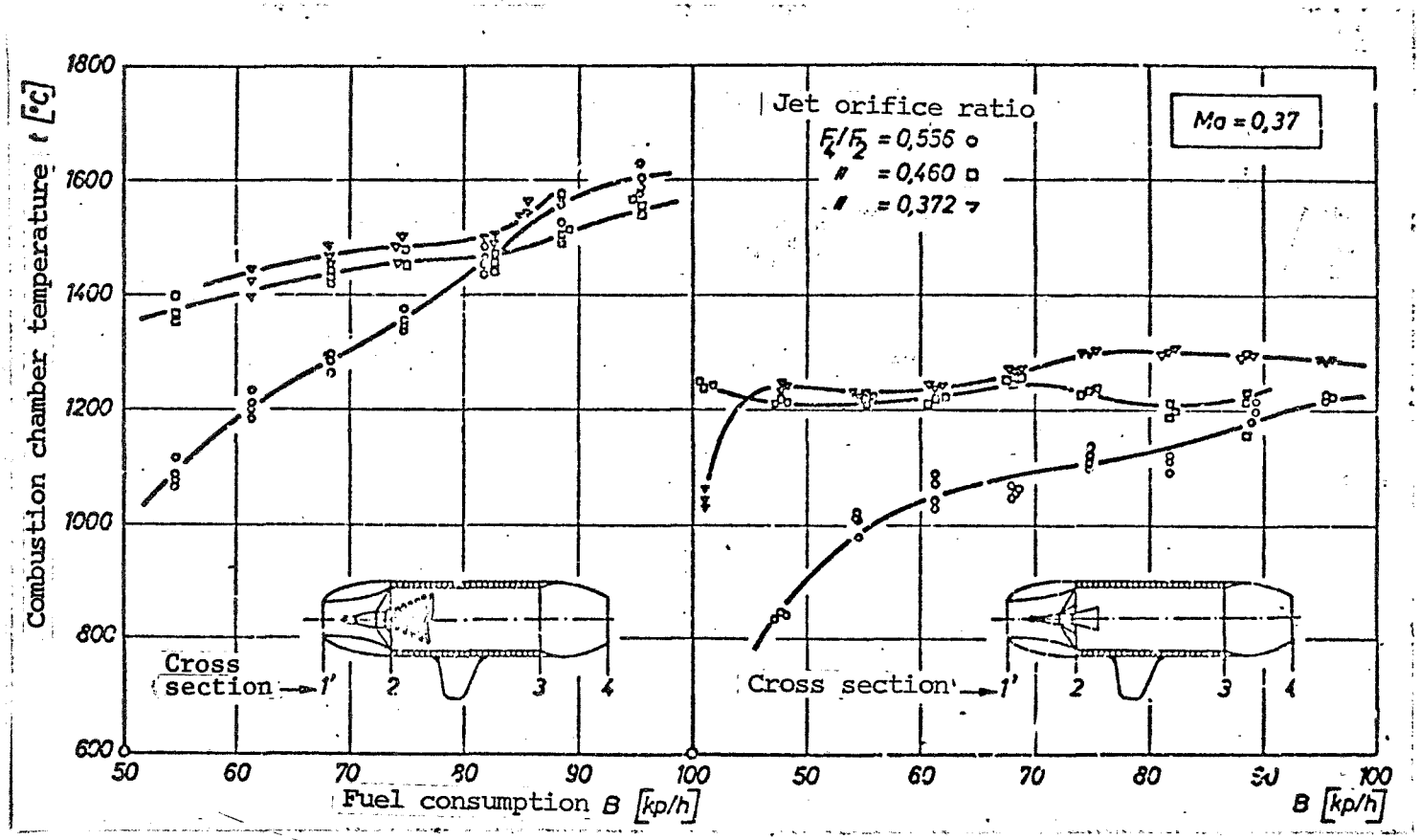

Engine of Figure 33 with fuel prevaporization.

Engine of Figure 32 with fuel prewarming.

Figure 21. Combustion chamber temperature at the center of the engine on cross section 3.

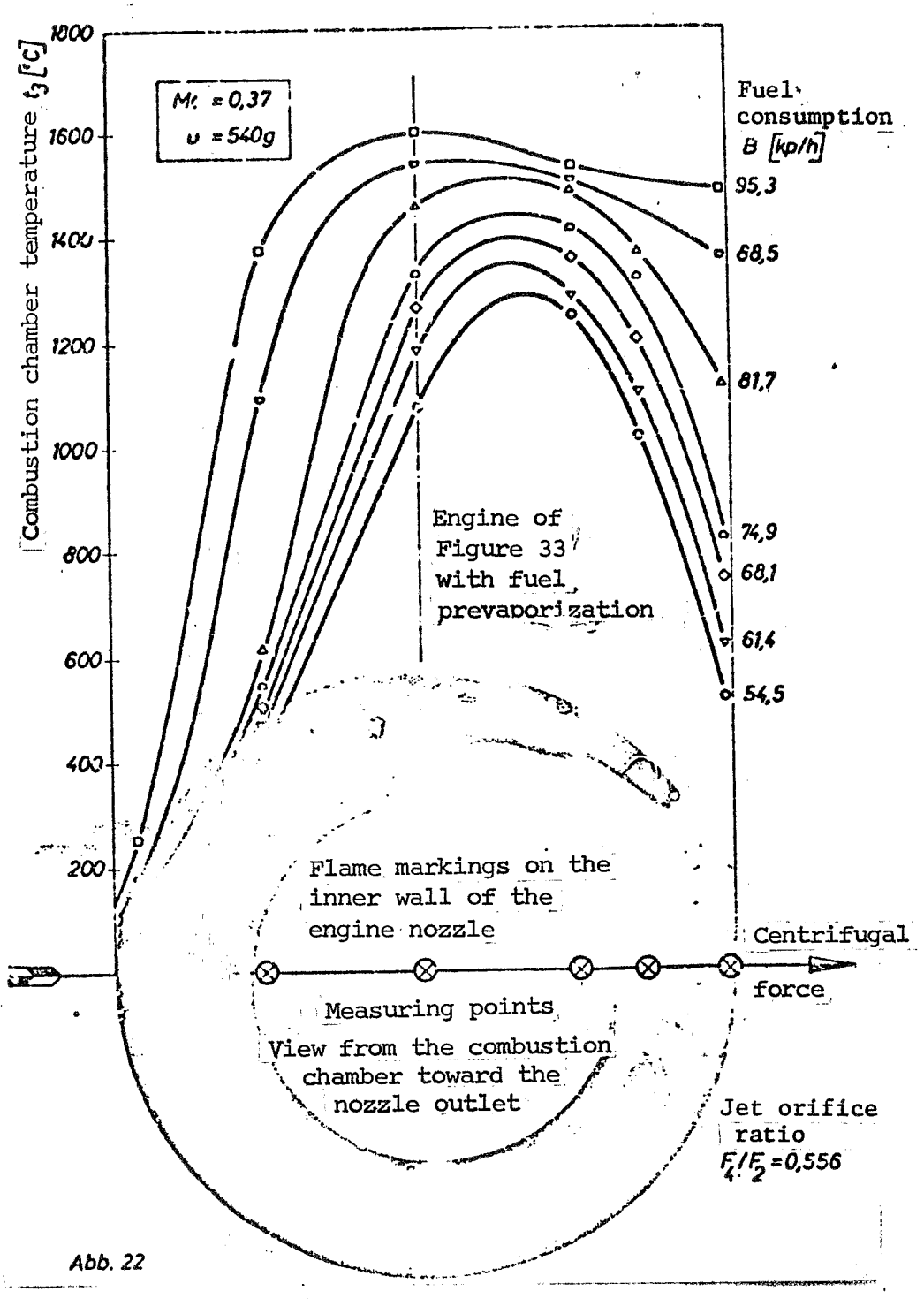

Figure 22. Effect of centrifugal force on the combustion chamber temperature distribution in the plane of rotor rotation at cross section 3.

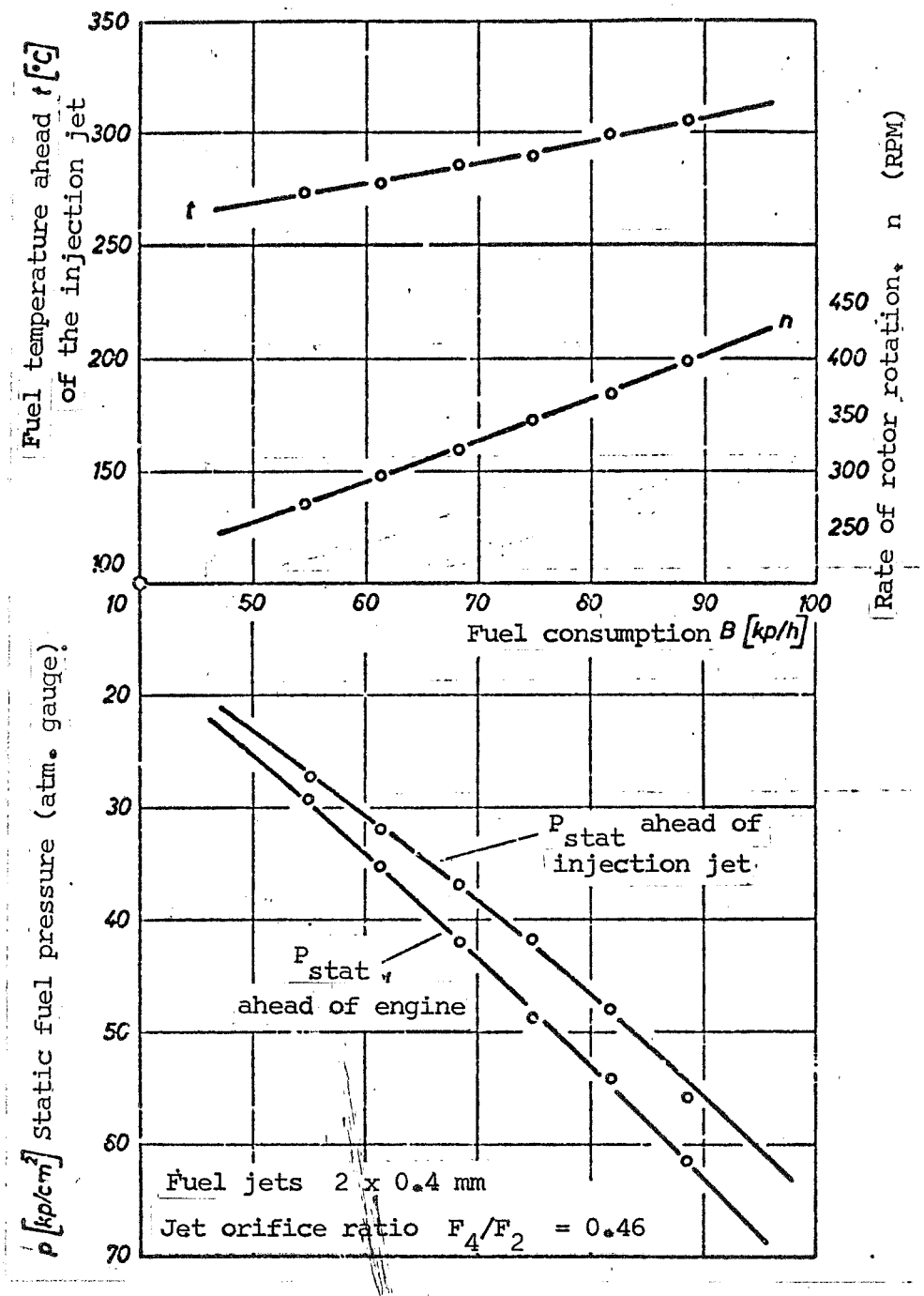

Figure 23. Runout with burning engine (Figure 33); fuel valve completely open; i.e., p is a function of (n) only.

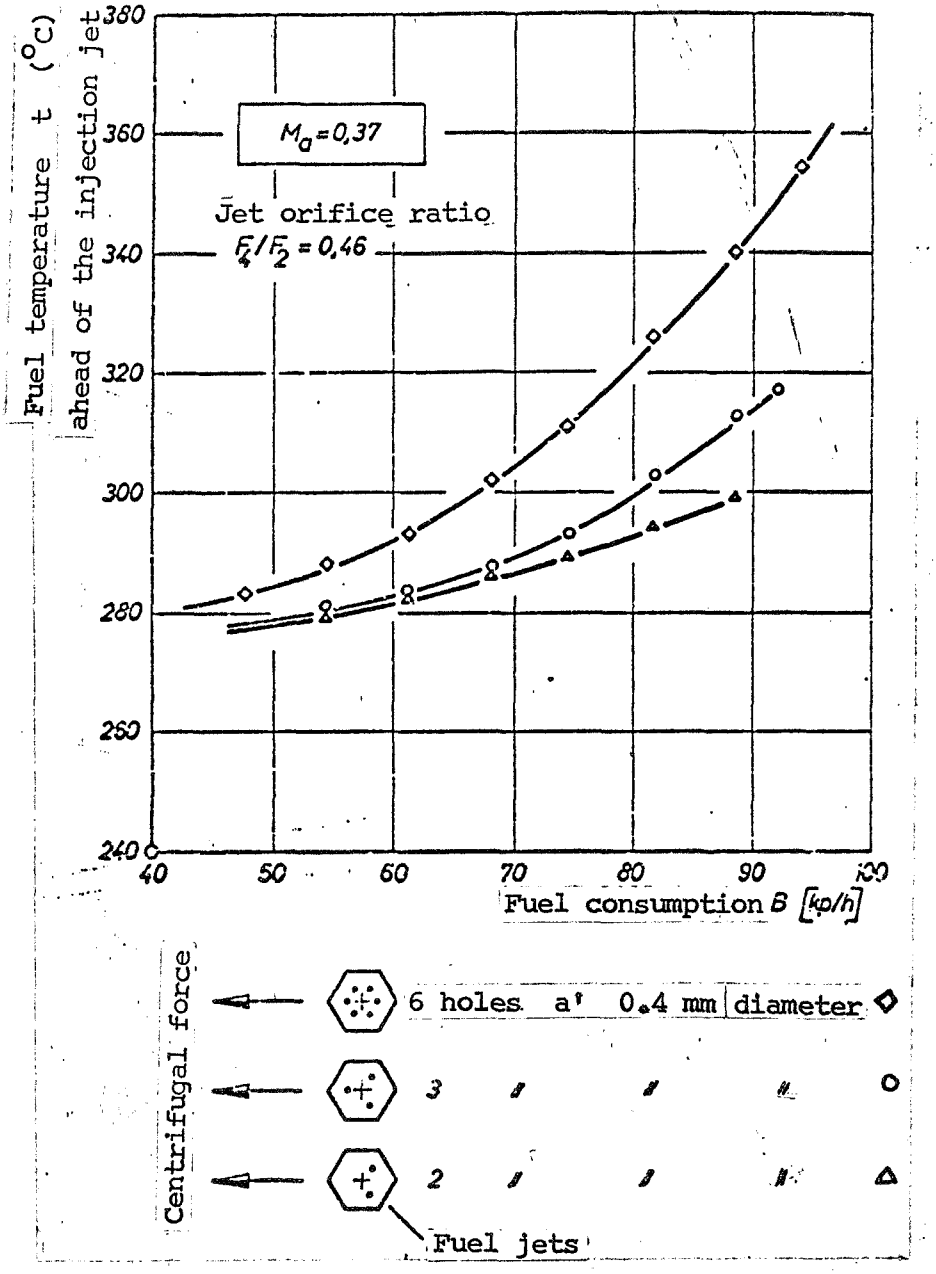

Figure 24. Effect of the fuel jet parameter on the fuel temperature.

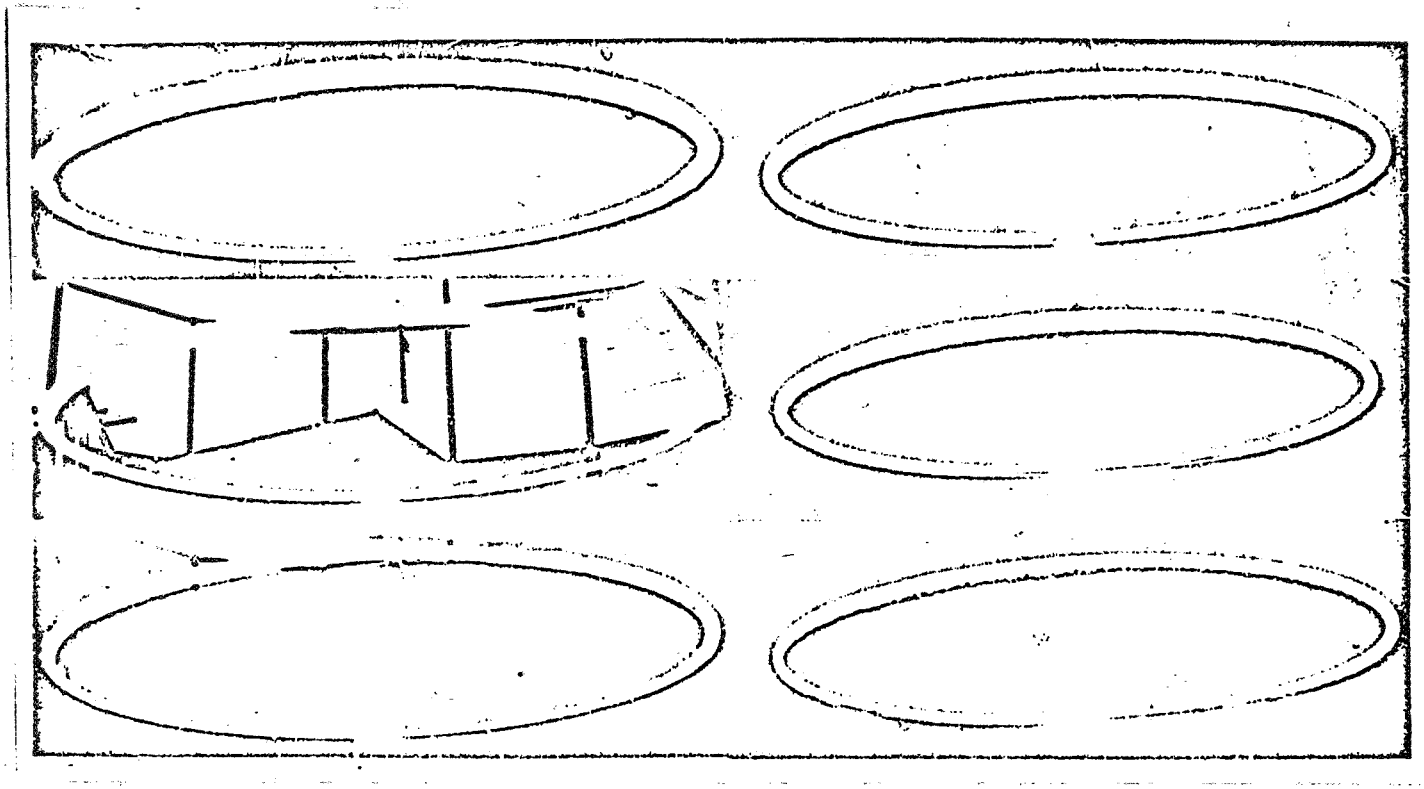

Without fuel prevaporization

With fuel prevaporization

Figure 25. Flame pictures of the ramjet engines of Figures 32 and 33. Fuel flow from top to bottom. B = 95, 82, 68 kp/hr. Exposure time 15 seconds, diaphragm 8.

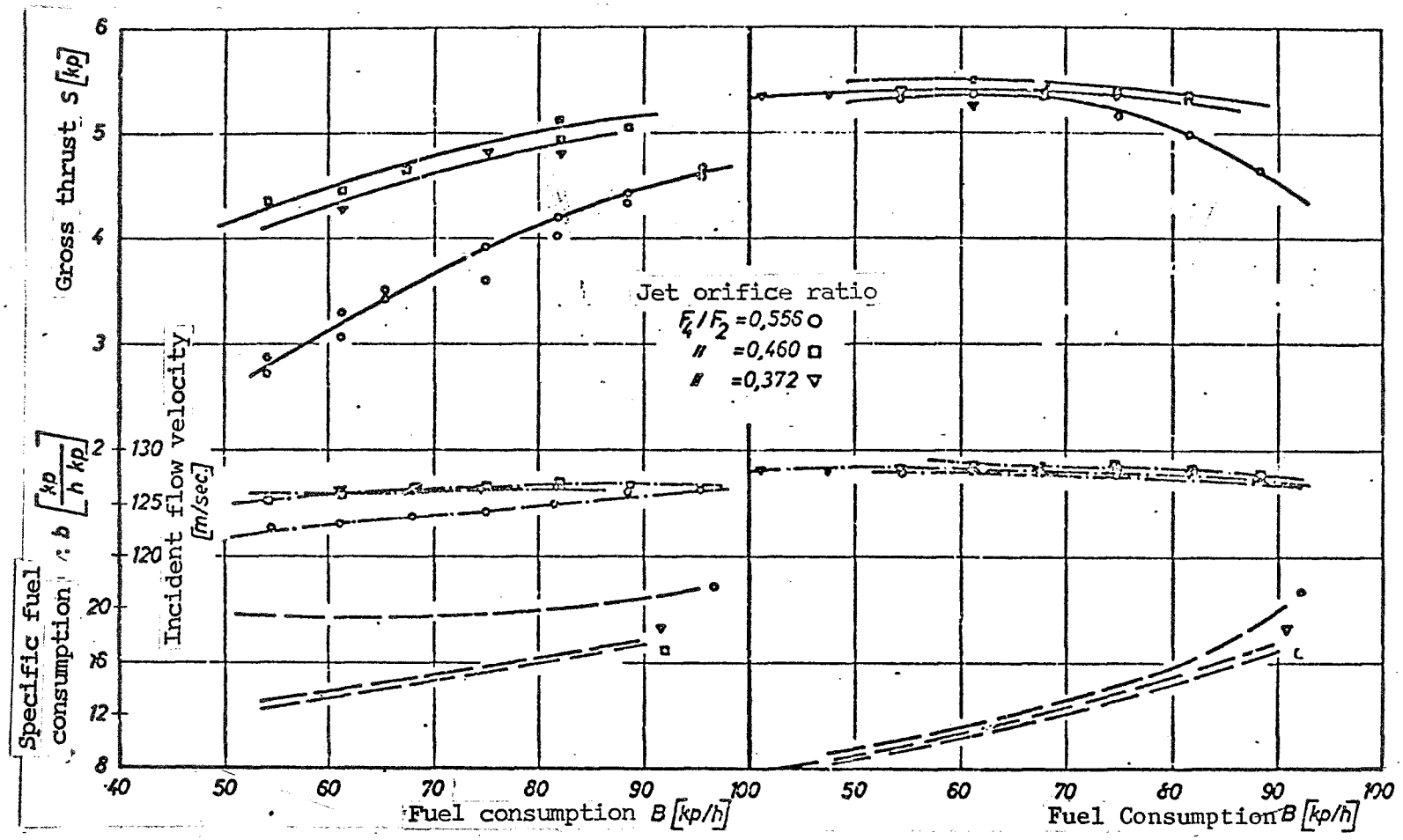

Engine of Figure 33 with fuel prevaporization.

Engine of Figure 32 with fuel prewarming.

Figure 26. Efficiency curves of the ramjet engines with fuel prevaporization or fuel prewarming.

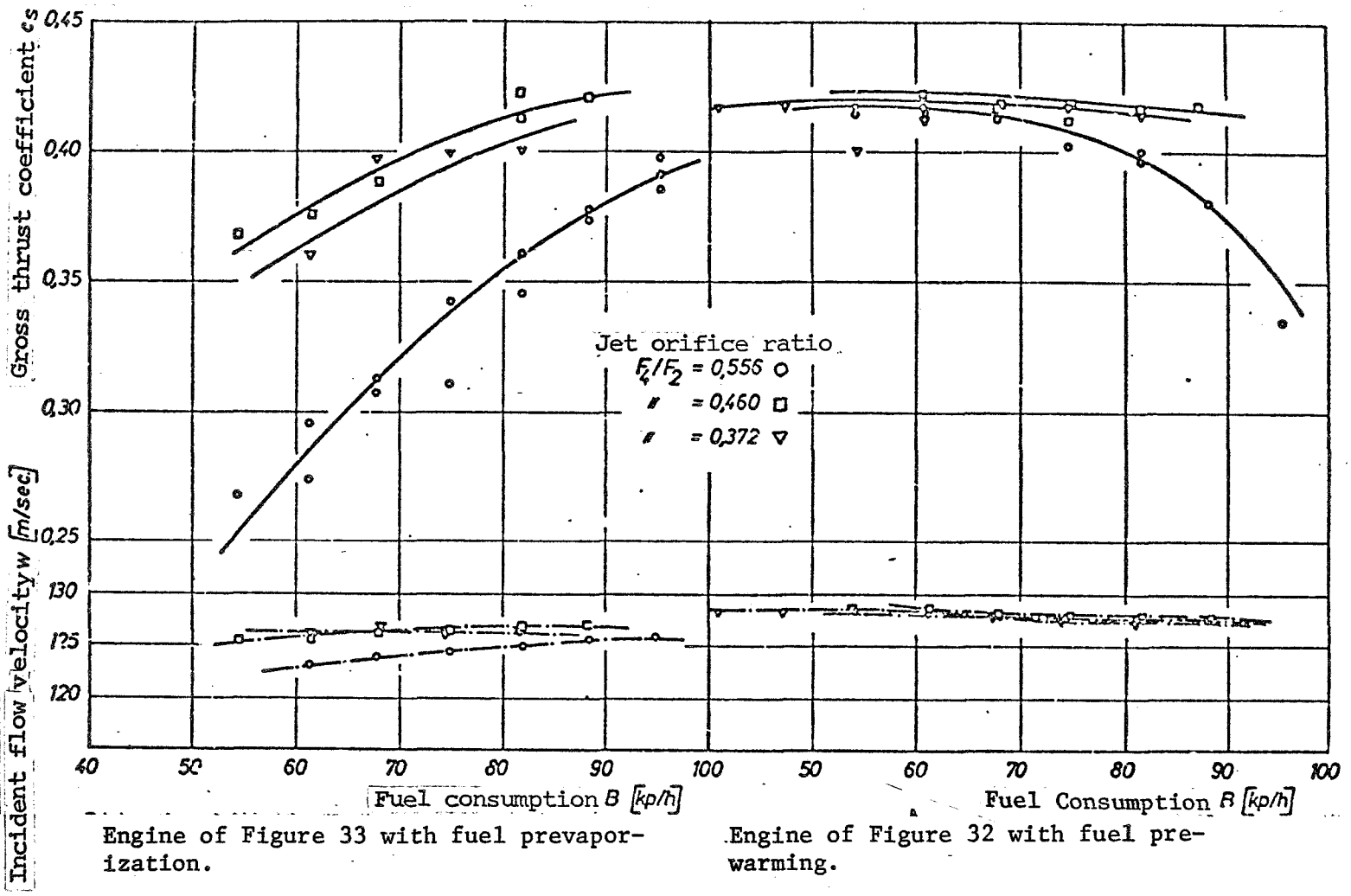

Engine of Figure 33 with fuel prevaporization.

Engine of Figure 32 with fuel prewarming.

Figure 27. Gross thrust coefficient of the ramjet engines with fuel prevaporization or fuel prewarming.

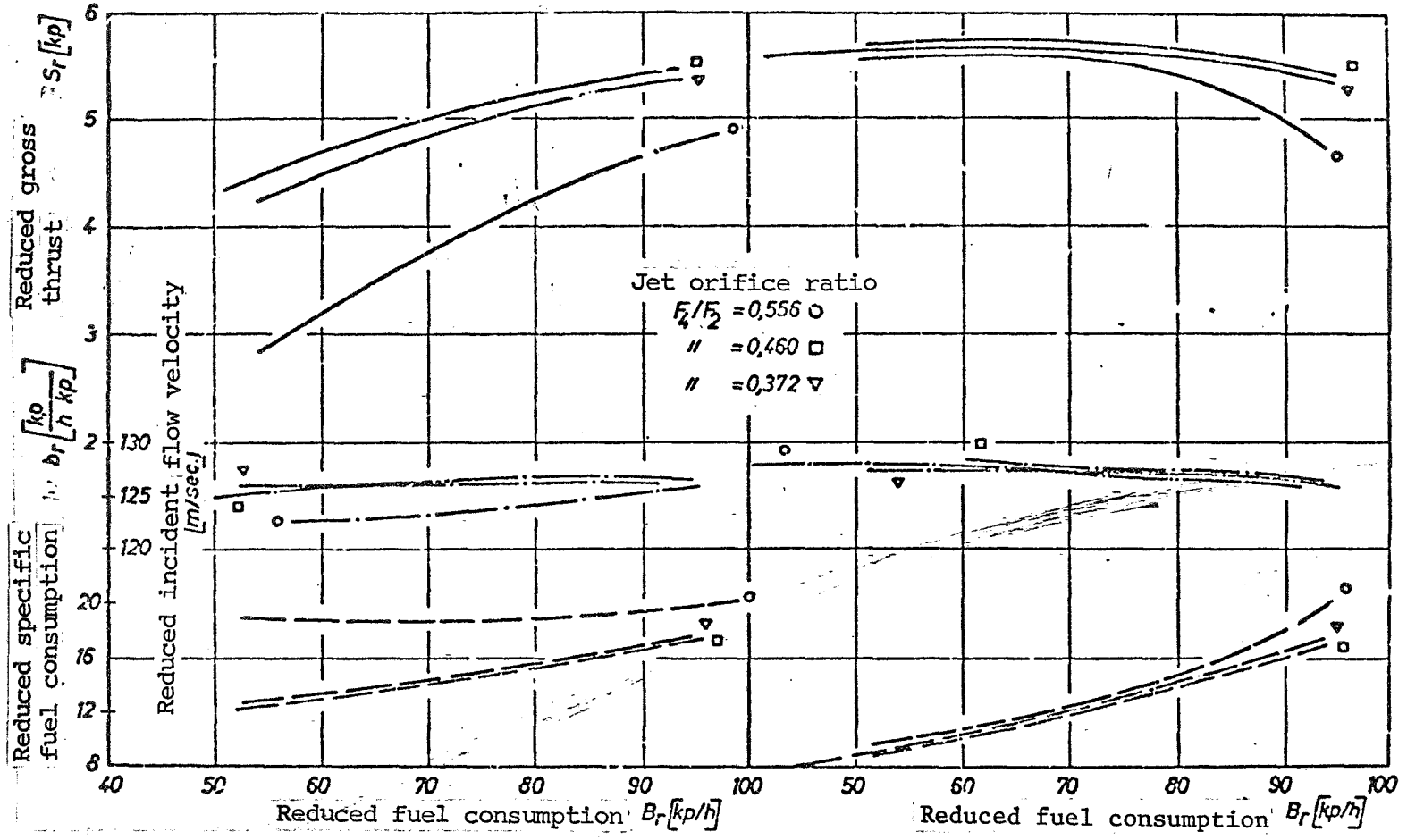

Engine of Figure 33 with fuel prevaporization.

Engine of Figure 32 with fuel prewarming.

Figure 28. Reduced efficiency curves of the ramjet engines with fuel prevaporization and fuel prewarming.

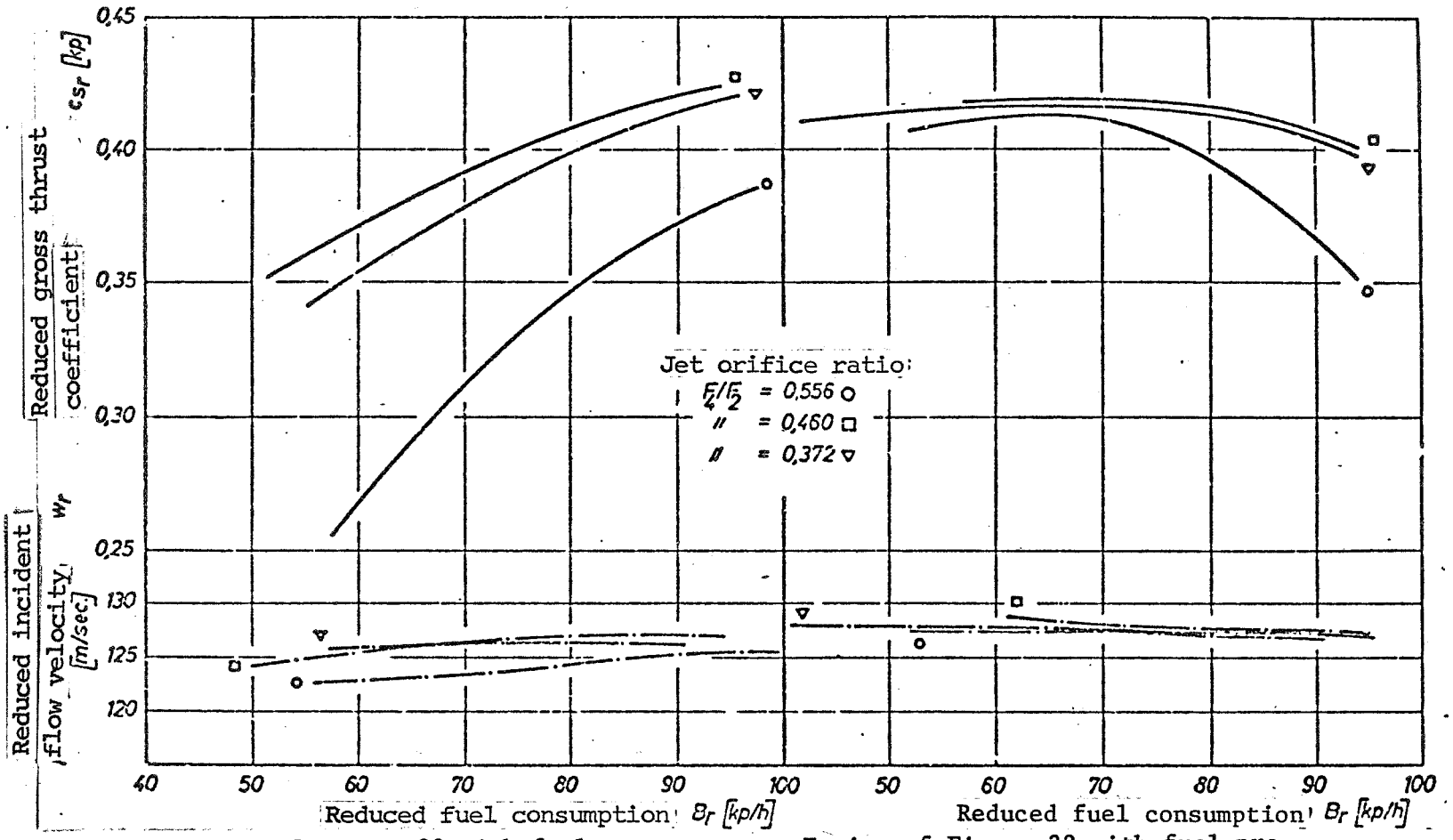

Engine of Figure 33 with fuel prevaporization.

Engine of Figure 32 with fuel prewarming.

Figure 29. Reduced gross thrust coefficient of ramjet engines with fuel prevaporization or fuel prewarming.

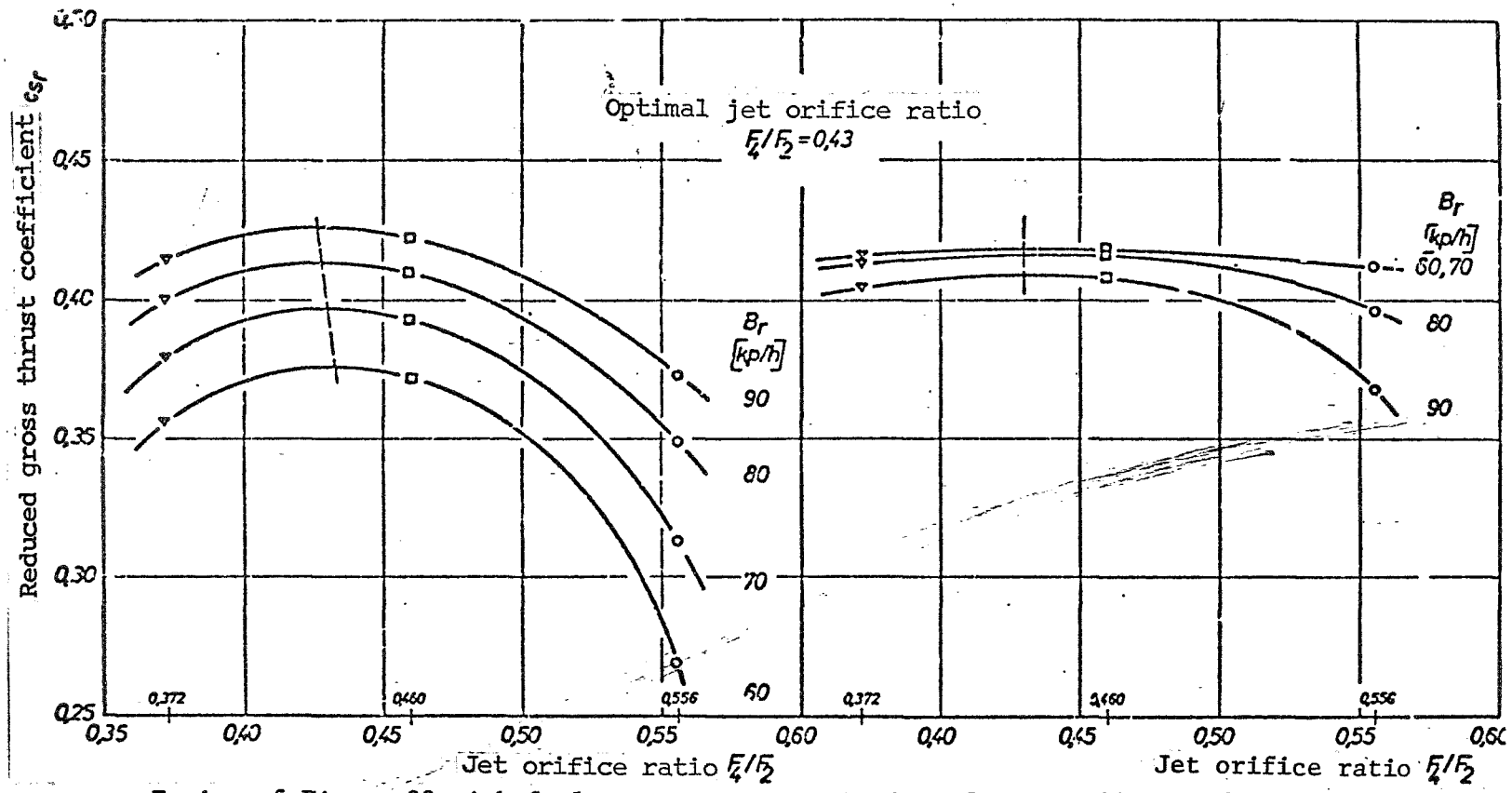

Engine of Figure 33 with fuel prevaporization.

Engine of Figure 32 with fuel prewarming.

Figure 30. Optimum jet orifice ratio F_4/F_2 for the test ramjet engines.

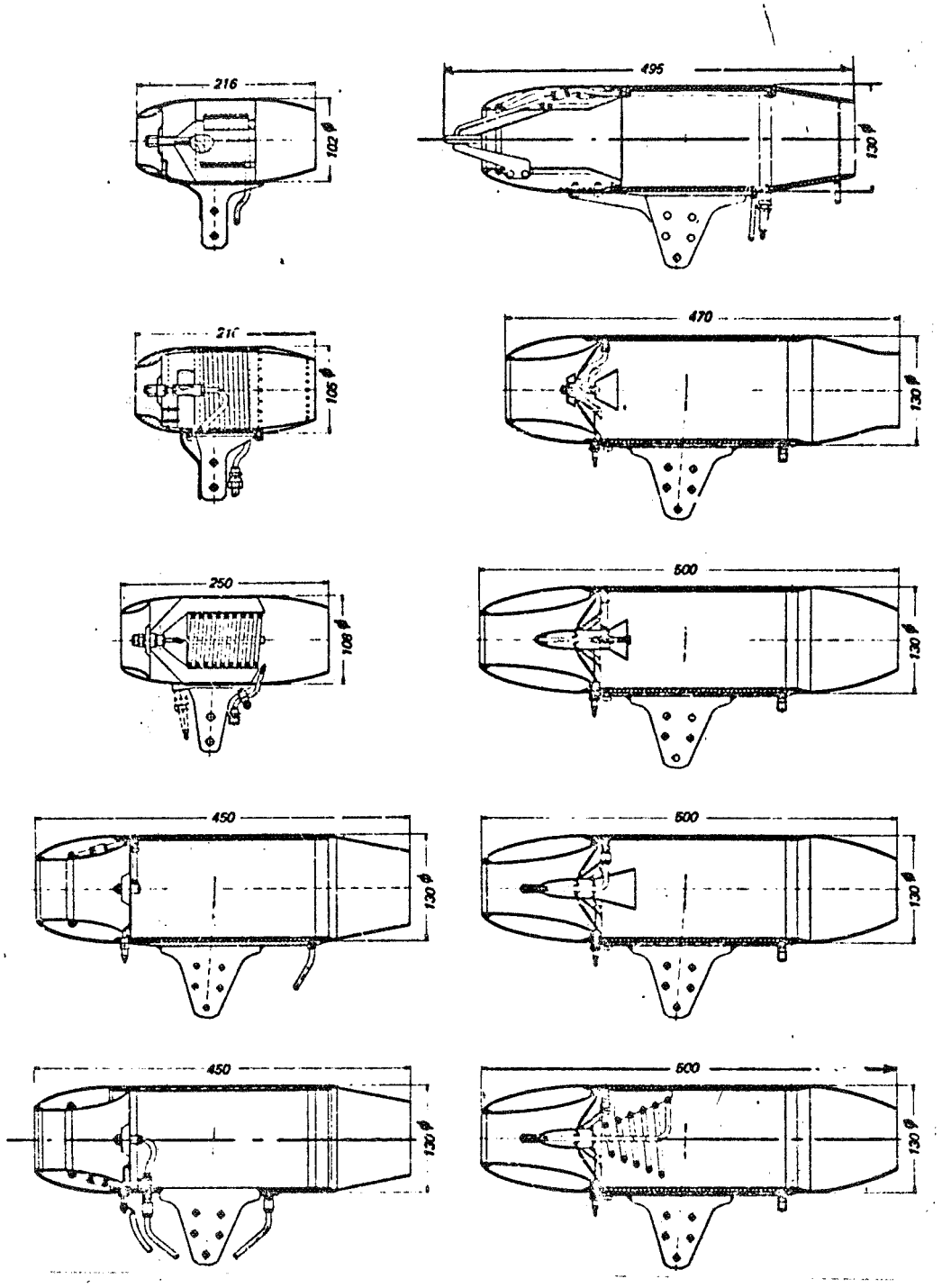

Figure 31. Stages in development of the experimental ramjet engines.

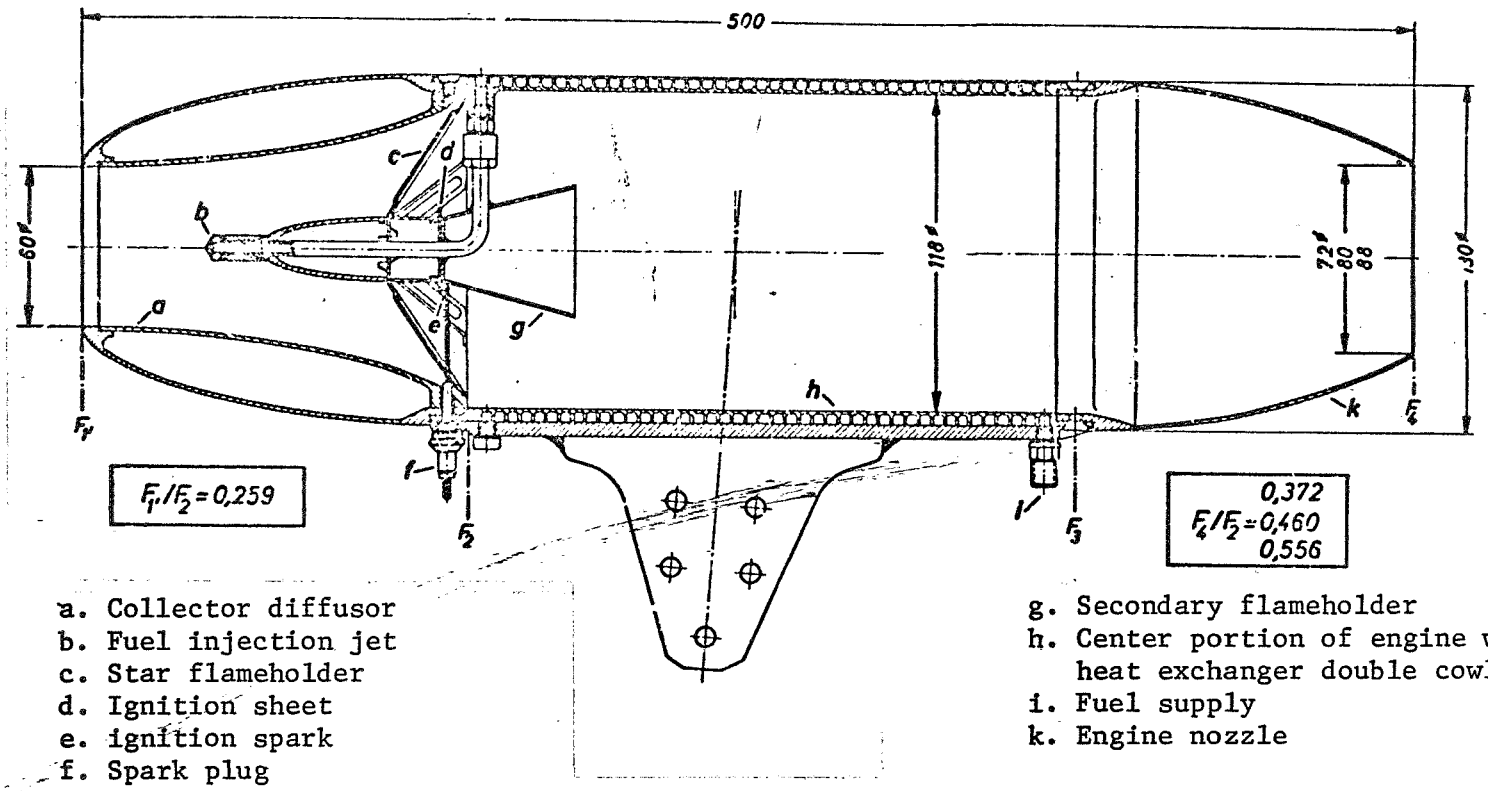

a. Collector diffusor
b. Fuel injection jet
c. Star flameholder
d. Ignition sheet
e. ignition spark
f. Spark plug
g. Secondary flameholder
h. Center portion of engine with heat exchanger double cowling
i. Fuel supply
k. Engine nozzle

Figure 32. Experimental ramjet engine with fuel prewarming.

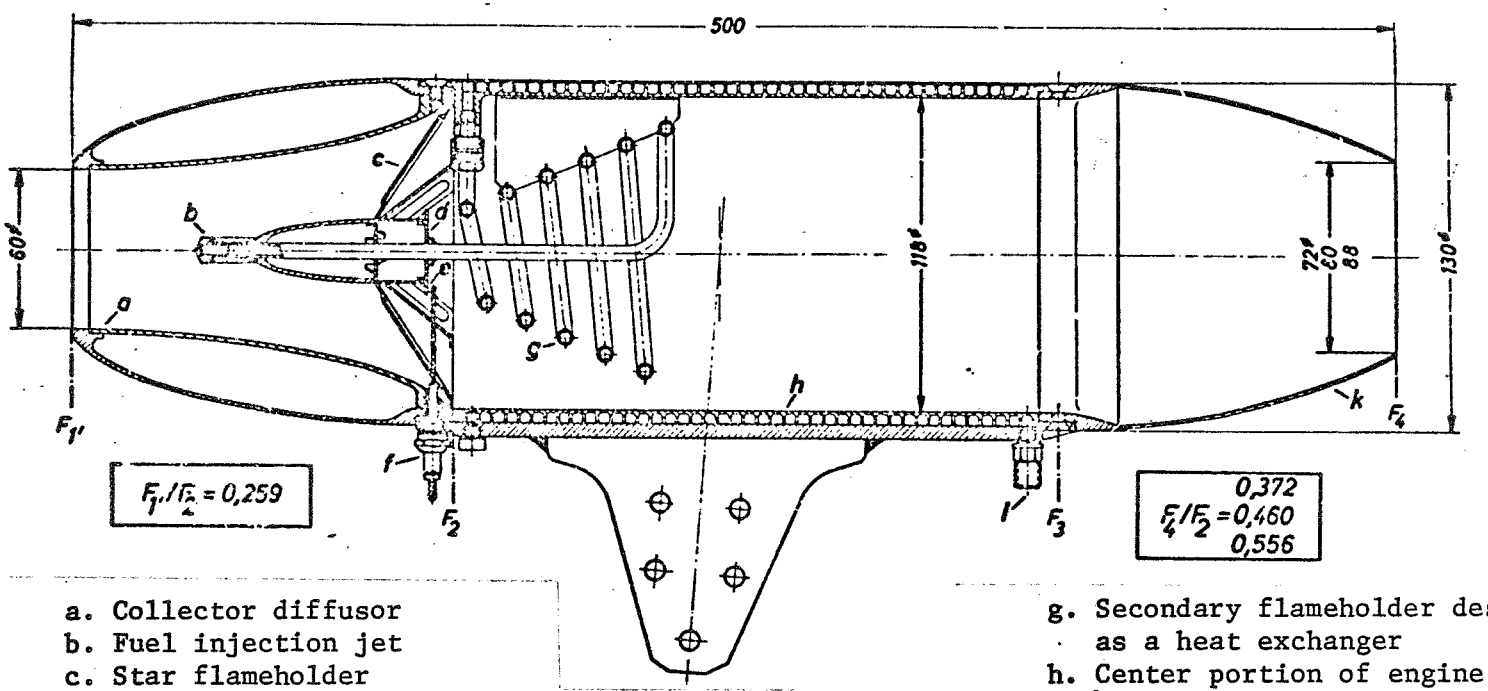

a. Collector diffusor
b. Fuel injection jet
c. Star flameholder
d. Ignition sheet
e. Ignition spark
f. Spark plug
g. Secondary flameholder designed as a heat exchanger
h. Center portion of engine with heat exchanger double cowling
i. Fuel supply
k. Engine nozzle

Figure 33. Experimental ramjet engine with fuel prevaporization.

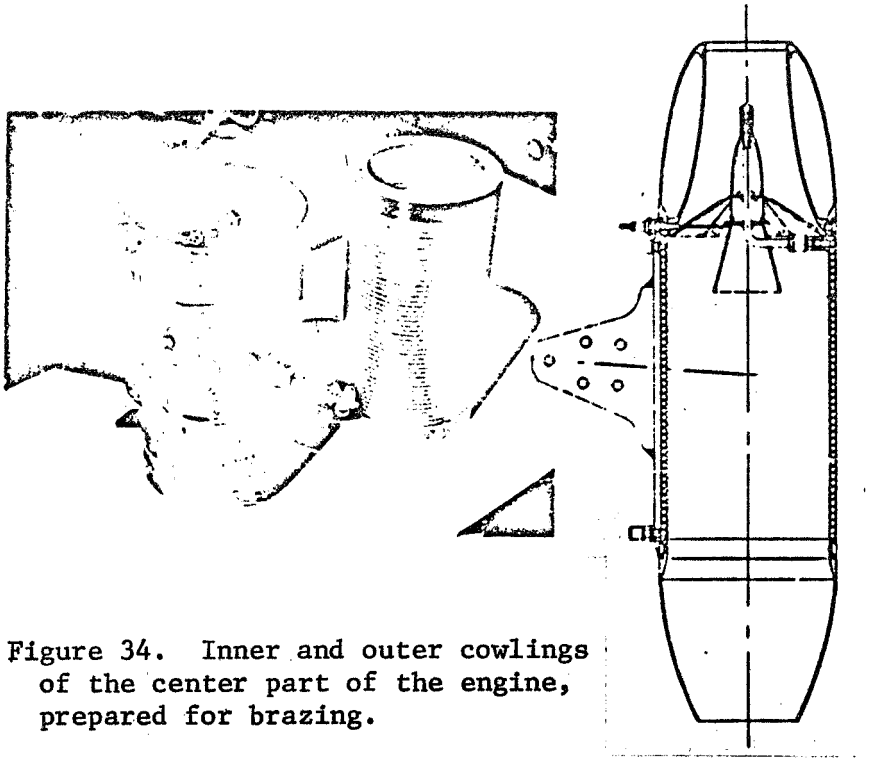

Figure 34. Inner and outer cowlings of the center part of the engine, prepared for brazing.

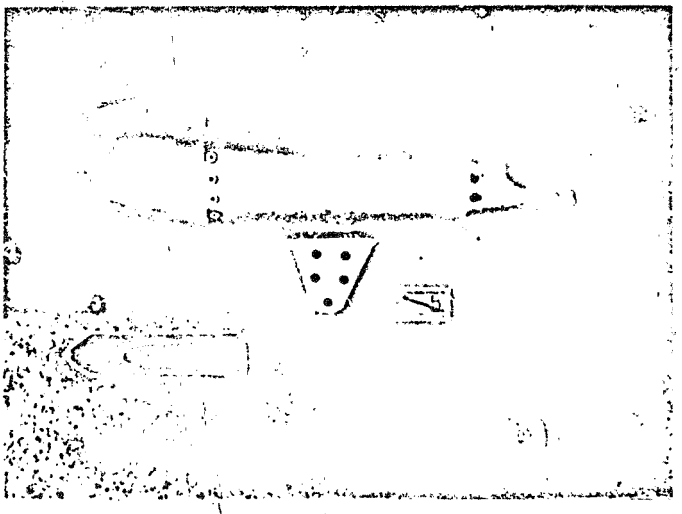

Figure 35. The ramjet engine with special spark plug which was used for the test runs.

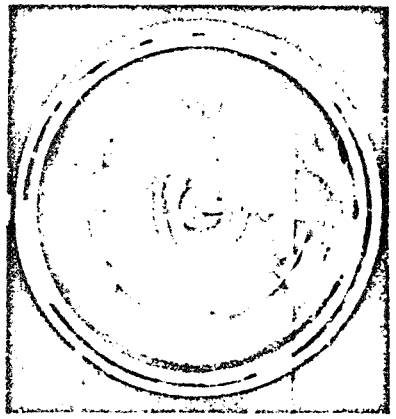

Conical secondary flameholder.

Figure 36

Flameholder system with injection jet.

Obstruction of the inner cross section of the engine

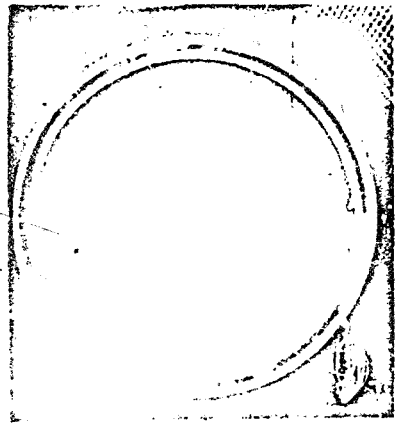

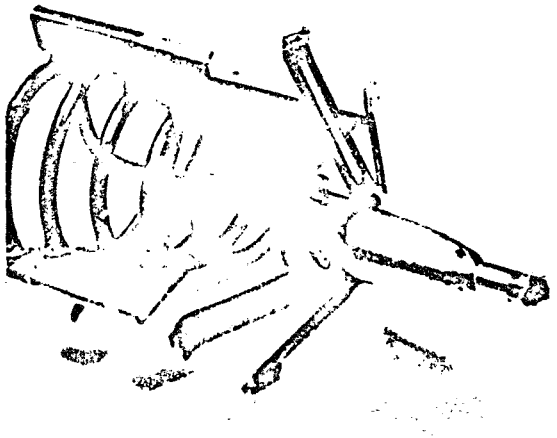

Figure 37

Secondary flameholder as heat exchanger.

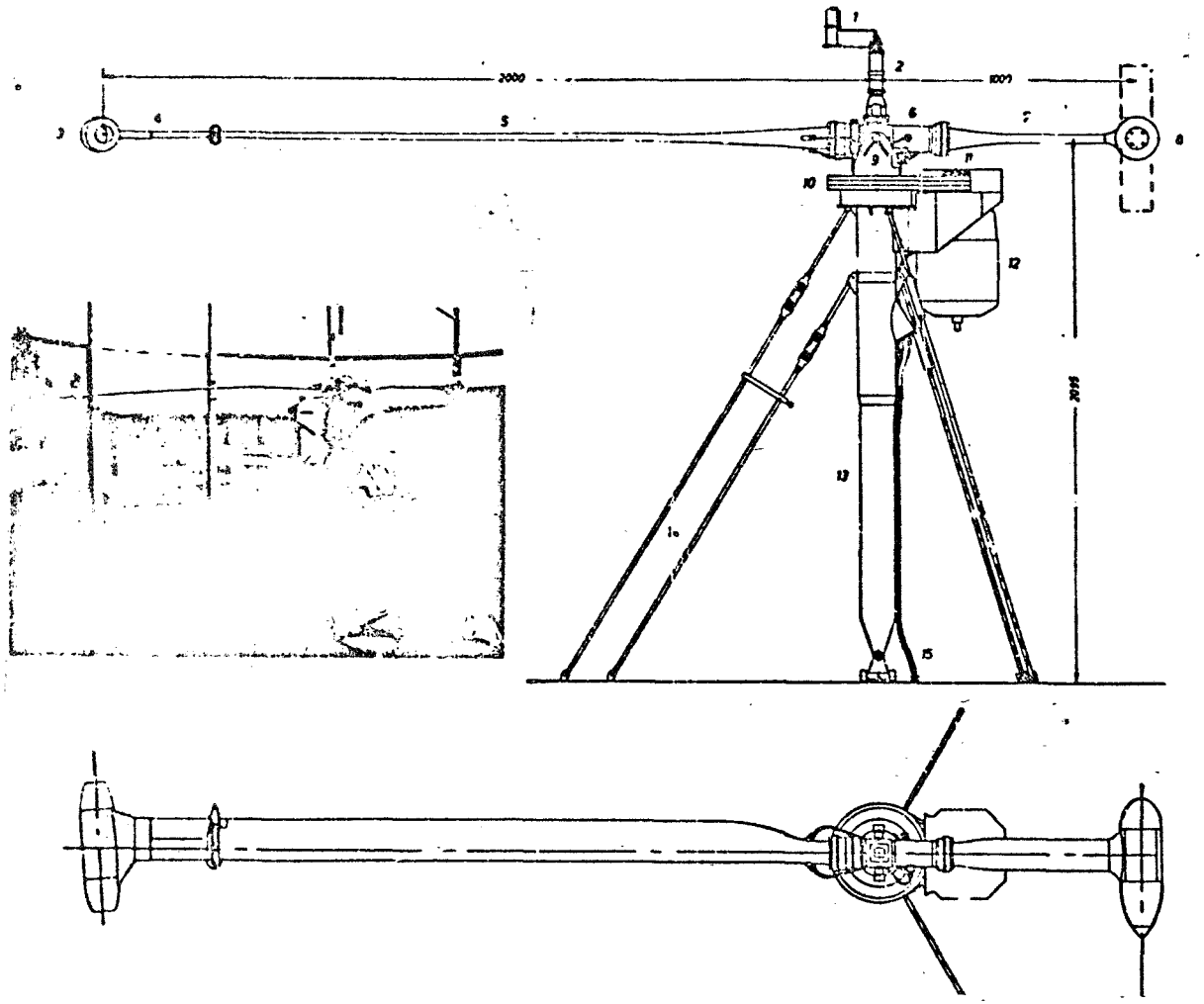

1. Measuring lines
2. Slip ring
3. Ramjet engine
4. Connecting piece
5. Long rotor arm
6. Rotor center section
7. Short rotor arm
8. Counterweight with air brakes
9. Tower head
10. V belt drive
11. Free-wheeling drive connector
12. Electric motor
13. Tower mast
14. Tower guys
15. Fuel and power supply

Figure 38. Rotating arm test stand for ramjet engines.

Figure 39. Rotor flange and intermediate connecting piece with ramjet engine.

Arrangement of the measuring pickups and transducers for pressure and temperature measurements at the ramjet engine.

a. Measuring point IV
b. Measuring point III
c. Fuel supply
d. Plug for thermocouple
e. Rotor made of glass fiber-reinforced plastic
f. Separable steel connecting piece

g. To measuring point I
h. Measuring point II (Chromel/Alumel thermocouple)
i. Measuring point V
k. Spark plug
l. Propane gas supply

m. Miniature pressure gauges
n. Platinum-rhodium/platinum thermocouple for measurement of combustion chamber temperature
o. Flange covering

a. Front covering
b. Weight plates (lead, steel)
c. Center section with air brakes
d. Rear covering
e. Governor
f. Short rotor arm
g. Electric positioning motor (linear actuator
h. Position potentiometer
i. Intermediate flange
k. Rotor center section
l. Rotatable flange (connection of the long rotor arm)
m. Rotor bearing housing

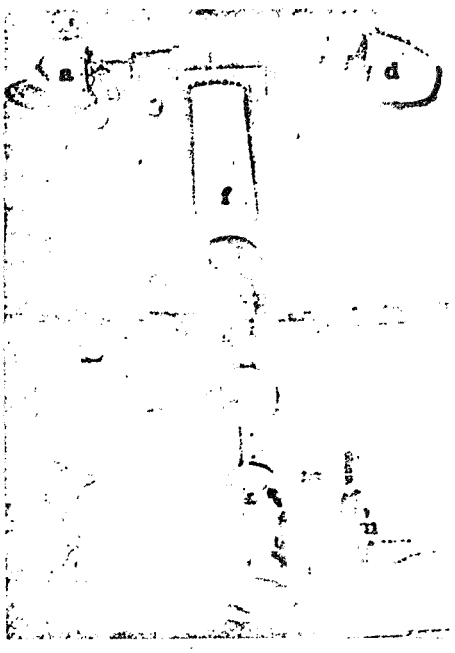

Figure 40. Rotor center section, short rotor arm, and counterweight of the rotating arm test stand.

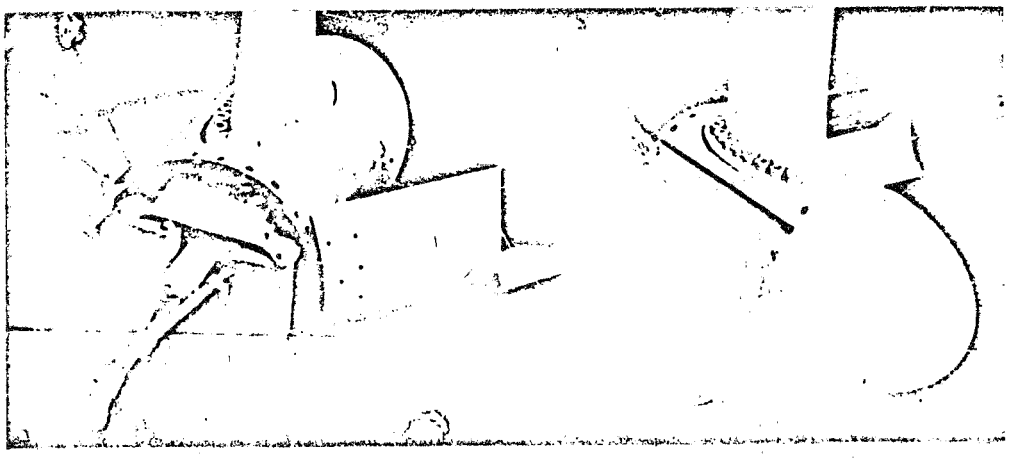

Figure 41. Rotor counterweight and air brake of the rotating arm test stand.

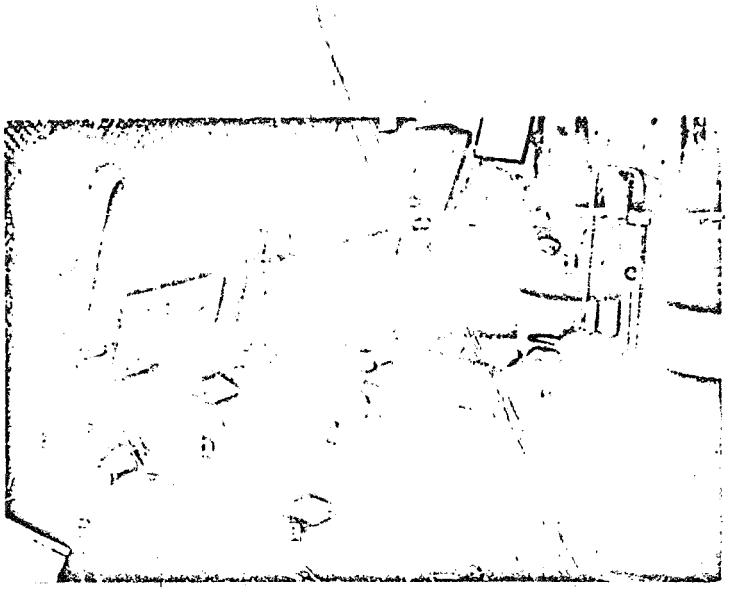

Figure 42. Control desk of the test stand system.

a. Switch table
b. Control tachometer
c. "gas lever" for remote activation of the fuel valve
d. Fuel storage
e. Liquid fuel flow meter
f. Air pump for fuel supply
g. Propane gas pressure reducing valve
h. Propane vaporizer

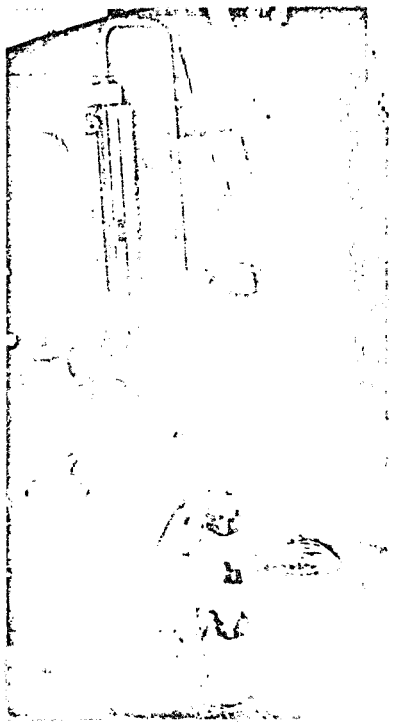

Figure 43. Fuel control system.

Figure 44. Element for transmission of two fuel lines, ignition current, and current for the positioning motor of the air brakes from the stationary to the rotating part of the tower head.

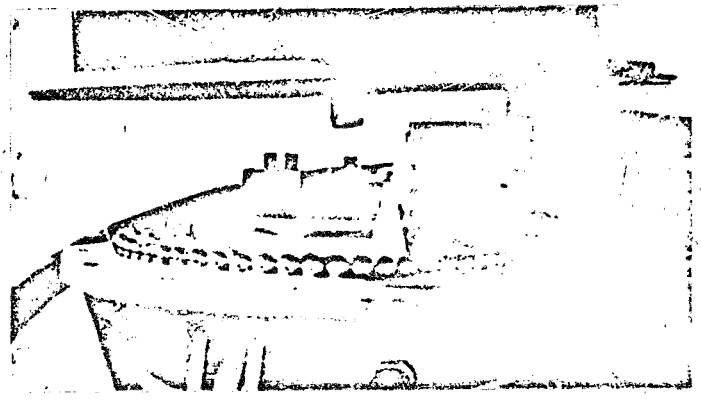

Tower head bearing with the elements shown above built in.

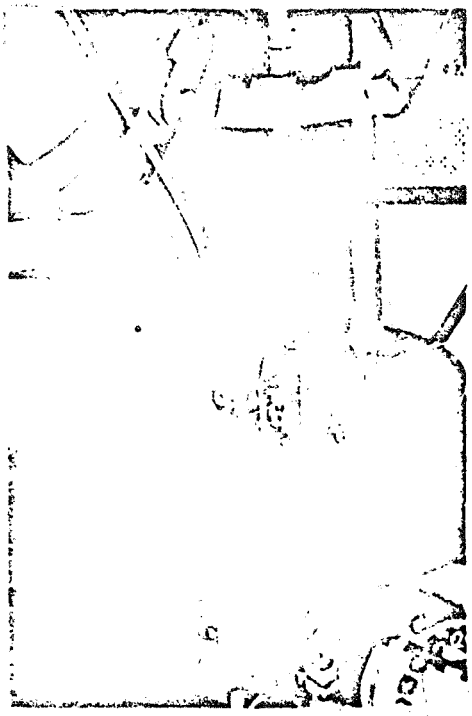

Figure 45. Tower head with tachometer pick-up.

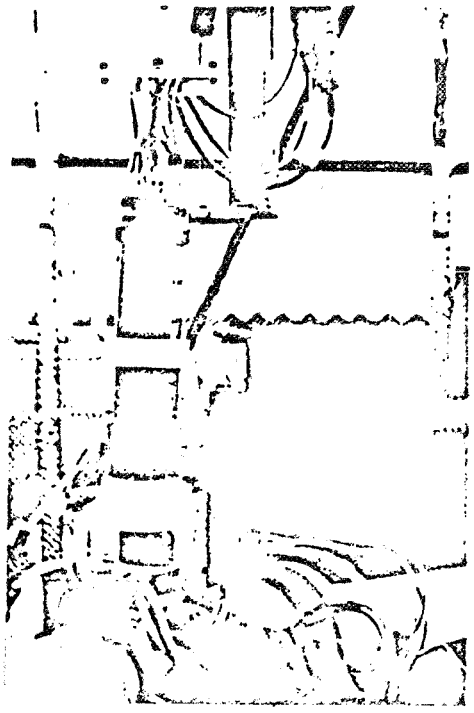

Figure 46. Measuring slip ring with 21 wipers.

a. Bright/dark ring, with permanent magnets inset.
b. Magnetically inductive pickup.
c. Photoelectric pickup.

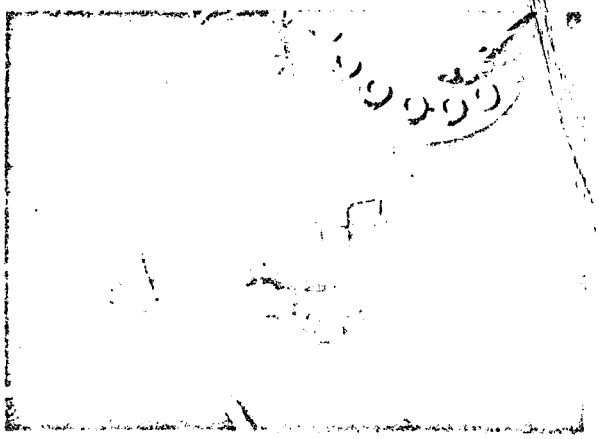

Figure 47. Tower head and rotor center section with added rotational moment pickup (inductive force gauge) which can be mounted on the cover.

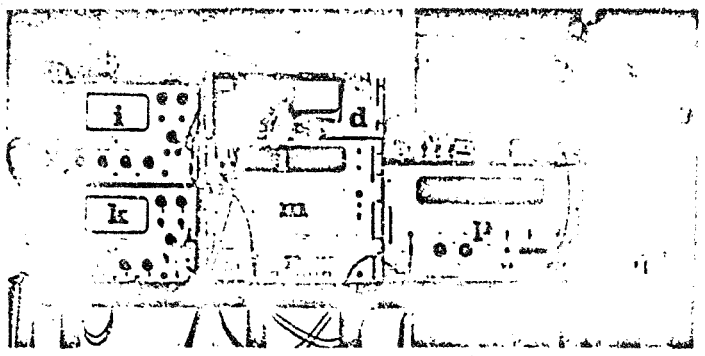

Figure 48: System for measurements on the ramjet engine at the rotating arm test stand.

a. Filter section (temperature measurement)
b. Amplifier for Chromel/Alumel thermocouple
c. Amplifier for Platinum-rhodium/Platinum thermocouple
d. Carrier frequency bridge for measurement of rotational moment (inductive)
e. Delay line
f. Range switch for the analog-digital converter
g. Power supply for Schmitt trigger (4 6V batteries)
h. Schmitt trigger for measuring rate of rotation
i. Carrier frequency measuring bridge for measurement of fuel pressure (strain gauge full bridge)
k. Carrier frequency measuring bridge for measurement of fuel pressure (strain gauge full bridge)
l. Visual indicator for analog-digital converter
m. Analog-digital converter
n. Measuring point switch
o. Filter section (rotational moment measurement)
p. Frequency counter for measurement of rotational rate
q. Printer

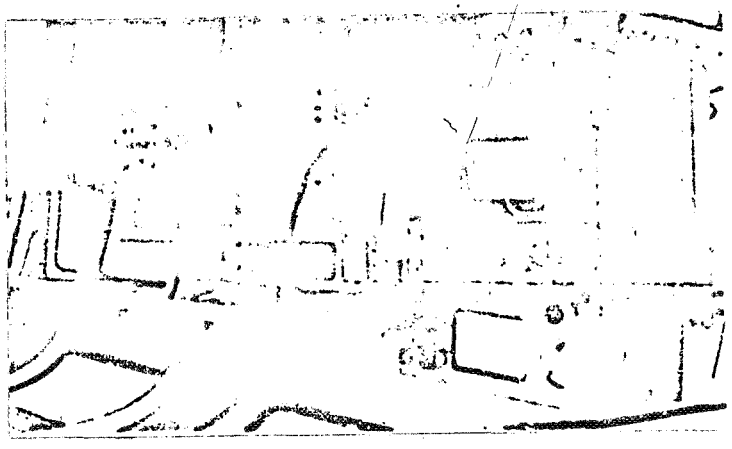

Figure 49. Arrangement of the measuring equipment shown above in the measuring van.

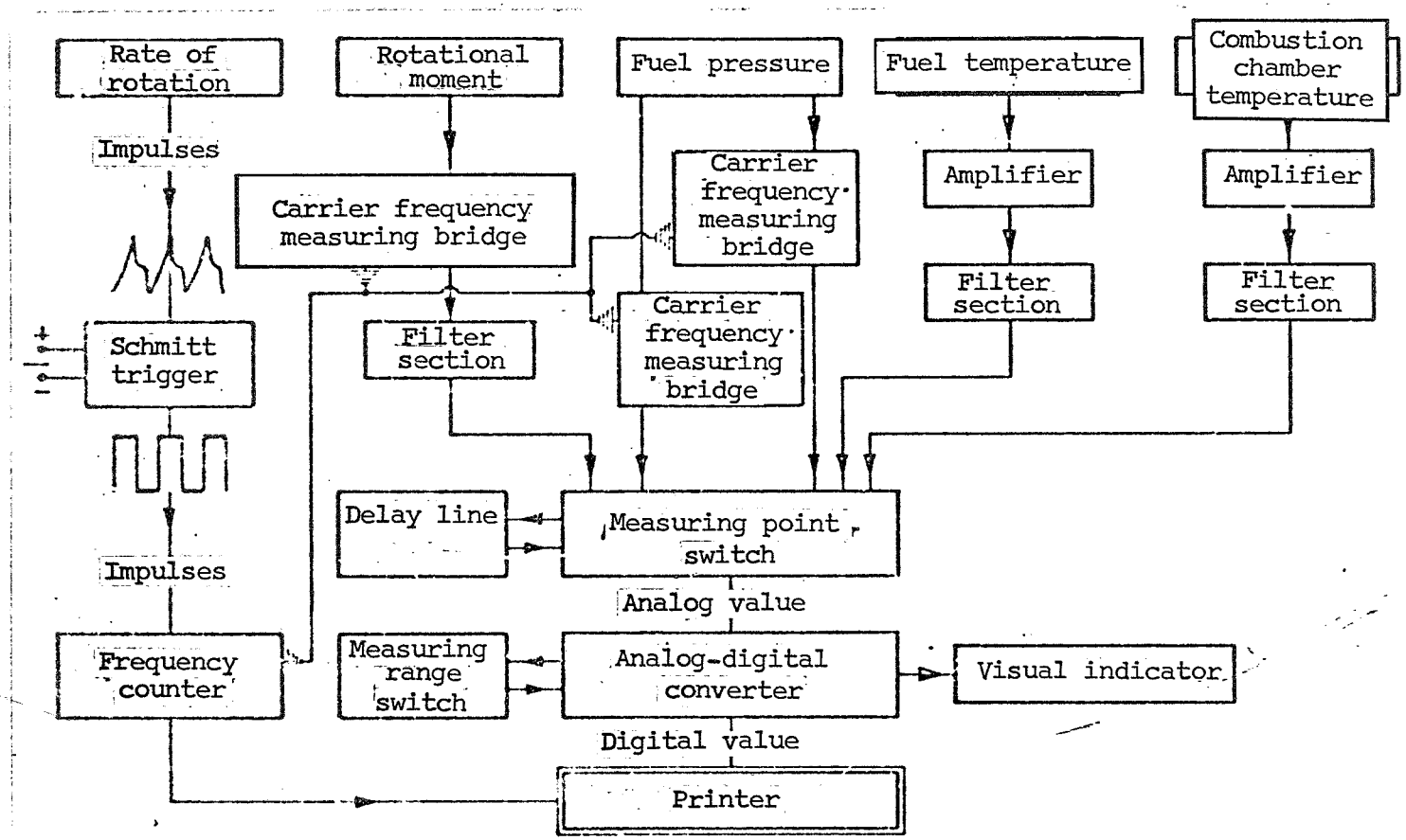

Figure 50. Block diagram of the measuring system.

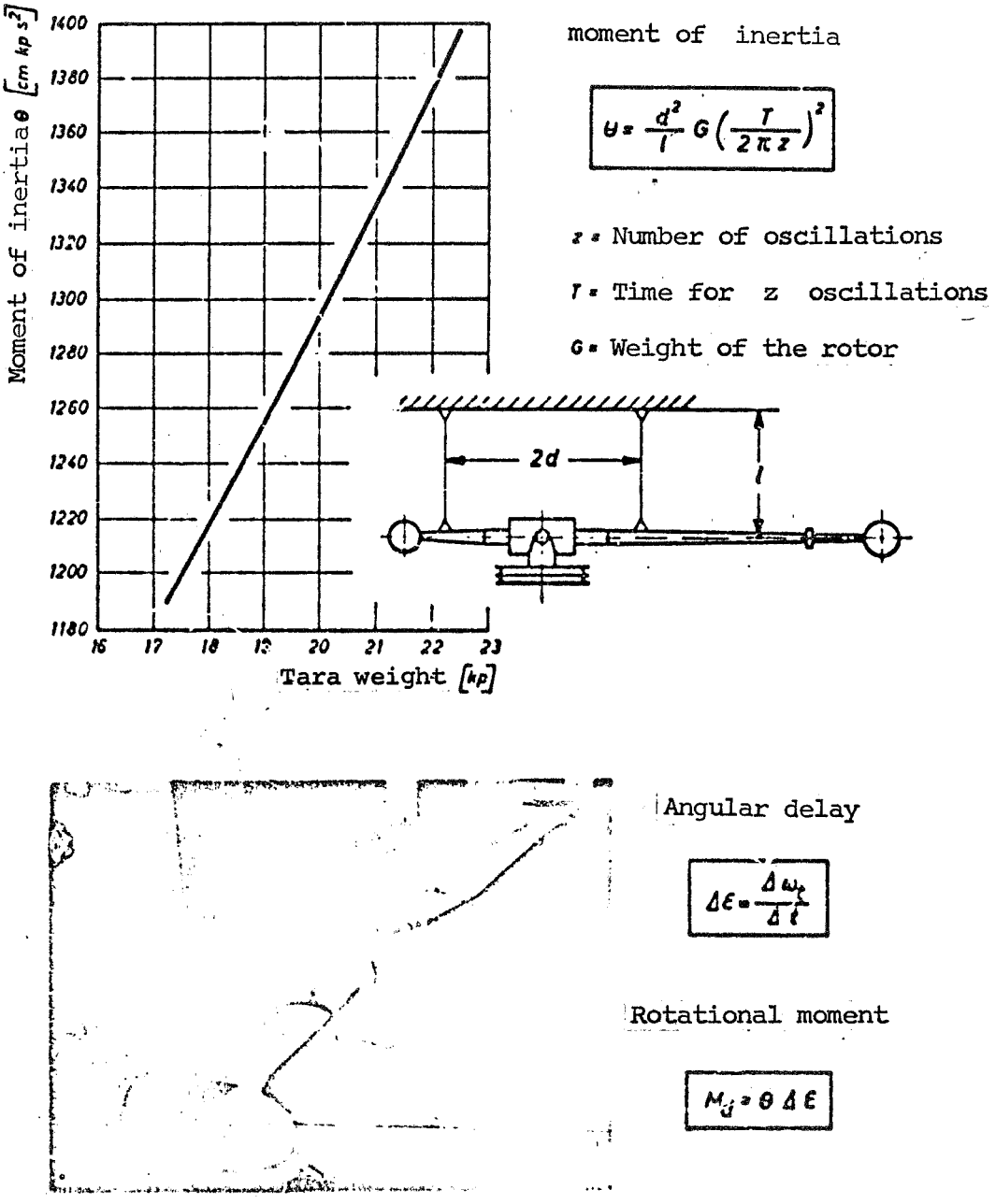

Figure 51. Experimental determination of the moment of inertia for the rotor.

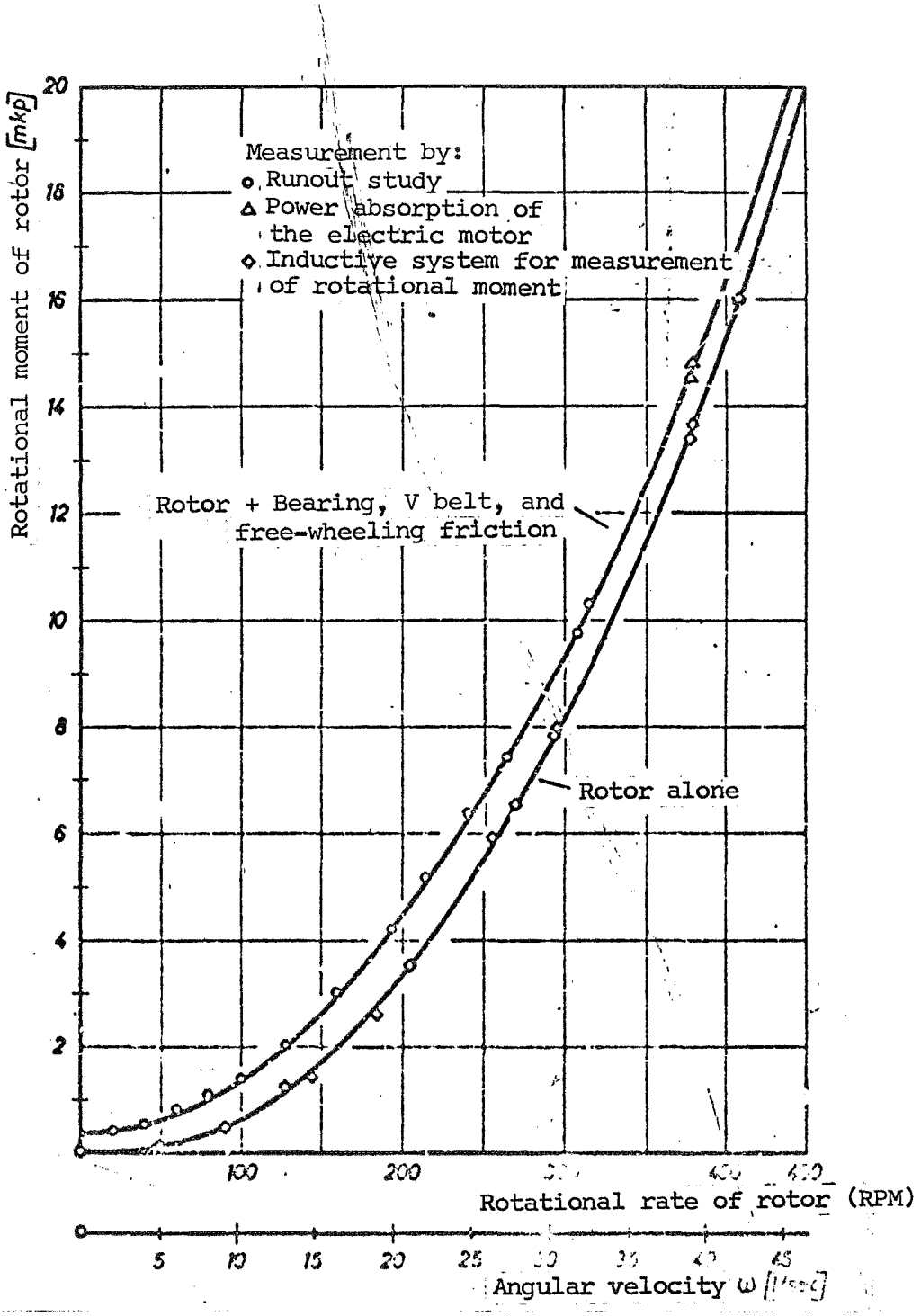

Figure 52. Rotational moment of the rotor with ramjet engine as a function of the rate of rotation.

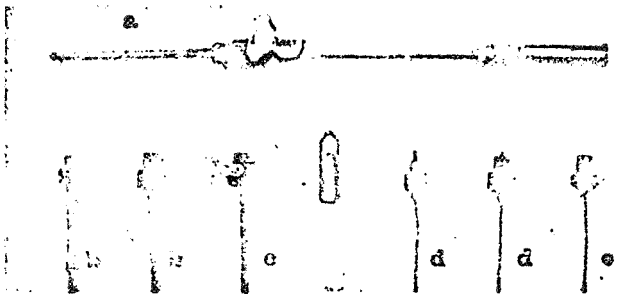

Figure 53. Temperature and pressure pickups

a. Platinum-rhodium/platinum sheathed thermocouple for measurement of combustion chamber temperature
b. Fuel pressure pickups
c. Injection jet with transducer for fuel static pressure
d. Fuel temperature pickups (Chromel/Alumel sheathed thermocouples)
e. Injection jet with Chromel/Alumel sheathed thermocouple

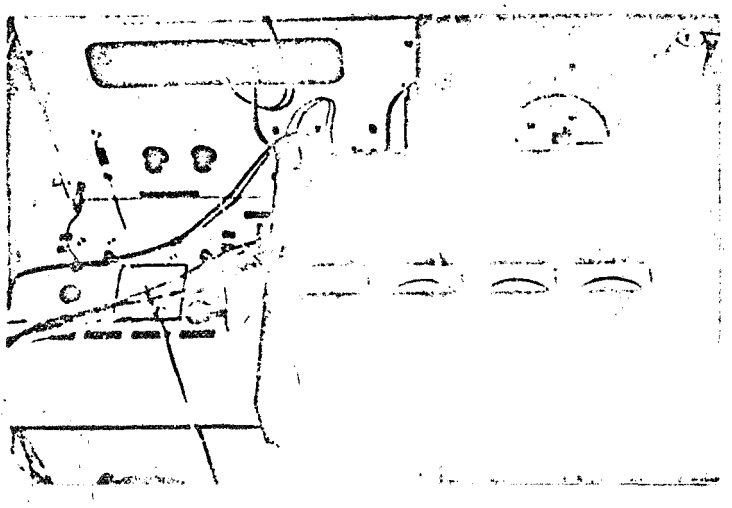

Figure 54. Power measuring box for determination of the power taken up by the drive motor.

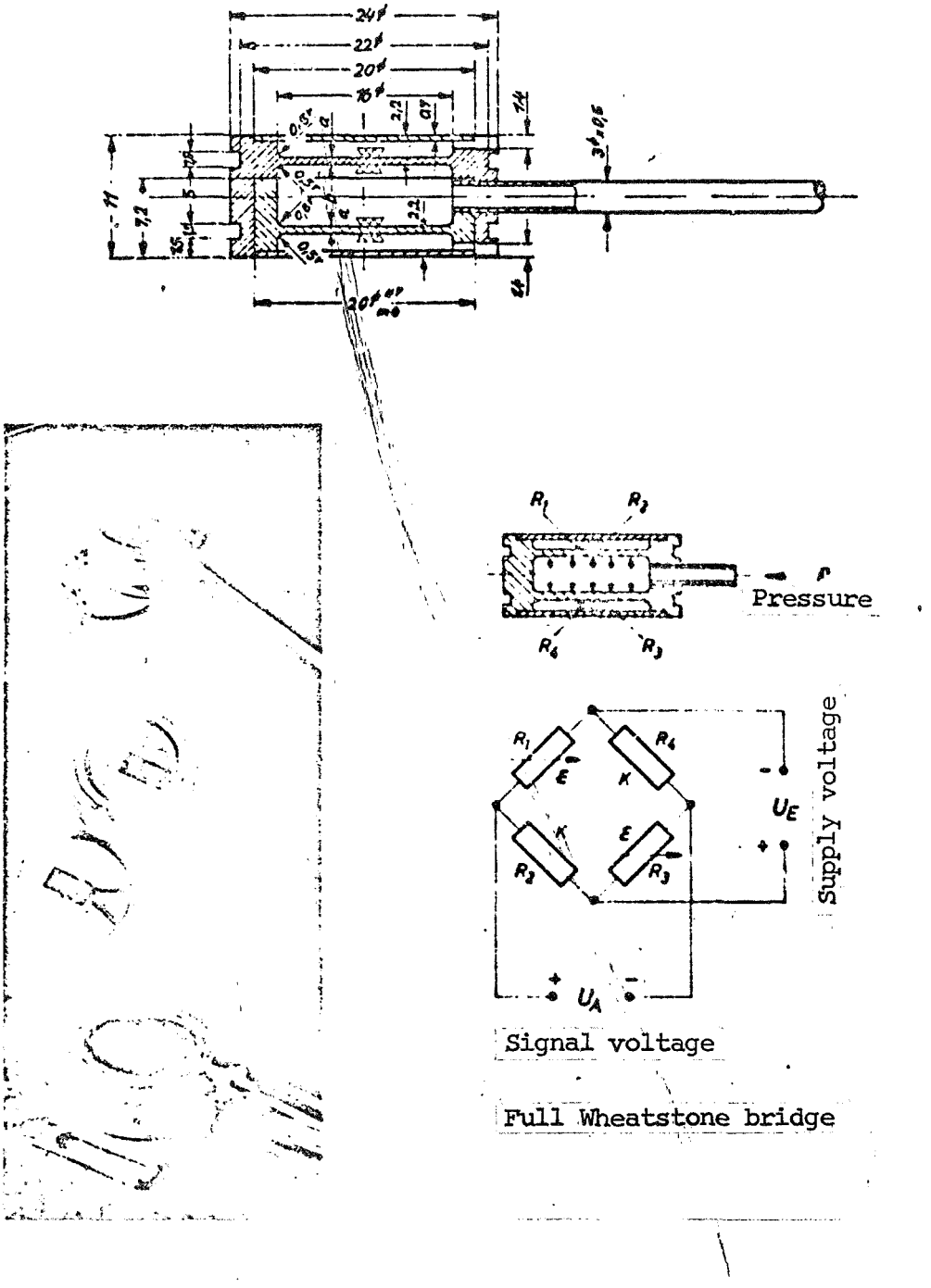

Figure 55. Miniature pressure transducers.

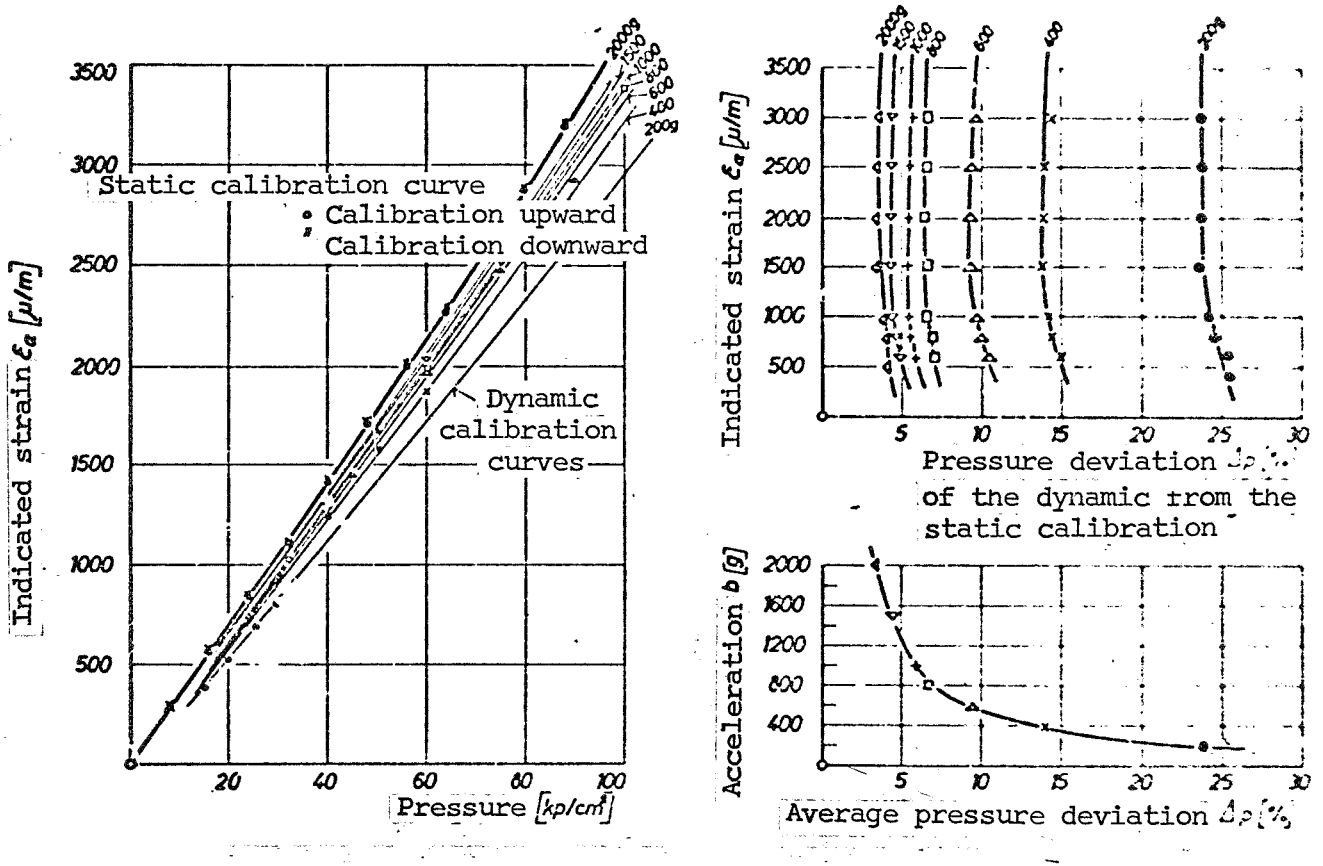

Figure 57. Static and dynamic calibration of the miniature pressure transducer MD 100/2.

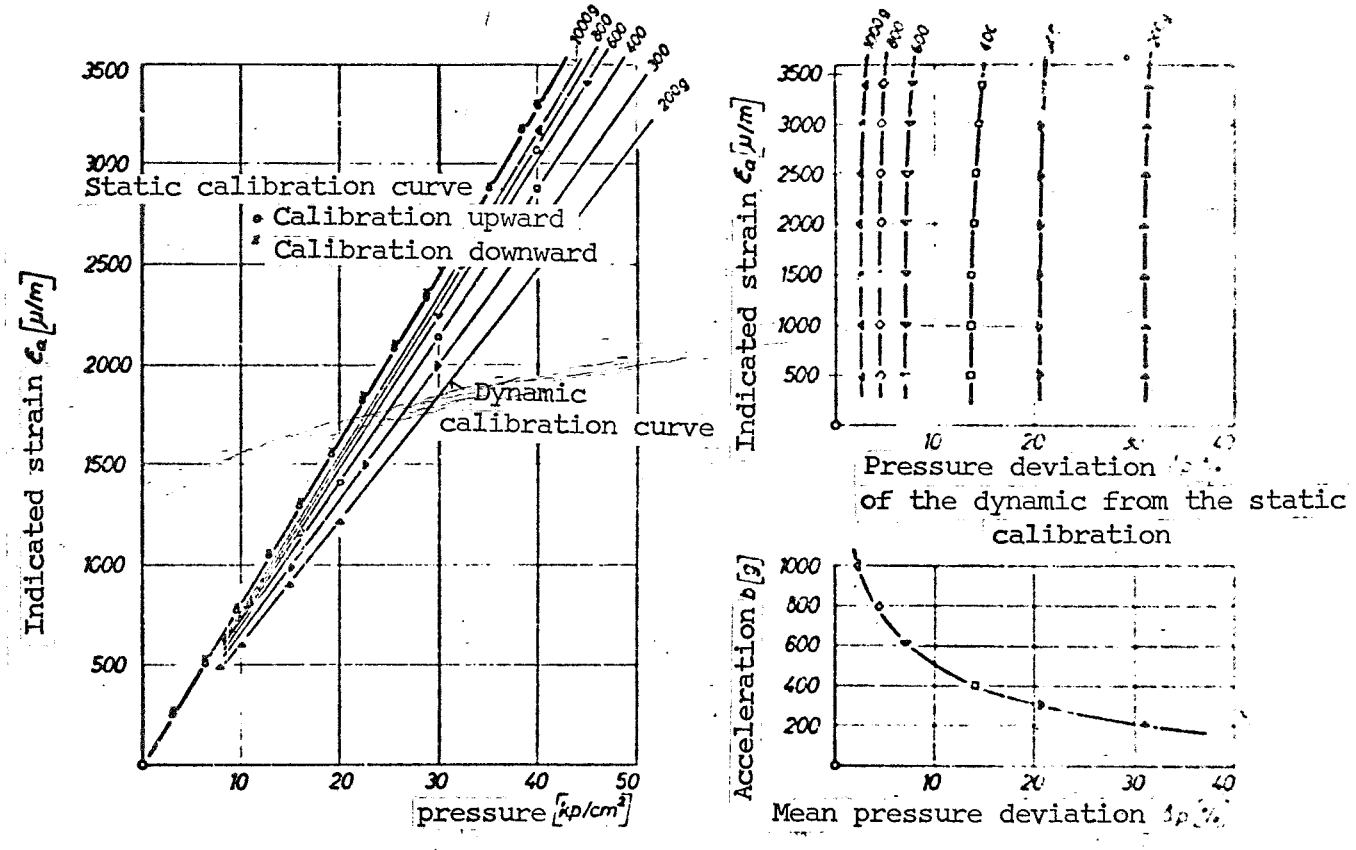

Figure 56. Static and dynamic calibration of the miniature pressure transducer MD 50/2.

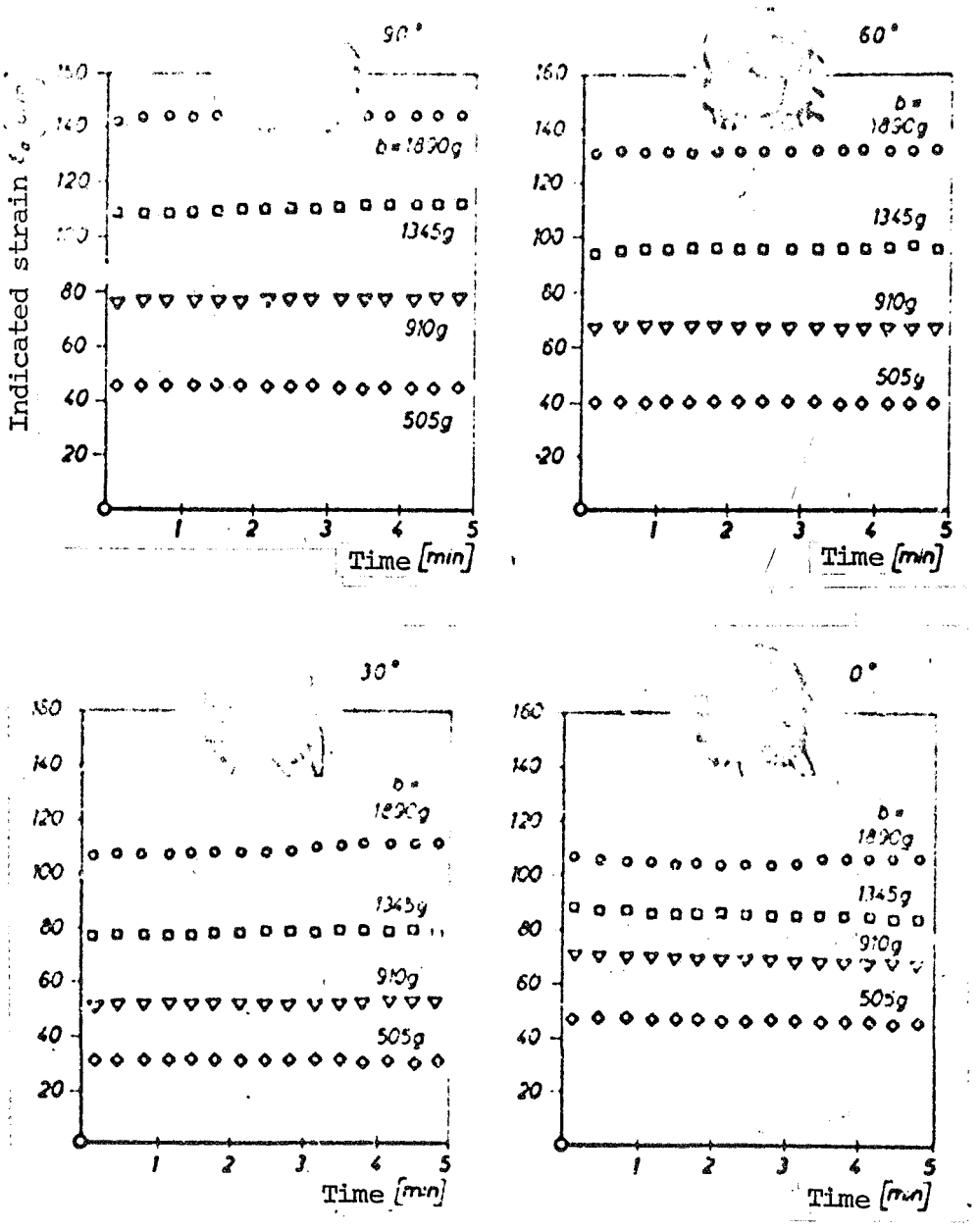

Figure 58. Effect of centrifugal force on the applied strain gauges as a function of the time and the orientation with respect to the direction of stress at constant acceleration.

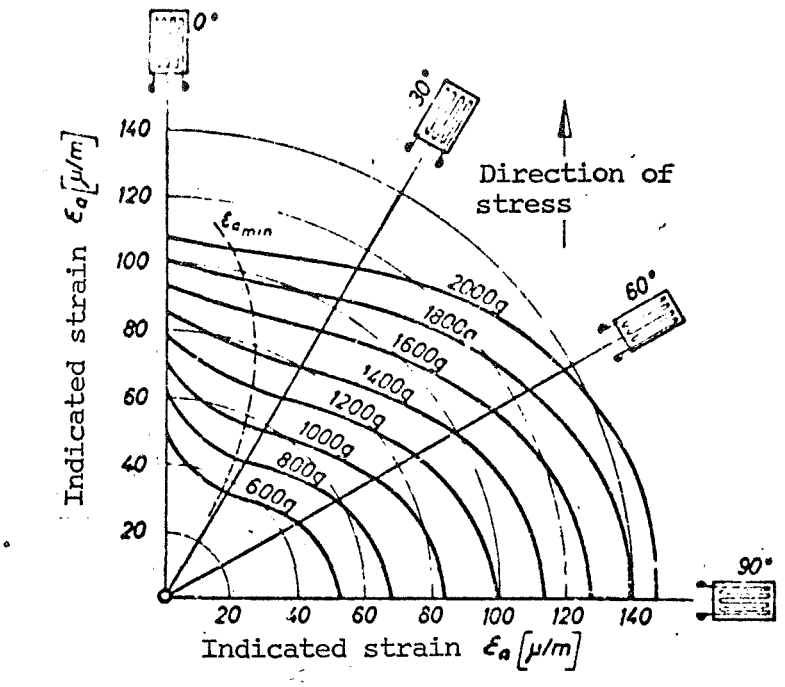

Figure 59. Effect of centrifugal force on the applied strain gauges as a function of the orientation with respect to the direction of stress.

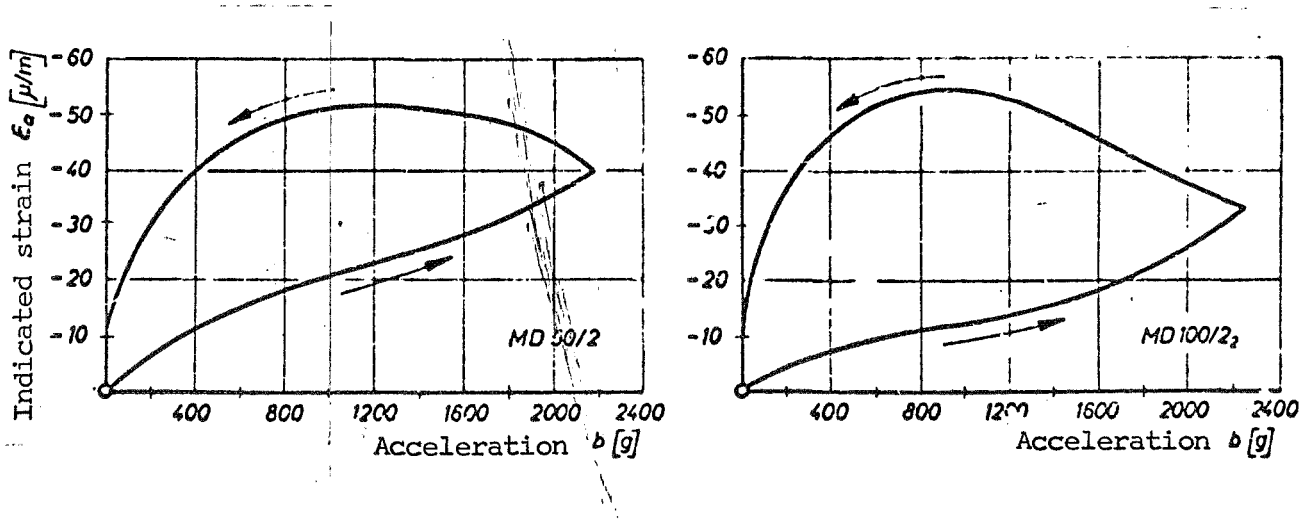

Figure 60. Effect of centrifugal force on the miniature pressure transducers MD 50/2 and MD $100/2_2$ without pressure loading.

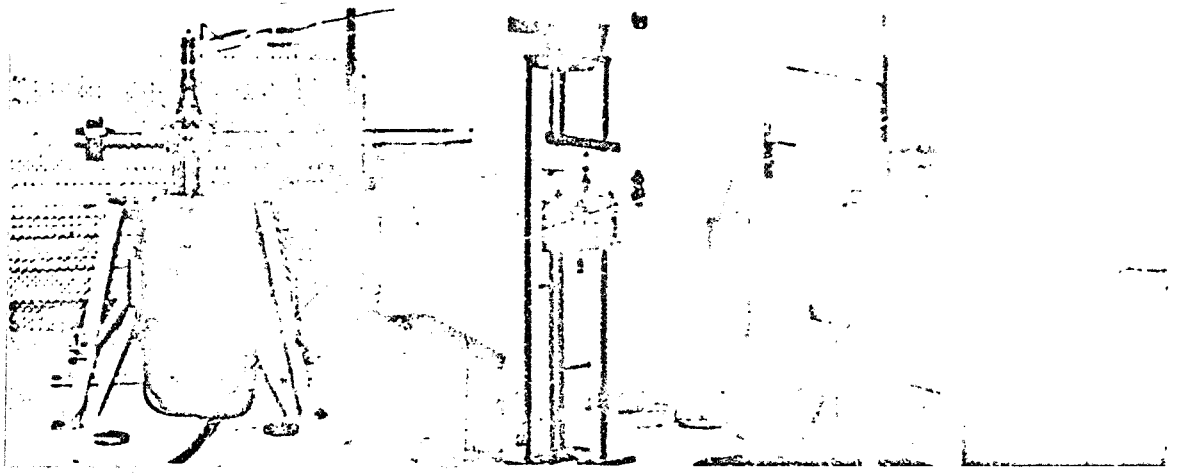

Figure 61. Centrifugal test stand for the miniature pressure transducers.

a. Carrier frequency measuring bridge
b. Analog-digital converter
c. Pressure sampling remote control
d. Range switch
e. Direct current regulator
f. Frequency counter (for measuring rate of rotation)
g. Printer
h. Monitoring mirror

Figure 62. Positioning of the test samples in the end of the rotor arm on the centrifugal test stand.

REFERENCES

1. Orlicek, A. F., and H. Pöll. Hilfsbuch für Mineralöltechniker (Manual for Petroleum Technologists). Die Eigenschaften von Kohlenwasserstoffen, Mineralölprodukten und Hilfstoffen (First Volume: The Properties of Hydrocarbons, Petroleum Products, and Auxiliary Materials). Springer-Verga, Vienna, 1951.

2. Grosse, L. Arbeitsmappe für Mineralölingenieure (Working Portfolio for Petroleum Engineers). VDI-Verlag GmbH, Dusseldorf, 1951.

3. Schmidt, E. Heat Transfer Through Fins. Z. VDI, Vol. 70, 1926, VDI-Verlag GmbH, Berlin, pp. 885-889 and 947-951.

4. Schmidt, Th. E. The Thermal Efficiency of Finned Surfaces. Proceedings of the German Society for Low-Temperature Technology, (DKV), DKV working paper 2-02, Verlag C. F. Müller, Karlsruhe, 1950.

5. Hausen, H. Wärmeübertragung im Gegenstrom, Gleichstrom und Kreuzstrom (Heat Transfer in Countercurrent, Concurrent, and Cross Flow). Springer-Verlag, Berlin-Gottingen-Heidelberg, 1950.

6. VDI-Wärmeatlas, Berechnungsblätter für den Wärmeübergang (VDI Heat Atlas, Papers for Calculating Heat Transfer). VDI-Verlag GmbH, Düsseldorf, 1957.

7. Eckert, E. Measurement of the Total Radiation from Water Vapor and Carbon Dioxide in Mixtures with Nonradiating Gases at Temperatures up to 1300°C. VDI Research Number 387, VDI-Verlag GmbH, Berlin, 1937, p. 19.

8. Gröber-Erk-Grigull. Grundgesetze der Wärmeübertragung (Fundamentals of Heat Transfer). Third Revised Edition, Third Improved and Extended Printing, Springer-Verlag, Berlin-Göttingen-Heidelberg, 1963.

9. Bosnjakovic, F. Technische Thermodynamik (Engineering Thermodynamics). First part, Fourth Edition, Verlag Theodor Steinkopf, Dresden and Leipzig, 1956.

10. Bosnjakovic, F. Thermodynamic Limitations in Heated Pipe Flow. Fifth Study Course for Space Flight Technology, Volume III, Thermo-Gas Dynamics 213b, German Society for Flight Sciences, Stuttgart, 1966.

11. Radin, E. J. and P. J. Carpenter. Comparison of the Performance of a Helicopter-type Ramjet Engine Under Various Centrifugal Loadings, NACA RM L53H18a, Washington, October, 1953.

12. Powell, R. D. and J. P. Shivers. An Experimental Investigation of a Flat Ramjet Engine on a Helicopter Rotor. NACA RM L55F28, Washington, January 4, 1956.

13. Sänger-Bredt, I. Design Tables for Ramjet Engines, Part 1. Contributions from the Research Institute for Physics of Jet Engines, No. 4, Verlag Flugtechnik Stuttgart/Ernst von Olhnausen, July 1956.

14. Ruden, P. Plane Symmetric Intake Diffusors. Yearbook of German Air Travel Research, Kommissionsverlag R. Oldenburg, Munich and Berlin, 1941, pp. 1377-1387; or German Air Travel Research F. B. 1209, 1940; Translation, NACA TM 1279, Washington.

15. Ruden, P. Wind Tunnel Measurements with Plane, Symmetric Intake Diffusors. Yearbook of German Air Travel Research, Kommissionsverlag R. Oldenburg, Munich and Berlin, 1941, pp. 1388-1397.

16. Brödel, W. The Theory of Plane Intake Diffusors. German Air Travel Research U. M. 716, 1943, Translation, NACA TM 1267, Washington.

17. Küchemann, D. and J. Weber. The Intake Problem with Engine Cowlings. Contributions of the German Academy for Air Travel Research, No. 117, 1943.

18. Küchemann, D. and J. Weber. Aerodynamics of Propulsion. McGraw-Hill Publishing Company Ltd., London-New York-Toronto, 1953.

19. Baals, D. D., N. F. Smith, and J. B. Wright. The Development and Application of High-Critical-Speed Nose Inlets, NACA TR 920, Washington, 1949.

20. Hütter, U. Propellers and Helicopter Rotor Blades of Fiber-Reinforced Plastics. Yearbook of the WGL, Verlag Friedr. Vieweg & Sohn, Bruanschweig, 1960, pp. 374-381.

21. Hütter, U. Load-Bearing Aircraft Parts of Glass Fiber Reinforced Plastics. Z. VDI-Luftfahrttechnik, Vol. 6, No. 2, VDI-Verlag GmbH, Düsseldorf, 1960.

22. Hütter, U. Highly Stressed Light Construction Parts of Glass Fiber Reinforced Plastics. Z. Kunststoffe 50, Carl Hanser Zeitschriften-verlag GmbH, Munich, 1960, pp. 318-324.

23. Quick, A. W. A Procedure for Investigation of Exchange Processes in Turbulent Streams Behind Bodies with Separated Flow. DVL Report No. 12, Westdeutscher Verlag, Cologne and Upladen, 1956.

24. Lorin, R. Propulsion by Direct Reaction and Its Application to Aviation. L'Aerophile. Numerous articles on this question, 1907-1913.

25. Lorin, R. A Simple Experiment Relating to Propulsion by Direct Reaction. L'Aerophile, 1913, p. 514; Abstract: Z. Flugsport, Vol. 31, No. 1, January 1939, p. 4.

26. Lambermont, P. and A. Pirie. Helicopters and Autogyros of the World. Cassell & Company Ltd., London, 1958, pp. 78-79.

27. Sänger, E. Ramjet Propulsion. Z. Luftfahrttechnik, VDI-Verlag GmbH, Düsseldorf, July 1956, pp. 131-140.

28. Spremberg, P. First Test Flight with the "Sänger Ramjet Engine". Z. Weltluftfahrt, Vol. 1, No. 10, 1949, p. 215.

29. Berry, M. Little Henry the Ramjet Helicopter. American Helicopter, Vol. 6, December 1947, p. 10.

30. McLarren, R. McDonnell Flies Ramjet Helicopter. Aviation Week, Vol. 47, November 1947, p. 14.

31. Holm, H. Hiller HJ-1, YH-32 Helicopter. Aeronautical Engineering Review, October 1953, pp. 48-53.

32. Lawrence, F. Hiller Jet Engine Awarded CAA Certification. American Helicopter, November 1954, pp. 11, 16-17.

33. Verhage, Ir. G. F. The Two-Engine Ramjet-Helicopter "Kolibrie". Luchtvaarttechniek 4, 31 August 1956, pp. 27-32.

34. International Meeting on Ramjets and Rockets, Freudenstadt, 6-8 February, 1956. Contributions from the Research Institute for Physics of Jet Propulsion, Stuttgart, No. 6. Verlag Flugtechnik Stuttgart/Ernst von Olnhausen, September 1956.

35. Hütter, U., S. Armbrust, P. G. Grüninger, F. Lachnit, H. Letsche. Light Helicopter with Ramjet Engines JS-71. German Helicopter Study Society, Stuttgart Airport, Report 43-3, March 1960.

36. Alvermann, W. and J. Lambrecht. Some Problems of Fuel Supply for Jet Engines. Motortechnische Zeitschrift, Vol. 19, No. 6, August 1958.

37. Allen, S. Combustion Chamber with Fuel Vaporizing Pipes for Internal Combustion Turbine Plants. U. S. Patent Specification 2,522,081, 1947. Abstract: Aircraft Engineering, Vol. 23, No. 263, January 1951.

38. Williams, F. D. M. Multiple Fuel Jet Burner and Torch Igniter Unit with Fuel Vaporizing Tubes. U. S. Patent Specification 2,541,900, 1948. Abstract: Aircraft Engineering Vol. 23, No. 270, August 1951.

39. Williams, F. D. M. Vaporizer System for Combustion. U. S. Patent Specification 2,548,087, 1950. Abstract: Aircraft Engineering, Vol. 23, No. 270, August 1971.

40. Heath, D. P. Jet Combustion Device Embodying Pretreatment of Fuel Before Combustion. U. S. Patent Specification 2,628,475, 1946. Abstract: Aircraft Engineering, Vol. 25, No. 293, July 1953.

41. Meschino, R. G. Annular Fuel Vaporizer for Gas Turbine Engines. U. S. Patent Specification 2,646,664, 1949. Abstract: Aircraft Engineering, Vol. 25, No. 298, December 1953.

42. Howes, L. D. Reverse-Flow Vaporizer with Single Inlet and Plural Outlets. U. S. Patent Specification 2,727,358, 1952. Abstract: Aircraft Engineering, Vol. 28, No. 327, May 1956.

Translated for National Aeronautics and Space Administration under Contract No. NASw-2035, by SCITRAN, P. O. Box 5456, Santa Barbara, California, 93103.